CHAPTER 1

Introduction

Abstract

Autophagy is a process of cellular self-degradation in which portions of the cytoplasm are sequestered within cytosolic double-membrane vesicles and delivered to the lysosome/vacuole. This process occurs in all eukaryotic cells and is partly a stress response; autophagy is induced during starvation and hypoxia. However, autophagy also plays a role during development and is associated with a range of diseases. Accumulating data also suggest the involvement of autophagy in aging. For example, the role of various hormones and nutrient sensing pathways in life span extension may involve autophagy. Similarly, autophagy is the primary mechanism for removing damaged organelles, such as mitochondria, which may have a direct impact on aging. Here, we review the role of autophagy, with an emphasis on the signaling pathways that are involved in regulation, and the consequences of autophagy induction with regard to aging.

Introduction

Autophagy, an evolutionarily conserved catabolic pathway in eukaryotic cells, plays an important role in stress response and the degradation of damaged cytosolic components (113). There are three general types of autophagy that can deliver intracellular materials into lysosomes for degradation: macroautophagy, microautophagy, and chaperone-mediated autophagy (CMA). CMA is restricted to a subset of proteins bearing a particular pentapeptide motif. Furthermore, CMA involves the translocation of unfolded substrates across the lysosome membrane and, therefore, is unable to accommodate large protein aggregates or organelles. Unlike CMA, both micro- and macroautophagy involve dynamic membrane rearrangements resulting in the ability to enwrap large structures, such as organelles. Microautophagy refers to the sequestration of cytosolic materials through direct invagination of the lysosomal membrane. In contrast, during macroautophagy, double-membrane cytosolic vesicles, termed autophagosomes, sequester the cytoplasm and deliver the cargo to the lysosome/vacuole for degradation (264).

Although autophagy is mainly considered a bulk sequestration process, selective autophagy to degrade damaged or excess organelles, such as mitochondria (mitophagy) (128), peroxisomes (micropexophagy and macropexophagy) (47), endoplasmic reticulum (ER; reticulophagy) (265), parts of the nucleus (piecemeal microautophagy of the nucleus) (189), and even ribosomes (ribophagy) (116) also have been reported. Most of the autophagy-related pathways mentioned above share similar molecular components and morphological features. In addition to catabolic degradation, in the yeast *Saccharomyces*

cerevisiae, Pichia pastoris, and *Candida albicans*, a biosynthetic pathway, the cytoplasm to vacuole targeting (Cvt) pathway, also uses the autophagy machinery to deliver the vacuolar hydrolase aminopepetidase I (264). A schematic diagram of autophagy-related pathways is shown in Fig 1.1.

The autophagy process can be dissected into several steps: induction, vesicle nucleation, cargo sequestration, autophagosome expansion and completion, vesicle fusion with the lysosome/vacuole, degradation, and nutrient recycling (73, 131). The identification of many autophagy-related (*ATG*) genes provides insight into the molecular machinery of the autophagy process. Among 32 *ATG* genes that have been identified so far, the majority of them function at the step of autophagosome membrane formation. Depending on their function, the Atg proteins can be classified into different groups: the Atg1 protein kinase complex is involved in autophagy induction and also acts along with Atg2 and Atg18 to regulate the cycling of the integral membrane protein Atg9; Atg14 is part of the phosphatidylinositol 3-kinase complex that is required for vesicle nucleation; the Atg8 and Atg12 ubiquitin-like conjugation systems are involved in autophagosome formation, and Atg8 controls the size of the autophagosome; and Atg9, Atg23, and Atg27 are thought to be part of the complex that delivers membrane needed for autophagosome production (73, 126, 255, 256).

Owing to the increasing understanding in the biological functions of autophagy, the significance of this process in diseases, aging, and immunity has been recognized (73). Among the different functions of autophagy that have been studied, growing evidence supports a role of autophagy in life span extension. For example, mutations that decrease mitogen-responsive pathways, such as in the insulin/insulin-like growth factor 1 (IGF-1)

receptor and target of rapamycin (TOR), as well as a reduction in food intake, are known

to increase life span from yeast to mammals, although the mechanisms of these pathways

in aging regulation is not clear (12). Results from various studies indicate that autophagy

may play an important role as a downstream effector of these life span regulatory

pathways. One focus of this review is, therefore, the interaction between macroautophagy

(referred to as autophagy hereafter) and several distinct longevity regulatory pathways. In

addition, mitochondrial respiration and alteration have been linked to aging.

Mitochondria can regulate autophagy through the generation of ROS. The role of this

autophagy induction, however, can serve as an important intervention for either

mitochondrial turnover to maintain homeostasis or as a signal for autophagy-associated
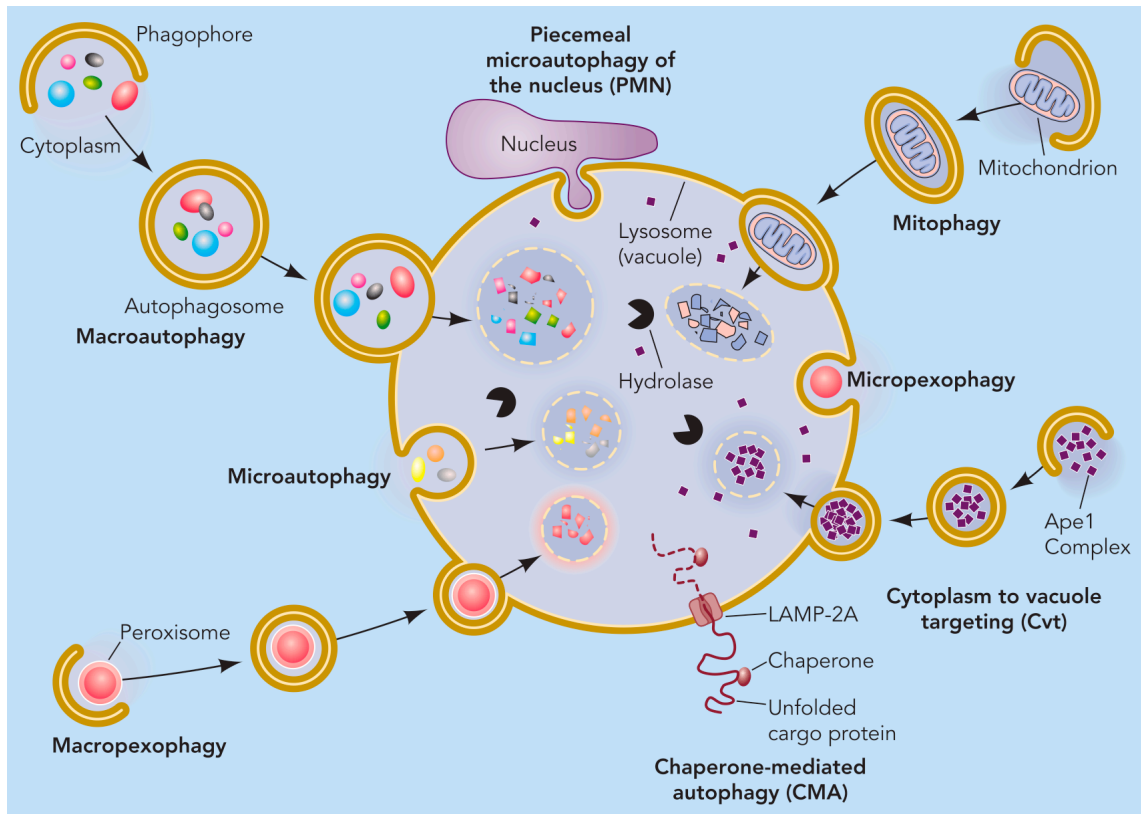
cell death.

Figure 1.1. Schematic diagram of selective and nonselective autophagy. Three fundamentally different modes of autophagy are macroautophagy, microautophagy, and chaperone-mediated autophagy. Depending on the specificity of the cargos, autophagy can be a selective or a nonselective process. During nonselective autophagy, a portion of the cytoplasm is sequestered into a double-membrane autophagosome, which then fuses with the lysosome/vacuole. In contrast, the specific degradation of peroxisomes in certain conditions can be achieved by either a macro- or microautophagy-like mode, termed macropexophagy and micropexophagy, respectively. Piecemeal microautophagy of the nucleus allows the degradation of a portion of the nucleus. The specific degradation of mitochondria, termed mitophagy also takes place. A biosynthetic pathway in yeast also shares similar morphological features. Note that this schematic illustrates aspects of autophagy in both yeast cells and higher eukaryotes.

Autophagy and Aging

Aging cells gradually accumulate various deleterious changes, resulting in a decline in cellular function and eventually leading to cell death and disease. The accumulation of damaged macromolecules and organelles is one of the most persistent changes in aging cells (226) and is associated with the decline of different catabolic pathways (37). Autophagy deficiency during aging has been proposed to be the main cause of this biological "waste" accumulation (36). In support of this theory, it has been found that loss-of-function in autophagy genes resulting in intracellular accumulation of damaged proteins and organelles in mice, accelerates aging, and life span shortening in *S. cerevisiae*, *Caenorhabditis elegans*, and *Drosophila melanogaster* (83, 117, 146). In contrast, elevating autophagy activity increases life span in *Drosophila* and rescues aged cells from accumulating dysfunctional mitochondria (211). Moreover, the failure in the clearance of proteins due to the decline of autophagy is associated with age-related pathogenesis in neurodegenerative diseases. For example, the conditional knockout of Atg5 or Atg7 in the nervous system causes neurodegeneration in mice (62, 114). Similarly, the *Drosophila* p62 homolog Ref(2)P, which is associated with neural aggregates and inclusion bodies found in various neural degenerative disorders (270), accumulates in the brain of autophagy-defective young flies (159). Thus, autophagy plays a cytoprotective role in preventing the accumulation of disease-causing proteins. However, the fact that autophagy is associated with cell death under certain settings might suggest its involvement in different aspects of aging. For instance, overexpression of autophagy genes or inducing autophagy in apoptosis-deficient cells can lead to cell

death (132). It is important to point out, however, that the latter situations may be nonphysiological. There is at present little, if any, direct evidence that autophagy normally causes cell death. Instead, it is likely to act primarily as a cytoprotective response.

Signaling, Aging, and Autophagy

Results from different organisms indicate that decreasing the activity of conserved nutrient-sensing signaling pathways, including insulin/IGF-1, TOR, protein kinase A (PKA), and protein kinase B (PKB), can extend life span. This phenomenon suggests that the conserved nutrient responsive pathways can affect life expectancy in evolutionarily diverse species. Interestingly, autophagy is sensitive to nutrient availability and is negatively regulated by these signaling pathways. The link between autophagy and nutrient sensing pathways that regulate life span has been demonstrated in many studies.

The insulin/IGF-1 pathway

In *C. elegans*, several long-lived mutants carry gene mutations that correspond to the components of the insulin/IGF-1 signaling pathway. For instance, mutations in *daf-2*, encoding the insulin/IGF-1 receptor, *age-1*, which encodes the catalytic subunit of the phosphatidylinositol 3-kinase (PtdIns3K), and *pdk-1*, which encodes phosphoinositide-dependent protein kinase 1 (PDK1), extend life span (104, 148, 170). The longevity regulated by this pathway is through attenuation of insulin/IGF-1, the downstream PI3K signaling, and in part by the upregulation of downstream stress response genes through the forkhead FoxO-related transcription factor (DAF-16) (123). Loss-of-function in DAF-18, a homologue of the phosphatase and tensin homolog on chromosome 10 (PTEN), de-suppresses the activity of PtdIns3K, thus inhibiting the longevity phenotype of *daf-2* and *age-1* mutants (119) (Fig 1.2).

Similar life span extension effects also appear in *Drosophila*. Flies with loss-of-function mutations in the insulin-like receptor (224), or its receptor substrate (*chico*) (32), or gain-of-function in a FoxO-like transcription factor (77) result in significantly increased life span. However, the longevity effect in mammalian systems is rather ambiguous probably due to the complexity of the metabolic pathways. A variety of mutations down-regulating insulin-like signaling activity can extend mammalian life expectancy. Mice heterozygous for the IGF-1 receptor, as well as dwarf mice with mutations in Pit1dw, Prop1df, and Ghr genes, are long-lived and have reduced plasma insulin and/or IGF-1 (14, 17, 34). In contrast, the variable effects on life span in mice with tissue-specific loss-of-function mutations in the insulin receptor, and the developmental and multiple endocrine defects in IGF-1-deficient animals complicates the interpretation of the data on the role of IGF-1 in aging (14). It is interesting to note that a recently identified aging suppressor gene, Klotho, in mice can block insulin-mediated glucose uptake, suppress the phosphorylation of insulin and IGF-1 receptors as well as repress already activated insulin receptors, thus resulting in increased longevity (118). Klotho mice show better oxidative stress resistance at the cellular and organismal level by inducing manganese superoxide dismutase (MnSOD) expression through activation of stress response FoxO forkhead transcription factors (258). The increasing resistance to oxidative and metabolic stress by upregulating FoxO transcription factors in long-lived mutant animals is thought to contribute, at least in part, to the long life span. Growing evidence shows that mammalian forkhead family transcription factors influence the life span of stem cells, control stress response gene expression, and have tumor suppressor functions (8).

It has been known for years that autophagy can be induced by low insulin levels during fasting, whereas high insulin levels are suppressive (156). However, the link between insulin/IGF-1 in longevity and autophagy is not clear. Several lines of evidence suggest that autophagy is involved in aging regulation through the insulin/IGF-1 signaling pathway. Depletion of *C. elegans* BEC-1, whose counterpart is yeast Atg6 and the human tumor suppressor Beclin 1, inhibits the increased longevity phenotype in the *daf-2* mutant, and slightly shortens the life span of wild-type animals (146). Similarly, knocking down *ATG7* and *ATG12* through double-stranded RNA (dsRNA) partially suppresses the life span extension in *daf-2* mutants and causes significant shortening of the mean but not the maximum life span of wild-type worms (66). Furthermore, *bec-1*, *atg-18*, and *lgg-1* (LC3/Atg8) mutants partially inhibit the increased longevity of *daf-2* mutants (229). Theses results suggest that autophagy and other parallel pathways may regulate life span through insulin/IGF-1 signaling. For example, the ubiquitin-proteasome system and the heat shock factor HSF-1, which controls stress-inducible gene expression and protein folding homeostasis, is also required for the life span extension of *daf-2* mutations (155).

The downstream insulin/IGF-1 components, forkhead transcription factors, also regulate autophagy activities. Accordingly, activation of FoxO in the *Drosophila* fat body induces autophagy in feeding larvae, whereas a null mutation of FoxO decreases starvation-induced autophagy (85). Similarly, FoxO3, the closest mammalian ortholgue of daf-16, which is associated with the long-lived phenotype of *daf-2* mutants in *C. elegans* as discussed previously, is necessary and sufficient to induce autophagy in skeletal muscles (141, 142). Thus, autophagy stimulation following a decrease in IGF-1-

PtdIns3K-Akt signaling can occur in a FoxO3-dependent manner. All together, these findings imply that autophagy can function downstream of insulin/IGF-1 to regulate life span (Fig. 1.2).

TOR

The insulin/IGF-1 pathway negatively regulates autophagy through the target of rapamycin (TOR), which also plays an important role in aging (81). TOR is a highly conserved serine/threonine protein kinase that regulates cell growth and proliferation in response to growth factors, nutrient signals, and energy status (167). There are two functionally distinct TOR complexes in yeast, TORC1, which is rapamycin-sensitive and regulates cell growth, translation initiation, and responses to nutrients, and TORC2, which is rapamycin-insensitive and regulates cytoskeletal remodeling (136). Inactivation of TOR signaling results in several physiological characteristics of starvation, including activation of autophagy (193). In yeast, TORC1 controls autophagy though Atg1, Atg13, and Atg17 (30, 90). Inactivation of TORC1 by rapamycin treatment or nitrogen starvation alters the phosphorylation state of Atg13, possibly facilitating an interaction with Atg1 kinase, which may induce autophagy (90).

There are two types of aging in yeast that can be used as models for higher eukaryotes: the replicative life span (RLS), which is measured by the number of daughter cells that a mother cell can produce before senescence (88), and chronological life span (CLS), which is determined by the length of time a non-dividing cell can survive (178). The yeast RLS has been suggested to be a model of aging for mitotically active cells, whereas the CLS has been modeled as post-mitotic cell aging (139). Defects in TORC1

11

signaling have been shown to increase yeast life span both replicatively and chronologically (15, 88). Long-lived animals with mutations resulting in decreased TOR signaling have also been reported in *C. elegans* (238). Decreasing TOR signaling by RNAi knockdown of TOR, *let-363/CeTor*, or the TOR accessory protein raptor, *daf-15*, extends adult life span (238). In *C. elegans*, the longevity effect of TOR deficiency is mediated by autophagy based on the finding that mutations in *bec-1*, *unc-51* (yeast Atg1 ortholog), and *atg-18* completely abolish the long-lived phenotype seen in *let-363/CeTor* RNAi-treated animals (229). In *Drosophila*, overexpression of an upstream TOR inhibitor (Tsc1-Tsc2), a downstream effector, dS6K (which may act through a feedback loop to suppress TOR), or dominant negative forms of dTOR extend life span (92). A recent study further suggests that autophagy is required for the life span extension in TOR signaling-deficient mutants (88) (Fig 1.2).

Amino acid starvation increases CLS in yeast through reduced TOR signaling (178). For instance, deletion of Gln3, a GATA transcription factor controlled by TOR, upregulates many permeases, integral membrane proteins that transport specific amino acids across the membrane, and amino acid biosynthetic enzymes. Deletion of several Gln3-regulated permease genes, such as the general amino acid permease Agp1, increases yeast CLS (178). In higher eukaryotes, decreasing cellular amino acid levels by either reducing the dietary source or reducing uptake in permease or transporter mutants also promotes longevity though reducing TOR signaling (149, 176).

Evidence supporting the interaction between TOR and insulin/IGF-1 pathways to control life span comes from genetic studies of *C. elegans* and mammalian systems (81, 238). The life span of *daf-2* nematodes is not further extended with RNAi knockdown of

let-363/CeTor. These two mutants share similar phenotypes other than life span extension. However, unlike *daf-2* animals, the life span extension of *let-363/CeTor* does not require the activity of the forkhead transcription factor DAF-16, indicating that TOR may act downstream of, or in parallel with, DAF-16 (41). In worms, the transcription of DAF-15, the Raptor-like regulatory TOR interacting partner, is inhibited by DAF-16 indicating that TOR may act downstream of DAF-16 (41, 81).

RAS/PKA

In addition to TOR, Ras/cAMP-dependent protein kinase A (PKA) also regulates autophagy in various organisms (21). The RAS/PKA pathway plays an important role in cell proliferation, stress response, and longevity (227). In yeast, in response to nutrient rich conditions, two redundant Ras GTPase, Ras1 and Ras2 (RAS), activate adenylate cyclase (encoded by the *CYR1* gene) to produce cAMP. Binding to cAMP allows the dissociation of the PKA catalytic subunits, Tpk1, Tpk2, and Tpk3 (177). In a study using a sequence-based proteomic approach to identify PKA substrates in *S. cerevisiae*, three autophagy-related proteins were identified: Atg1, Atg13, and Atg18. These proteins act at an early step of autophagy, which agrees with the observation that activation of Ras/PKA inhibits early in the process (20). Constitutive activation of PKA by depleting its regulatory subunit Bcy1 suppresses autophagy induction during nutrient-depletion and can override the inactivation of TORC1, indicating that PKA acts as a negative regulator for autophagy (20, 266). (Fig 1.2)

Mutations that result in attenuation of Ras/PKA signaling, such as in *ras2Δ*, increase both the RLS and CLS in yeast strains (45, 137). This CLS increase requires the

downstream effectors Msn2 and Msn4 (46, 244). Nutrient depletion would first activate Rim15, a glucose-responsive kinase that integrates and transduces TOR, PKA, and Sch9 signals in response to nutrients. Active Rim15 upregulates the expression of the stress-response transcription factors Msn2 and Msn4, which subsequently results in the transcription of genes involved in stress response, such as superoxide dismutase (SOD) (23). However, many studies suggest that downstream stress-response genes, such as *MSN2*, *MSN4*, and *RIM15*, are involved in extension of CLS but have opposite effects on RLS. Similarly in superoxide dismutase (SOD) mutants, the RLS is shortened. One possible explanation is that the stress-resistance genes that contribute to the CLS may affect the budding process, thus reducing the RLS (214). Ras/PKA also regulates the life span in mammals based on the observation that type 5 adenylyl cyclase knockout (CA5-KO) mice live 30% longer than their wild-type littermates (260). In the CA5-KO mice, the growth hormone level is decreased; suggesting that the insulin signaling is these mice is also decreased. Given the fact that attenuation of Ras/PKA signaling is associated with longevity, and that Ras/PKA negatively regulates autophagy, it can be speculated that the longevity effect of Ras/PKA may be mediated through autophagy. However, the link between autophagy and Ras/PKA in life span regulation still needs to be tested.

PKB/Sch9

Sch9 is a serine/threonine protein kinase and its kinase domain is homologous to yeast PKB, *C. elegans* AKT-1, AKT-2, and mammalian protein kinase B (PKB/Akt) (35, 46). Sch9 is also involved in nutrient sensing, oxidative stress resistance, and cell size control (82). PKA and Sch9 may function in parallel, and they share many targets to

control several physiological events, such as growth, cell cycle progression and glycolysis (137, 227). In yeast, similar to Ras/PKA signaling mutants, transposon insertional *sch9* mutants show CLS that is three times longer than the wild type. Life span extension in *sch9* mutants as well as mutants defective in PKA is mediated by the serine/threonine kinase Rim15 and the downstream stress resistance transcription factors Msn2/4 (244).

Sch9 is a negative regulator for autophagy. Hyperactivation of Sch9 partially suppresses autophagy when TOR is inactivated by rapamycin. Inactivation of both PKA and Sch9 without inactivating TORC1 can induce autophagy, and inactivation of all three has an additive effect indicating that these factors may, at least in part, regulate autophagy in parallel (266). Msn2/4 and Rim15 are involved in PKA- and Sch9-mediated autophagy regulation (266). Although there is no direct evidence, it is reasonable to link the longevity phenotype of PKA and Sch9 signaling-attenuated mutants with autophagy activation. Future experiments are needed to elucidate the interaction between autophagy and PKB-regulated life span extension.

PKA, Sch9, and TOR may control some cellular processes in concert. Indeed, these kinases integrate nutrient signaling and regulate cell growth (174, 194, 197). A functional interaction between the corresponding pathways has been suggested because of the overlapping downstream targets and the similar phenotypes in cells deficient in either pathway (213, 249). Additionally, these pathways, along with insulin/IGF-1 signalings, have been linked to life span regulation in diverse species as discussed above. This supports the idea that decreased activity in conserved nutrient sensing pathways extends life span, that this is a common phenomenon in diverse species, and that

autophagy may act downstream of these pathways to accomplish this beneficial effect

(178).

LKB-AMPK

AMPK functions as an energy sensor. In response to metabolic stress conditions,

AMPK activates several cellular processes to restore normal energy levels, such as

glucose uptake and glycolysis (63). AMPK functions to extend life span in *C. elegans* (6)

and to promote autophagy in human cell lines (133). Paradoxically, in *Zmpste24*-null

mice, a model of human Hutchison-Gilford progeria characterized by premature aging,

there is an extensive basal activation of autophagy due to the activation of LKB1-AMPK

and inhibition of TOR (143). It is possible that the nuclear structure abnormalities in

these progeroid mice are due to a defect in lamin A maturation, which may through an

unknown mechanism trigger a series of anti-aging responses, such as the use of

alternative metabolic pathways and the induction of autophagy activity. However, this

adaptive response is unable to compensate for the cellular defects, which then lead to the

chronic activation of autophagy. This chronic autophagic response may overcome its

beneficial anti-aging effects, resulting in premature death of the mutant mice (143).
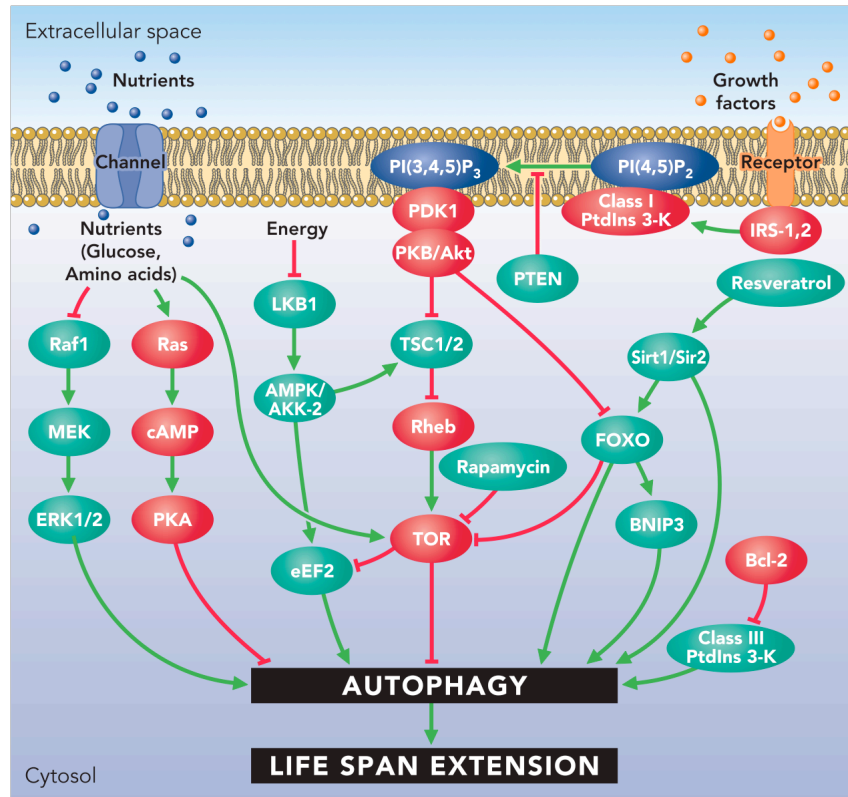
Figure 1.2. Schematic representation of signaling pathways regulating autophagy. The pink components represent the factors that inhibit autophagy, whereas the green ones represent the stimulatory factors for autophagy. The TOR signaling pathway plays a central role in autophagy regulation. In mammalian system the insulin/IGF-1 signaling pathway regulates autophagy through TOR. However, there are TOR-independent mechanisms of regulation, such as those involving Ras/PKA, Raf-1, and LKB1. The downstream transcription factor of the insulin/IGF-1 pathway, FoxO, also has been reported to activate autophagy, which is independent of TOR signaling. Sirt1/Sir2, which is activated under calorie restriction conditions, has been shown to activate autophagy and promote longevity. Please see the text for details.

Calorie Restriction

Caloric/calorie restriction (CR) refers to the limiting of dietary energy intake while maintaining essential nutrient levels. In various species, CR has been shown to extend life span, slow aging, and delay the onset of age-associated diseases, such as cancer, diabetes, neurodegeneration and cardiovascular diseases (144). For instance, CR suppresses several forms of radiation- or carcinogen-induced cancers in rodents (56). In humans, CR lowers cholesterol, blood pressure, blood glucose, and plasma insulin (69). In mice, a 30%-50% reduction of caloric intake increases the average and maximum life span 20-50% compared with *ad libitum* fed control mice (245). The beneficial effects of CR in primates are the improvement of aging biomarkers, such as blood pressure (195, 196). A study of an Okinawan population shows that CR may contribute to average and maximum life span extension and lower the risk of age-related chronic diseases (248).

How does CR work? CR causes the gene-expression profile to shift toward increasing protein turnover, damage repair, and stress response while attenuating age-associated gene induction (120, 121). Insight may come from long-lived mutants carrying mutations in conserved nutrient-responsive pathways: insulin/IGF-1, TOR, PKA, PKB/Sch9. As discussed previously, mutations that cause the attenuation of these pathways have similar effects on life span increase as that of CR. A recent study indicates that the TOR and PKB/Sch9 signaling pathways may mediate the life span regulation of CR (88, 134, 244). Removal of either asparagine or glutamate from the media induces a starvation response and increases survival through inactivation of TOR (178). Moreover,

18

CR fails to further increase yeast RLS seen in *tor* and *sch9* mutants, indicating the involvement of these two pathways in CR-mediated RLS extension (86, 88).

CR reduces plasma insulin levels; however, the involvement of the insulin/IGF-1 pathway in CR-mediated longevity remains in debate. Exposure of *daf-2* mutant worms to CR conditions further extends life span, suggesting that CR and the insulin/IGF-1 signaling pathway may function in parallel to regulate aging (72). Life span extension by reducing glycolysis requires DAF-16 (61, 124), and decreased glucose metabolism is a common feature in CR and mutants attenuated in TOR, PKA, PKB/Sch9, and insulin/IGF-1 signaling activities (41). The above result links the insulin/IGF-1 pathway to the metabolic changes associated with CR, but the connection between CR and the insulin/IGF-1 signaling pathway is more apparent in flies and mice. CR does not further extend life span in *chico* mutant flies (carrying a mutation in the insulin receptor substrate) and long-lived growth hormone receptor/GH-binding protein knockout (GHRKO) mice, indicating that the insulin/IGF-1 pathway may mediate the CR effect (16, 34, 172).

CR and Autophagy

CR may reduce the activity of TOR, PKA and PKB/Sch9 signaling, and as a result decrease protein synthesis and metabolic changes (96). Decreasing these nutrient responsive pathways may induce autophagy. Since the degree of autophagy activity is responsive to the nutrient levels, it is logical to speculate that autophagy might be induced under CR conditions (117, 153). Indeed, CR maintains autophagy activity at juvenile levels and reverses the age-related decline of autophagy activity in rat hepatocytes and cardiomyocytes (250). Some data suggest that the effects of CR in

longevity are mediated through reducing TOR activity and activation of autophagy in organisms form yeast to mammals (60, 115, 229). For example, autophagy is induced in *eat-2* (*eating-defective-2*) worms, where the function of the feeding organ has been disrupted, and show increased life span, supporting the idea that autophagy induction is coupled with CR-mediated longevity (229). The knockdown of *bec-1* and *atg7* by RNAi treatment suppresses the long-lived phenotype associated with CR. Moreover, loss of function in *bec-1* and *unc-51* (yeast *ATG1*) completely inhibit the increased longevity of the *eat-2* mutant indicating that autophagy is required for the CR-mediated longevity (229).

Sir2

In addition to the conserved nutrient sensing signaling pathways, the sirtuin gene family that functions in maintaining genome stability is also found to regulate aging, although the relationship between CR and sirtuin genes as well as their effect on aging remains controversial. The name sirtuin comes from the yeast protein silent information regulator 2 (Sir2), the first member identified in this family. Through a screen, the SIR complex was identified as a regulator for RLS (95). In yeast, Sir2 activity is required for the longevity effect of CR (57). *SIR2* encodes a histone deacetylase that was identified to be involved in silencing the mating type loci (*HML* and *HMR*), telomeres, and ribosomal DNA (rDNA) locus *RDN1* (55).The Sir2-associated RLS extension mainly occurs through suppressing the recombination of repetitive rDNA and the formation of extra-chromosomal circular forms of rDNA (55, 212). The histone deacetylase activity of Sir2 is nicotinamide adenine dinucleotide (NAD+)-dependent, which allows the regulation of

its activity depending on metabolic status and changes in the NAD+/NADH ratio. CR

may increase the NAD+ ratio, thus increasing Sir2 activity to promote longevity (228).

However, beneficial effects of CR still can occur in yeast defective in respiration (86).

The link between Sir2 and CR has been reported, although some studies are in

conflict regarding the role of Sir2 in life span extension by CR (96). In the case of yeast,

Sir2 activity correlates with yeast RLS under CR conditions. Deletion of *SIR2* shortens

the yeast RLS, whereas elevation of its activity leads to longevity (87, 134). However,

Sir2 shortens the CLS (44). Overexpression of Sir2 in worms (*sir-2.1*) extends life span

by up to 50%. Sir-2.1 functions upstream of DAF-16 in the insulin/IGF-1 signaling

pathway (228). In adult worms, complete starvation increases life span to a greater extent

than CR. This type of life span extension is independent of insulin/IGF-1 signaling and

Sir-2.1 (60). *Drosophila* Sir2 (dSir2) is required for the life span-extension effect of CR

(192). In Sirt1 (mammalian Sir2 orthologue) knockout mice, the physiological and

behavioral pattern associated with CR does not occur, suggesting that Sirt1 mediates the

effects of CR (27). The Sirt1 activator resveratrol activates Sirt1 and extends life span in

mice fed with a high-calorie diet and in fish (10, 233). Furthermore, Sirt1 activates fatty

acid mobilization from white adipocytes under CR in 3T3-L1 adipocytes. Upregulation of

Sirt1 stimulates lipolysis and reduction in fat, which is sufficient to extend life span in

mice (175). On the other hand, results in some types of mammalian cells and tissues

suggest that Sirt1 might accelerate aging. Sirt1$^{-/-}$ mice embryonic fibroblasts (MEFs)

extend replicative life span that is correlated with increasing proliferative capacity under

oxidative stress (31). Evidence also suggests that Sir2/Sirt1 is part of the regulation loop

in the insulin/IGF-1 pathway. Forkhead transcription factors are targets of Sir2, and in

worms Sir2 modulates the activity of DAF-16 (228) (Fig 1.2). Similarly, mammalian

Sirt1 deacetylates FoxO transcription factors (19, 38). Moreover, Sirt1 represses IGF

binding protein 1 expression. Sirt1-null mice have increased production of IGF binding

protein 1 and show several phenotypes correlated with long life span (129). In addition to

Sirt1, among seven mammalian Sir2 homologs, some may have similar functions to Sir2.

For instance, Sirt6 binds to chromatin and suppresses genome instability by enhancing

resistance to DNA damage, and Sirt6 knockout mice show accelerated aging phenotypes

and age-associated pathology (157).

A recent study demonstrates the ability of Sirt1 to induce autophagy.

Overexpression of Sirt1 induces autophagy in both normal growth and starvation

conditions, but not in the dominant negative *sirt1* mutant, suggesting that Sirt1 alone is

sufficient to induce autophagy even in the presence of nutrients (122). Atg5, Atg7, and

Atg8 are acetylated by Sirt1 in an NAD^+-dependent manner and the acetylation levels are

reduced under starvation conditions, suggesting that Sirt1 can adjust autophagy activity to

match the metabolic status (122). In *sirt1*$^{-/-}$ mice, embryonic heart tissues and neonatal

tissues within the first 3 h after birth show increased p62 levels, which serves as an *in*

vivo marker for impaired autophagy (13, 122). Some phenotypes of *sirt1*$^{-/-}$ closely

resemble *atg5*$^{-/-}$ mice, such as the accumulation of abnormally shaped mitochondria, early

mortality, and abnormality of energy-responsive pathways (117, 122). Moreover,

mammalian Sirt1 has a cellular protective role against certain forms of neurodegeneration

(7). Enhanced Sirt1 might mimic CR conditions to induce autophagy, which then

promotes damaged protein and organelle removal to protect against age-related diseases.

Future studies are needed to elucidate the link between sirtuin-mediated life span

extension and the regulation of autophagy.

ROS, Mitochondria, Aging, and Autophagy

Mitochondria and aging

Accumulation of mitochondrial DNA (mtDNA) mutations as well as a decline in mitochondrial function is a common feature in aging cells (243). Studies performed in humans reveal a decline of ATP production with age (210). Similarly, some age-related diseases are associated with mitochondrial alterations. For instance, hearing loss in aged animals is associated with mitochondrial dysfunction and mtDNA mutations (259). Mitochondria are the primary source, and a target, of reactive oxygen species (ROS) and the production of ROS is proposed to play an important role in aging (65). The mitochondria theory of aging, a variant of the free radical theory of aging, proposes that ROS production during respiration causes accumulation of oxidative damage in mitochondria and mtDNA, which would eventually lead to aging and death (65). Electron leakage at the electron transport chain (ETC) during respiration, through both detoxification enzymes and non-enzymatic reactions, can generate ROS. ROS cause oxidative damage to mtDNA and inhibition of the ETC, resulting in even higher levels of ROS production. This "vicious cycle" in the end leads to cellular function decline and aging (3).

According to the mitochondria theory of aging, one would assume that the rate of aging would correlate with the ROS level produced at mitochondria. Additionally, reducing ROS production or decreasing respiration might retard the aging process. Nevertheless, evidence both supports and contradicts the ROS theory of aging as shown in Table 1.1 and Table 1.2. Furthermore, respiration rate and ROS production are not proportional to each other. Instead, ROS production is determined by the state of the ETC

24

(243). For example, in long-lived fly mutants expressing human uncoupling protein

UCP2 in mitochondria of fly neurons there is increased respiration, enhanced oxidative

stress resistance, and decreased ROS production (52). Life span extension is observed in

mutants displaying both increased and decreased respiration, and mild increases in ROS

are seen in long-lived mutant flies and worms with partial disruption of the mitochondrial

ETC (150, 180).

Table 1.1 Evidence to support the ROS theory of aging

Organism	Experimental Finding	Reference
Yeast	Long-lived mutants with down regulation of the RAS/PKA pathway show increasing SOD2 expression	(173)
	tor1 mutant with CLS extension has high respiration rate, low ROS production	(15)
C. elegans	Long-lived *daf-2* animals show increasing MnSOD level	(71)
	Catalase is required for life span extension in *daf-C* and *clk-1* mutants	(225)
	gas-1 with mutation in subunit of complex I has increased ROS level and is short-lived	(94)
	isp-1 has increasing SOD-3 mRNA level	(49)
	Overexpression of Cu-ZnSOD and catalase extend life span	(168, 171)
Drosophila	Long-lived *mth* mutants increase resistance to oxidative stress	(135)
	clk-1 is long-lived with reduced ROS production	(48)
	Short-lived *mev-1* has increased superoxide anion and higher nuclear DNA damage and mutations	(79, 204)
	Overexpression of CuSOD extends mean life span up to 48%	(220)
	Overexpression of MnSOD extends mean life span up to 37%	(219)
	p66^{shc} mice show increased oxidative stress resistance and longevity	(147)
Mouse	Heterozygous mclk1 (orthologue of clk-1) mice display increased life span	(130)

Table 1.2   Evidence contradicting the ROS theory of aging

Organism	Experimental Finding	Reference
Drosophila	Overexpression of mitochondrial adenine nucleotide translocase (ANT) has lower membrane potential and ROS production but no effect on life span	(150)
	Simultaneous overexpression of both MnSOD and catalase ectopically targeted to mitochondrial matrix results in decreased H_2O_2 release and increased oxidative stress but is short-lived	(11)
	Feeding SOD mimetic drug (exogenous antioxidant) can rescue the pathology associated with oxidative damage, but fails to extend life span	(140)
	Overexpression of CuSOD, MnSOD or thioredoxin has no effect on life span extension	(169, 205)
Mice	Homozygous transgenic mice with a 2 to 5-fold elevation of Cu/ZnSOD in various tissues have reduced life span; hemizygous mice with 1.5 to 3-fold increase in Cu-ZnSOD have no effect on life span	(74)
	Heterozygous null mutation of SOD2 (MnSOD) shows no difference in mean or maximum life span and no aging biomarker accumulation	(234)
	Long-lived naked mole-rats (NMRs) have similar MnSOD, catalase and glutathione peroxidase (cGPx) with physiologically equivalent age-matched CB6F1 mice. They appear to have high level of oxidative damage even at a young age	(4)
Honey bee	Longevity of queen honey bee is involved in other mechanisms than increased antioxidant gene expression	(33)

A class of long-lived mutants, Mit, in *C. elegans* paradoxically display

mitochondrial dysfunction, and most of the affected genes encode components of the

ETC (5, 125, 158). The mechanism attributed to the life span extension has been the

subject of intense study. The life span of long-lived respiration-defective nematodes is

further increased by a mutation attenuating the insulin/IGF-1 pathway (40). This additive

effect on life span extension suggests that the insulin/IGF-1 signaling pathway and

mitochondrial respiration machinery function in parallel in life span regulation. Several

hypotheses have been proposed to explain the possible metabolic strategies that could

account for the long life span. One of the intriguing hypotheses is that autophagy is

required for longevity of Mit mutants (239). In long-lived mitochondrial respiration

mutants, *atp-3* (ATP-synthase-3), which encodes a subunit of the mitochondrial ATP-

synthase (239), and *clk-1* (clock abnormal-1), defective in ubiquinone synthesis (48, 158),

additional knockdown of autophagy genes, such as *unc-51*, *bec-1* or *atg18*, suppresses the

life span (229). This demonstration suggests that the life span regulation that corresponds

with the mitochondrial respiration system is mediated by autophagy.

Mitochondria and autophagy

Mitochondrial dysfunction leads to changes in membrane potential, ROS

production, ATP production, and Ca^{2+} homeostasis. In response to these changes, cells

induce compensatory pathways, including autophagy (99, 239). This preferential

degradation of damaged mitochondria before inducing apoptotic cell death is believed to

be either a mechanism for mitochondrial quality control and/or an important

cytoprotective response (99, 163). It is suggested that mitochondrial ROS production acts

as a redox signal to regulate autophagy (199). Although ROS-dependent oxidative damages are associated with age-related disorders, at low concentration ROS function as signaling molecules in a number of biological processes, such as defense against invasion of microorganisms, and cell growth (22). ROS damage may induce mitochondrial permeability transition (MPT) and provide a signal leading to induction of autophagy (191). Accumulating evidence suggests that the outcomes of autophagy induction, including those mediated by ROS, can either promote cell survival or may be associated with cell death (151). In the latter case, however, it may be that the autophagic response was insufficient to prevent cell death, which thus occurs with "autophagic features".

ROS formation following starvation, rapamycin treatment or ischemia/reperfusion conditions is essential for autophagy induction (28, 145, 199). Several studies suggest that ROS act as a positive signal to regulate autophagy. A recent finding shows that ROS are required to induce autophagy under starvation conditions, and treatment with antioxidative agents abolish the subsequent autophagosome formation (199). Nutrient starvation leads to mitochondrial H_2O_2 accumulation partially through a class III PtdIns3K. A direct target for oxidation by H_2O_2 is Atg4, a protease essential for autophagy. Oxidation of this protein leads to inhibition of its deconjugation activity (199), which allows the accumulation of phosphatidylethanolamine-conjugated Atg8 on the autophagosome membrane, an important step in autophagosome formation (256). Based on this observation, a model for the regulation of Atg4 activity is that the H_2O_2 generated from mitochondria forms a gradient which results in a corresponding gradient of Atg4 activity; Atg4 closer to the mitochondria is less active compared with Atg4 further away in the cytosol, thus regulating the status of Atg8 lipidation and autophagosome formation

29

(198). Additionally, ROS generation and mitochondrial lipid peroxidation are suggested to induce mitophagy (107, 108).

Treatment with the caspase inhibitor zVAD promotes necrotic cell death when induced by lipopolysaccharides or cell death ligands (240, 257). Autophagy is induced in macrophages challenged with lipopolysaccharides when caspase activation is inhibited. ROS production is increased in these macrophages, and the induction of autophagy results in caspase-independent cell death (257). It is possible that, in this event, ROS might be involved in autophagy induction, because superoxide treatment results in cell death with autophagic features in these same cells. In another cell line, murine L929 fibrosarcoma, a similar event occurs when caspases are inhibited by zVAD (268). Unexpectedly, catalase is selectively degraded by autophagy upon zVAD treatment, leading to ROS accumulation in mitochondria, and ultimately cell death (269). In contrast, a recent finding suggests that autophagy plays a protective role preventing zVAD-induced cell death in L929 cells (252). In this study, autophagy induced by rapamycin or serum deprivation protects against z-VAD-induced cell death. In addition to caspase inhibition, zVAD is able to inhibit lysosomal cathepsin and calpain activities, which are required for autophagy in mammalian cells (39). The cell death reported previously might be due to the block of autophagy at a late stage through inhibition of calpain and/or other additional unknown effects of zVAD (252).

Mitochondrial dysfunction can be induced by mitochondrial ETC inhibitors. For instance, the ETC complex I and II inhibitors, rotenone and TTFA, induce cell death with autophagic features in transformed/cancer cell lines through ROS production (27). In contrast, the same ETC inhibitors fail to induce ROS generation and cell death with

autophagic features in non-transformed primary mouse astrocytes (27), suggesting that induction of autophagic cell death may be a strategy for cancer treatment especially for those tumors where the cells are resistant to apoptosis. Indeed, several antitumor drugs may rely on this approach to kill cancer cells. For instance, an anti-cancer drug currently in phase II clinical trials, FK866, which targets a NAD biosynthesis enzyme to deplete intracellular NAD, is able to induce autophagic cell death in neuroblastoma (10, 11, 65, 67). Additionally, sodium selenite was demonstrated to induce cell death in several types of cancer through cell death with autophagic features, including malignant gliomas, which are resistant to apoptotic therapies. Sodium selenite can cause mitochondrial membrane potential collapse, high superoxide anion generation, and induction of mitophagy (88). This cell death was blocked by overexpression of Cu-ZnSOD or MnSOD but not catalase. The fact that superoxide generator treatment alone is sufficient to induce autophagic cell death in gliomas (88) supports the idea that mitochondria could regulate autophagy through ROS production.

The antitumor effect of another chemical, arsenic trioxide (As_2O_3) has been shown through upregulating BNIP3 and induced autophagic cell death in malignant glioma cells (83). BNIP3 is a BH3 domain-containing pro-apoptotic Bcl-2 family protein. Augmentation of the levels of either BNIP3 or another BH3 domain-containing pro-apoptotic protein, Bax, induces autophagic cell death (192). Autophagic cell death induced by overexpression of BNIP3 or Bax is dependent on the MPT and ROS accumulation (192). All together, these data suggest that through ROS generation mitochondria regulate autophagy activity. Autophagy and mitophagy induction may contribute to both cell survival and cell death; however, it is not clear what factors lead to

which fate. Understanding the mechanisms that underlie the decision for life or death mediated by autophagy would provide potential therapeutic value in treatments for cancer as well as mitochondrial-associated disease. Finally, it is important to note in some of the above situations that, although we refer to autophagic cell death, it has generally not been determined whether cell death is actually due to autophagy, and if so these situations are generally non-physiological in that they rely on various inhibitors and/or the absence of apoptosis.

Mitophagy

Mitochondria are degraded through autophagy and can be detected within double-membrane cytosolic vesicles (181). However, there have been some questions as to whether a selective form of mitochondrial degradation (mitophagy) actually occurs. The evidence for selective mitophagy comes primarily form yeast. A mitochondrial outer membrane protein, Uth1, and Aup1, a mitochondrial intermembrane space phosphatase related to mammalian PP2C, are apparently required for specific delivery of mitochondria into the yeast lysosome analog, the vacuole (22, 92, 182), although more recent data cast doubt upon these findings (271). Serum withdrawal promotes mitophagy of dysfunctional mitochondria or those with mtDNA mutations but spares the normal organelles in mammalian cells (56). Direct experimental evidence comes from the selective removal of depolarized mitochondria after laser-induced photodamage in living hepatocytes (100).

"Giant" mitochondria are commonly observed in aged cells, especially in long-lived post-mitotic cells, such as cardiomyocytes and skeletal muscle fibers (46). Elimination of dysfunctional mitochondria through mitophagy is proposed to retard aging

(56). These senescent mitochondria are often enlarged with mtDNA mutations and protein alterations due to oxidative damage accompanied by a lack of turnover. Through fusion and fission, mitochondria can complement the damaged unit by exchange of content and restore their function, which is thought to be a defense mechanism against mitochondrial dysfunction (144). However, depolarized mitochondria fail to undergo fusion and fission events and are targeted for autophagic elimination (189). Interestingly, inhibition of autophagy results in a lower inner membrane potential, which blocks mitochondria fusion, thus increasing the giant mitochondria accumulated in rat myoblasts and human fibroblasts (140). These findings imply that mitochondria removal by autophagy is a key mechanism for quality control.

What is the reason for the failure in mitochondria turnover in aged cells? One explanation is the age-associated decline in mitophagy (126). The decreasing autophagy activity may provide a cellular environment allowing the accumulation of dysfunctional mitochondria. This idea is supported by the ability of anti-lipolytic agents, which mimic nutrient starvation, to stimulate autophagy, to rescue aging cells from the accumulation of dysfunctional mitochondria in rat liver (23, 43). Additionally, injection of anti-lipolytic agents in mice has an anti-aging effect by decreasing plasma insulin, free fatty acids, and glucose, and increasing autophagic activity *in vivo* (44). Another possibility is that some dysfunctional mitochondria fail to be recognized by the autophagy machinery and thereby accumulate with age (110).

What signals induce mitophagy for mitochondrial turnover? Some evidence suggests that the mitochondrial permeability transition caused by ROS damage initiates mitophagy as discussed above. Along this line, certain mtDNA mutations may make the

33

organelle less prone to mitophagy degradation because the respiration defect leads to a decrease in ROS production and less oxidative damage, which might result in a decrease in the recognition signals for mitophagy (109). The MPT describes the phenomenon of the opening of nonspecific high-conductance permeability transition pores in the mitochondrial inner membrane. It is proposed that ROS cause oxidative damage to mitochondrial membrane proteins or mtDNA mutation resulting in abnormal protein synthesis, which then leads to defects in protein folding, aggregate formation, and the formation of nonspecific aqueous pores (109, 110). The opening of the pores leads to the MPT and may induce autophagy (113). At low concentration, ROS may cause mild oxidative damage and the MPT, inducing both autophagy and mitophagy and promoting cell survival (131). One example is the starvation-induced mitophagy in rat hepatocytes, which is mediated by the MPT (45). Another example suggests that mitophagy is an adaptive response that promotes cell survival by preventing ROS generation and maintaining redox homeostasis. In response to hypoxic conditions, the increasing generation of ROS by mitochondria is necessary to activate the transcription factor, hypoxia-inducible factor 1 (HIF-1) (58). HIF-1 then induces BNIP3 expression and subsequent mitophagy induction (171). BNIP3 augmentation could increase the free Beclin 1 level for autophagy induction by competing for binding to Bcl-2 (215), which inhibits autophagy by directly interacting with Beclin 1 (150) (Fig. 1.3). Similar phenomena are also observed in lungs and the lung epithelial cells of mice (215). Moreover, mitophagy also plays an essential role during development. For example, the complete elimination of mitochondria by mitophagy is required for the maturation of reticulocytes. A recent study shows that BNIP3L (NIX) is required for selective

sequestration of mitochondria into autophagosomes (165, 169). Similarly, BNIP3L is also involved in mitophagy during terminal erythroid differentiation. BNIP3L knockout mice develop anemia and show mitochondrial retention, and the red blood cells have a shorter life span *in vivo* (615). Both BNIP3 and BNIP3L are able to induce mitochondrial depolarization, cytochrome *c* release, and apoptosis when overexpressed (25, 26, 73). However, BNIP3L-mediated mitophagy in reticulocytes may not depend on mitochondrial depolarization since it is independent of Bax or Bak and is not blocked by an MPT inhibitor (165, 169).

Mitophagy can be induced when apoptosis is blocked. As mentioned above, in various transformed cells that are apoptosis deficient or upon inhibition of caspase activities, mitophagy induction results in cell death (28, 42). Among those cases, ROS generation plays a role in mitophagy induction. It is proposed that the ROS level can control the balance between life and death (20). Additionally, the extent of MPT resulting form oxidative damage may lead to different cellular responses, including autophagy, apoptosis, and necrosis as shown in Fig.1.3 (89, 109). At a low concentration of ROS, the stress level is just enough to lead to MPT; autophagy and mitophagy may be induced as a repair system for damaged mitochondrial removal. As the oxidative damage increases, mitochondria may no longer release factors that promote cell survival, and instead molecules that trigger apoptosis may leak out. Last, since the extreme oxidative stress causes severe MPT, neither autophagy nor apoptosis can progress due to ATP depletion. Thus, necrosis may take place. Whether autophagy/mitophagy leads to survival or contributes to death probably depends on the severity of mitochondrial damage, the

35

length of ROS exposure, or whether the autophagy machinery is overwhelmed by the
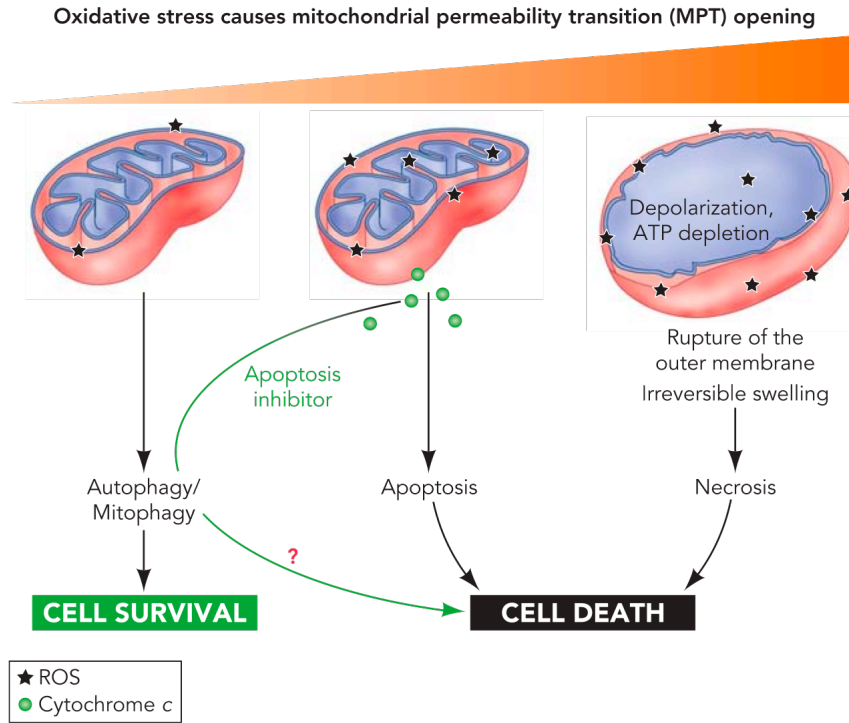
organelle damage.

Figure 1.3. Pathways activated in response to different degrees of oxidative stress. When the low oxidative stress is just enough to lead to the MPT, autophagy and mitophagy may be induced. As the oxidative damage increases, molecules such as cytochrome c may be released from mitochondria and trigger apoptosis. At the extreme, oxidative stress causes severe MPT or even the rutpture of the mitochondrial membrane, and neither autophagy nor apoptosis can provide adequate responses. Thus, necrosis may be induced. Under certain nonphysiological settings, where apoptosis is absent or inhibited, autophagic cell death may be induced. However, in this kind of cell death with autophagic features, it has generally not been determined whether cell death is actually due to autophagy or whether it still occurs despite the cytoprotective attempts of the induced autophagy pathway.

Concluding remarks

Autophagy is a major mechanism for the removal of damaged cellular structures and is critical to maintain cell survival. As demonstrated by various studies, autophagy genes are important for long-term viability. Signaling pathways that involve components such as insulin/IGF-1, TOR, PKA, and/or PKB, as well as dietary restriction are important for life span regulation. Autophagy induction in response to these signals may promote the removal of damaged proteins or organelles and maintain proper metabolism, which is crucial for cell survival (94).

Mitochondria play an important role in aging and regulate autophagy through ROS generation and the MPT (131). Autophagy induction signaled from mitochondria can result in enhanced survival or may possibly contribute to cell death. Uncovering the molecular mechanisms underlying autophagic regulation may help us to manipulate autophagy for therapeutic purposes.

CHAPTER 2

Atg27 Is Required for Autophagy-dependent Cycling of Atg9

Abstract

Autophagy is a catabolic pathway for the degradation of cytosolic proteins or organelles and is conserved among all eukaryotic cells. The hallmark of autophagy is the formation of double-membrane cytosolic vesicles, termed autophagosomes, which sequester cytoplasm; however, the mechanism of vesicle formation and the membrane sources remain unclear. In the yeast *Saccharomyces cerevisiae*, selective autophagy mediates the delivery of specific cargo to the vacuole, the analog of the mammalian lysosome. The transmembrane protein Atg9 cycles between mitochondria and the phagophore assembly site (PAS), which is the site of autophagosome biogenesis. Atg9 is thought to mediate the delivery of membrane to the forming autophagosome. Here, we characterize a second transmembrane protein, Atg27, which is required for specific autophagy in yeast. Atg27 is required for Atg9 cycling and shuttles between the PAS, mitochondria, and the Golgi complex. These data support a hypothesis that multiple membrane sources supply the lipids needed for autophagosome formation.

Introduction

Cell must be able to respond to changes in the environment. One process that cells use to respond to internal or external stress is autophagy. Autophagy is a degradative process responsible for the rapid degradation of damaged or unnecessary organelles and cytosol in the lysosome/vacuole (181). In addition, autophagy is involved in cellular remodeling, development, and aging and also plays a role in preventing a range of diseases including some types of cancer and neurodegeneration (131, 208). Autophagy is conserved among all eukaryotic cells. The hallmark of the autophagic process is the sequestration of cytoplasm into a double-membrane vesicle called the autophagosome, which then docks and fuses with the lysosome/vacuole, releasing the inner vesicle into the lysosome/vacuole lumen for degradation (181).

Autophagy can be a selective or a nonselective process. Studies in the yeast *Saccharomyces cerevisiae* have provided two examples of selective autophagy that morphologically and mechanistically overlap with non-selective autophagy. First when cells are shifted from growth on oleic acid, a condition in which peroxisomes are essential, to a preferred carbon source, the now superfluous peroxisomes are selectively degraded by a mechanism termed pexophagy (43). Another example is seen with import of the resident vacuolar hydrolase, amminopeptidase I (Ape1), which is targeted to the vacuole through the cytoplasm to vacuole targeting (Cvt) pathway. Both the Cvt pathway and pexophagy are examples of specific autophagy where the cargo, precursor Ape1 (prApe1), or peroxisomes are enwrapped in double-membrane vesicles and then transported from the cytosol directly to the vacuole lumen. In contrast to autophagy,

which is induced by starvation, the Cvt pathway is biosynthetic and is constitutive in vegetative conditions.

More than 25 novel AuTophaGy-related (*ATG*) genes in the yeast *S. cerevisiae* have been identified through genetic screens of yeast mutants blocked in one of these pathways (111). Studies of Atg components have provided some insight into the molecular basis for the autophagy process; however, there are many questions that remain to be addressed. One of the most intriguing questions is the origin of the membrane for the double-membrane Cvt vesicles or autophagosomes. Recent data suggest that Atg9 may mark the membrane that is donated to the forming sequestering vesicles (161, 186). Atg9 localizes to mitochondria and cycles between this compartment and the phagophore assembly site (PAS), the site of organization for Cvt vesicle and autophagosome formation (230). Recently, we showed that Atg23 and the actin cytoskeleton are needed for anterograde delivery of Atg9 to the PAS, whereas Atg1, Atg13, Atg2, Atg18, and the phophatidylinositol (PtdIns) 3-kinase, Vps34, are required for retrograde movement (183, 186). Here, we show that Atg27 is another transmembrane protein required for Atg9 cycling. The localization and transit pattern of the Atg27 protein is similar to that of Atg9 and is dependent on the latter protein. Atg27, originally named Etf1, was identified as a PtdIns(3) phosphate-binding protein that is a downstream effector of Vps34 (254). Because of the correction of a sequencing error in the *Saccharomyces* Genome Database, the true full-length Atg27 contains 75 additional amino acids at the N terminus relative to Etf1. We discovered that Atg27 is a type I transmembrane protein with an N-terminal signal sequence, resulting in a topology

opposite to that reported to Etf1. Atg27 function is required for specific types of

autophagy and for efficient bulk autophagy.

Results

Atg27 Contains an N-terminal Signal Sequence

We identified *atg27Δ* in a screen for mutants defective in the processing of the Cvt pathway cargo protein precursor aminopeptidase I (prApe1; and our unpublished results). The *ETF1* gene was simultaneously identified in a screen based on a missorting phenotype that was synthetic with a *vsp34^{ts}* mutant (254); however, the subsequent analysis of *ETF1* and its gene product were influenced by a sequencing error originally present in the *Saccharomyces* Genome Database. *ETF1* is allelic with *ATG27*, and the corrected full-length Atg27 protein is predicted to contain a signal sequence at the N terminus, based on the SignalP program (http://www.cbs.dtu.dk/services/SignalP). If the additional amino acids at the N terminus function as an authentic signal sequence, it would likely result in a membrane topology different from that published previously. Accordingly, we undertook a careful analysis of Atg27 biosynthesis.

There are three possible models of Atg27 topology (Fig. 2.1A). In model I, Atg27 has no signal peptide; with only a single transmembrane domain, Atg27 is in a type II orientation, in agreement with the prediction reported previously (254). The correct full-length Atg27 with an N-terminal signal sequence is shown in model II and III. In model II, the signal sequence of Atg27 is not cleaved, resulting in a protein with two transmembrane domains; both the N and C termini of Atg27 face the cytosol. In contrast, if model III is correct, the signal sequence of Atg27 is cleaved giving a type I membrane protein topology.

To distinguish among these models, we performed a protease protection assay (Fig. 2.1B). Yeast spheroplasts were osmotically lysed under conditions that retain the integrity of subcellular compartments and separated into supernatant and pellet fractions, and the pellet fractions were treated with exogenous protease. To monitor Atg27, we tagged the C terminus with the HA epitope; the resulting protein was functional (data not shown). As a control, we followed the cleavage of the vacuole membrane protein Pho8 in a *pep4Δ* strain, which is defective in the removal of the C-terminal propeptide. Pho8 was found only in the pellet fraction, indicating efficient separation of the cytosol from the membrane. The cytosolic tail of Pho8 was protease-accessible in the absence of Triton X-100, whereas the lumenally-oriented propeptide was cleaved only when the vacuolar membrane was solubilized by detergent, verifying that the vacuole, and presumably other osmotically sensitive compartments, were intact after spheroplast lysis. Atg27 was found in the P13 fraction as expected for a membrane-associated protein (Fig. 2.1B); however, the C-terminal HA tag of Atg27 was cleaved by protease both in the absence and the presence of detergent. This result suggested that the C terminus of Atg27 faced the cytosol, ruling out the topology predicted by model I.

To test the functionality of the Atg27 signal sequence, we performed an assay for invertase secretion. Invertase lacking its native signal sequence remains in the cytosol, whereas replacement with an endogenous signal sequence restores secretion to the preiplasm (110). We constructed an *ATG27-SUC2* fusion (A27I-28) containing the amino-terminal 28 amino acids of Atg27 fused to invertase lacking its endogenous signal sequence. As controls, we examined two previously characterized Pep4-invertase chimeras. P4I-23 and P4I-137 contain the Pep4 signal sequence (23 amino acids) and N-

terminal propeptide including the vacuolar targeting sequence (137 amino acids),

respectively (110). The P4I-23 chimeric protein was efficiently secreted into the

periplasmic space, whereas P4I-137 was efficiently retained within the cell, in agreement

with previous data (Fig. 2.1C). To have a comparable expression level with controls, an

overexpressed A27I-28 construct was used in this experiment; expression from the

endogenous *ATG27* promoter was below a practical level of detection by this assay. The

yeast strain expressing A27I-28 exhibited almost complete secretion of invertase activity

(Fig. 2.1C). After normalizing to the vector control, 95% of the invertase activity was

secreted with the A27I-28 chimera, suggesting that the N-terminal 28 amino acids can

function as a signal sequence.

To determine whether the N-terminal signal sequence of Atg27 is cleaved, we

used a molecular genetic approach. According to the SignalP program, there is a signal

sequence cleavage site between alanine at position 19 and leucine at position 20 in Atg27.

A proline residue at the -3 amino acid position would disrupt recognition of the signal

sequence cleavage site (242). We replaced the valine with a proline residue at the -3

position, creating Atg27^{V17P}, and examined the effect on signal sequence cleavage. In the

case of model II in which the signal sequence of Atg27 is not cleaved, the wild-type

Atg27 and Atg27^{V17P} would show a similar mobility after SDS-PAGE; however, if the

signal sequence is normally cleaved as shown in model III, Atg27^{V17P} would be ~2 kDa

larger than the wild-type Atg27. Protein extracts were prepared from cells expressing

Atg27-HA and Atg27^{V17P}-HA, and the position of Atg27 was monitored by western blot.

The molecular mass of Atg27^{V17P} was ~2 kDa larger than that of wild-type Atg27 (Fig.

2.1D), suggesting that the predicted cleavage site was disrupted by the V17P mutation.

These data suggest that Atg27 contains a signal sequence that is cleaved in normal cellular conditions.

As a final assessment of the functionality of the Atg27 putative signal sequence we examined the Atg27 topology by introducing a glycosylation site in the predicted lumenal region; Atg27 lacks endogenous glycosylation sites. Accordingly, glycosylation would confirm that the introduced sites had gained access to the lumen of the endoplasmic reticulum (ER). We introduced a canonical Asn-X-Thr N-linked glycosylation site by mutating glycine at position 105 to asparagine in the HA-tagged Atg27 plasmid. *atg27*Δ cells expressing Atg27^{G105N} were grown to early log phase and harvested, and cellular proteins were evaluated by western blot using an antibody against HA. Atg27^{G105N}-HA showed a slower mobility after SDS-PAGE compared with wild-type Atg27-HA (Fig. 2.1E). The shift in molecular mass corresponded to ~2-3 kDa, which would fit with the increase expected from the addition of a single glycosyl side chain. To confirm that the change in migration was due to glycosylation, we treated the lysate with endoglycosidase H. After endoglycosidase H treatment, the mobility of Atg27^{G105N}-HA was restored to that of wild-type Atg27-HA. As a control, Prc1 (carboxypeptidase Y, a vacuolar hydrolase known to be glycosylated) was examined from the same cell lysates and showed similar results indicating that the molecular mass shift of Atg27^{G105N} was due to the addition of sugar molecules. These results suggested that the major soluble domain of Atg27 translocated into the ER lumen. Taken together, these data indicate that Atg27 is a type I transmembrane protein with an N-terminal signal sequence. This topology is the opposite of that predicted from the previous studies (254).
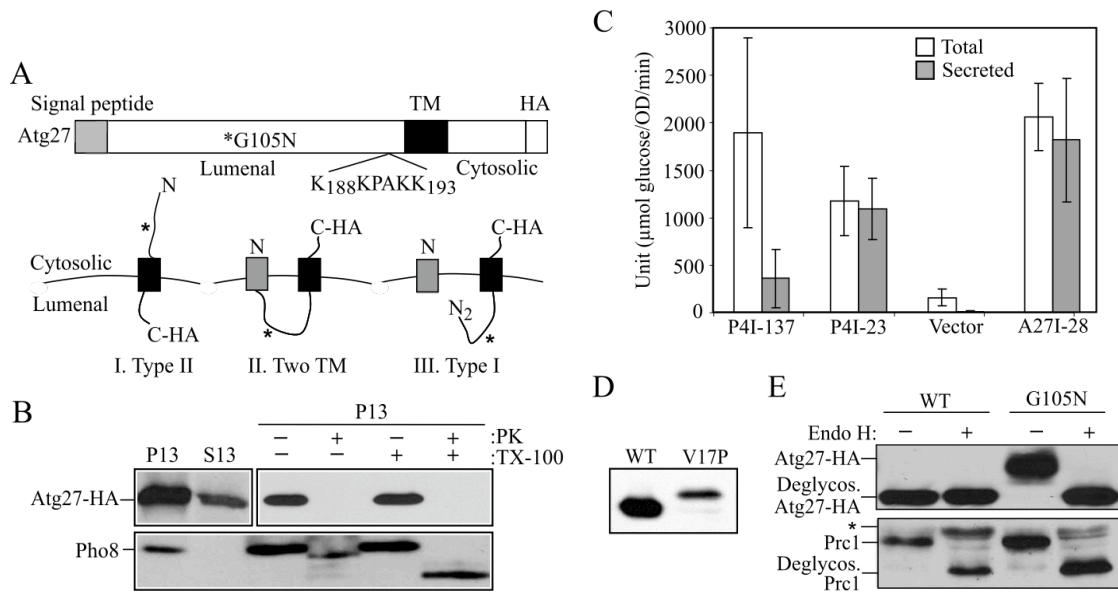
Figure 2.1. Atg27 is a type I transmembrane protein. (A) Schematic drawing of full-length Atg27. The full-length Atg27 protein contains 271 amino acids. Analysis of the primary amino acid sequence using the SignlP program indicates that Atg27 has a signal sequence (residue 1-19) and a transmembrane (TM) region (residues 199-122) according to TMHMM-prediction of helices in proteins (http://www.cbs.dtu.dk/services/TMHMM-2.0/), in a type I membrane topology. The putative PtdIns(3)phosphate-binding site (residues 188-193, KKPAKK) from the previous report (254) is indicated. Three possible membrane topologies for Atg27 are shown: I, type II transmembrane orientation; II, two transmembrane domains; and III, type I transmembrane protein. The asterisk marks the mutation introduced to replace glycine at position 105 with asparagine, creating a glycosylation site. (B) The C terminus of Atg27 is exposed to the cytosol. Atg27-HA (WLY1) and *pep4Δ* (TVY1) cells were converted into spheroplasts and then osmotically lysed. The cell lysates were centrifuged at 13,000 x g for 10 min to generate the pellet (P13) and supernatant (S13) fractions. The P13 fractions then were resuspended and subjected to treatment with 1% Triton X-100, proteinase K, both or neither on ice for 30 min. The lysates were then TCA-precipitated and analyzed by SDS-PAGE and western blot. (C) The N-terminal 28 amino acids of Atg27 are able to direct invertase secretion. Cells expressing invertase fusion proteins (P4I-137, P4I-23, empty vector [pSEYC306], or A27I-28) were grown to early log phase. The cells were collected and subjected to an invertase activity assay as described in Materials and Methods. (D) The signal sequence of Atg27 is cleaved. Cells expressing Atg27-HA (WT) or Atg27^{V17P}-HA (V17P) from the pAtg27-3xHA(416) or pAtg27^{V17P}-3xHA(416) plasmids were grown to early log phase. The protein extracts were analyzed by western blot and probed with monoclonal anti-HA antibody. (E) The lumenal region of Atg27 translocates into the ER. Cells expressing Atg27-HA (WT) and Atg27^{G105N}-HA (G105N) were grown to early log phase. The cell lysates were subjected to endoglycosidase H treatment as described in Materials and Methods. After resolution by SDS-PAGE, the samples were analyzed by western blot and probed with antibodies against Prc1 and HA, separately. The positions of glycosylated and deglycosylated forms of both proteins are indicated. The asterisk indicates cross-reacting bands.

Table 2.1. Yeast strains used in this study.

Strain	Genotype	Source or reference
SEY6210	*MATα ura3-52 leu2-3,112 his3-Δ200 trp1-Δ901 lys2-801 suc2-Δ9 mel GAL*	(190)
PJ69-4A	*MATα leu2-3,112 trp1-Δ901 ura3-52 his3-Δ200 gal4Δ gal80Δ LYS2::GAL1-HIS3 GAL2-ADE2 met2::GAL7-lacZ*	(80)
BY4742	*MATα his3Δ leu2Δ lys2Δ ura3Δ*	ResGen™
atg1Δ	BY4742; *atg1Δ::KAN*	ResGen™
FRY143	SEY6210; *pep4Δ::LEU2 vps4Δ::TRP1*	(30)
IRA001	BY4742; *PEX14-GFP::HIS3*	(183)
IRA002	BY4742; *PEX14-GFP::HIS3 atg1Δ::URA K.l*	(183)
JHY28	SEY6210; *pep4Δ::LEU2 vps4 Δ::TRP1 atg1Δ::HIS5 S.p.*	This study
JLY43	SEY6210; *ATG9-GFP::KAN atg27Δ::HIS5 S.p.*	This study
JLY44	SEY4210; *ATG9-GFP::HIS5 S.p.*	This study
JLY45	SEY6210; *ATG9-GFP::HIS5 S.p. atg1Δ::URA3*	This study
JLY47	SEY6210; *ATG9-GFP::KAN atg1Δ::URA3 atg27Δ::HIS5 S.p.*	This study
TN124	*MATα leu2–3,112 ura3–52 trp1 pho8::pho8Δ60 pho13Δ::URA3*	(162)
TN121	*MATa leu2-3,112 trp1 ura3-52 pho8::pho8Δ60 pho13Δ::URA3*	(75)
TVY1	SEY6210; *pep4Δ::LEU2*	(53)
Vps34^{tsf}	SEY6210; *vps34Δ::TRP1 pvps34^{tsf}::URA3*	(216)
WHY001	SEY6210; *atg1Δ::HIS5 S.p.*	(207)
WLY1	SEY6210; *ATG27-3xHA::TRP1*	This study
WLY2	SEY6210; *atg27Δ::TRP1*	This study
WLY3	TN121; *atg27Δ::TRP1*	This study
WLY5	SEY6210; *ATG27-GFP::HIS3*	This study
WLY6	SEY6210; *ATG27-GFP::HIS VRG4-RFP::TRP1*	This study
WLY8	SEY6210; *pep4Δ::LEU2 vps4Δ::TRP1 atg27Δ::HIS3*	This study
WLY11	SEY6210 ATG23-GFP::TRP1	This study
KTY29	SEY6210 ATG23-GFP::KAN *atg1Δ::URA3*	This study
KTY32	SEY6210 ATG23-GFP::KAN *atg9Δ::HIS3 S.k.*	This study
WLY05	SEY6210 *ATG27-GFP::HIS3*	This study
WLY11	SEY6210; *atg1Δ::URA K.l. ATG27-GFP::HIS3*	This study
WLY18	SEY6210; *atg13Δ::LEU2 ATG27-GFP::HIS3*	This study
WLY22	SEY6210; *atg27Δ::TRP1 pATG27-3xHA* (416)	This study
WLY26	SEY6210; *atg1Δ::URA S.k. atg9Δ::KAN ATG27-GFP::HIS3*	This study
WLY27	BY4742; *PEX14-GFP::HIS3 Atg27Δ::URA K.l.*	This study
WLY40	TN124; *atg27Δ::KAN*	This study
WLY41	SEY6210; *atg1Δ::LEU2 K.l. atg9Δ::KAN ATG27-GFP::HIS3 RFP-Ape1::LEU2*	This study
WLY59	JLY45; *atg27ΔC::TRP1*	This study

47

WLY51   SEY6210; *vps34Δ::TRP1 pvps34^{tsf}::URA3*   This study
WLY52   SEY6210; *atg14Δ::TRP1 ATG27-GFP::HIS3*   This study

Atg27 Is Required for the Cvt pathway and Pexophagy and for Efficient Bulk Autophagy

Previously, Atg27 was reported to be specifically involved in the Cvt pathway but not bulk autophagy (254). Because of the previously mentioned sequencing error, we decided that it was important to reinvestigate the phenotype of the *atg27Δ* mutation. We deleted the full-length *ATG27* gene and examined the role of Atg27 in the Cvt pathway by pulse-chase analysis of prApe1 processing (Fig. 2.2A). After delivery to the vacuole, the propeptide of prApe1 is removed resulting in a convenient molecular mass shift that can be followed to monitor delivery to the vacuole (112). Yeast strains were grown in SMD selective media, pulse-labeled with [^{35}S]methionine/cysteine for 10 min, and then subjected to a nonradioactive chase for 2 h at 30°C. Ape1 was immunoprecipitated from the cell lysates and then analyzed by SDS-PAGE and autoradiography. In a control *atg1Δ* strain defective in the Cvt pathway, prApe1 processing was blocked, whereas in wild-type cells, prApe1 was processed as expected (Fig. 2.2A). In the *atg27Δ* strain, even after a 2 h chase, prApe1 remained unprocessed. These data confirm that Atg27 is required for the Cvt pathway.

The Cvt and autophagy pathways can be broken down into several steps: induction, vesicle formation and completion, docking and fusion of the vesicle with the vacuole, breakdown of the cargo, and recycling. Most of the Atg proteins are involved in the vesicle formation step. To determine whether Atg27 acts during vesicle formation, we performed an Ape1 protease-sensitivity assay. If prApe1 is enclosed in a completed vesicle, the potentially protease-sensitive propeptide domain would be protected from exogenously added protease. Alternatively, if Atg27 is required for vesicle formation

49

and/or completion, prApe1 would be sensitive to the protease, and the resulting cleavage would result in a molecular mass shift. To block the delivery of prApe1 to the vacuole and subsequent prApe1 processing within this organelle, we used a *pep4Δ vam3^{ts}* strain that is defective for fusion of vesicles with the vacuole at the nonpermissive temperature and that cannot process the propeptide within the vacuolar lumen. Spheroplasts from the wild-type (*pep4Δ vam3^{ts}*) strain and from this strain deleted for the *ATG1* or *ATG27* gene were incubated at 37°C for 20 min to inactivate the Vam3 protein. The cells were then pulse-labeled with [^{35}S]methionine/cysteine for 10 min, followed by a nonradioactive chase reaction. After osmotic lysis the low-speed pellet fractions, which contained prApe1, were subjected to proteinase K treatment in the presence or absence of detergent. In the wild-type cells, prApe1 was protected from exogenously added protease and was digested only after the membrane was disrupted with detergent, reflecting a defect in vesicle formation and/or completion. Similarly, in the *atg27Δ* strain, an equivalent fraction of prApe1 was protease-accessible independent of detergent addition, indicating that the prApe1 was not completely enwrapped by the membrane. This result suggests that Atg27 functions in the vesicle formation/completion step.

Next, we extended our study to examine the role of Atg27 in the specific degradation of peroxisomes, termed pexophagy, and bulk or nonspecific autophagy. To test the role of Atg27 in pexophagy, we monitored the degradation of the peroxisomal integral membrane protein Pex14. The C terminus of Pex14 was chromosomally tagged with GFP. The induction of pexophagy results in delivery of peroxisomes into the vacuoles and Pex14 degradation, whereas the GFP moiety remains relatively stable within the vacuole. Thus, the appearance of free GFP correlates with pexophagy (183).

Pexophagy was induced as described in Material and Methods. In wild-type cells expressing Pex14-GFP, peroxisomes were delivered into the vacuoles upon pexophagy induction, represented by the appearance of free GFP (Fig. 2.2C). No free GFP was detected in the *atg1Δ* strain, indicating that the assay reflects an autophagic process. Pex14-GFP underwent processing in *atg27Δ* cells; however, there was a kinetic delay relative to the wild-type strain, indicating that Atg27 is required for efficient pexophagy.

In a previous study (254), *atg27Δ* cells were reported to process prApe1 after induction of autophagy by rapamycin. Analysis of prApe1 processing is not sufficient for monitoring autophagy, however, because prApe1 is a specific marker; import in starvation condition still utilizes specific components including the receptor Atg19 (201). Therefore, we performed additional experiments to test the role of Atg27 in nonspecific autophagy. To make a quantitative measurement of autophagy, we utilized Pho8Δ60, a truncated version of the vacuolar alkaline phosphatase, Pho8. Pho8Δ60 lacking the N-terminal transmembrane domain, is unable to enter the ER and accumulates in the cytosol; it is only delivered into the vacuole through autophagy (162). Once inside the vacuole this protein is cleaved and become enzymatically active. Thus, Pho8Δ60 activity serves as a marker for bulk cytosolic autophagy. The Pho8Δ60 activity was measured in wild-type, *atg1Δ*, and *atg27Δ* cells (Fig. 2.2D). As expected, *atg1Δ* cells that are defective in autophagy showed no increase of Pho8Δ60 activity after autophagy was induced. Wild-type cells showed Pho8Δ60 activity that increased after 2-4 h of starvation, whereas *atg27Δ* cells induced Pho8Δ60 activity to <50% of the wild-type level. The partial induction of Pho8Δ60 activity suggested that autophagy occurred in *atg27Δ* cells but not as efficiently as in wild-type cells.

The partial block in nonspecific autophagy led us to further analyze the role of

Atg27 through another biochemical approach, GFP-Atg8 processing. Atg8 is a ubiquitin-

like protein that is conjugated to phosphatidylethanolamine (75, 105) and is one of two

Atg proteins that remain associated with the completed autophagosome membrane.

Similar to Pex14-GFP, Atg8 is degraded after delivery into the vacuole, whereas the GFP

moiety is again relatively stable (207). Wild-type, *atg1Δ*, and *atg27Δ* cells were

transformed with a plasmid-based GFP-Atg8, grown in SMD medium and then subjected

to nitrogen starvation. At various time points, aliquots were removed and TCA-

precipitated and then subjected to western blot using anti-GFP antibody (Fig. 2.2E). In

wild-type cells, the amount of free GFP increased over time during starvation,

representing a functional autophagy pathway, whereas in autophagy-defective *atg1Δ* cells,

no free GFP was detected. In the *atg27Δ* mutant, there was a kinetic delay in free GFP

accumulation compared with the wild-type strain. This result agreed with the Pho8Δ60

analysis and further suggested that the *atg27Δ* mutant had an intermediate autophagy

defect.

Two possibilities may explain the intermediate autophagy defective phenotype

(Fig. 2.2D and E) of the *atg27Δ* mutant: a reduction of either autophagosome size or

autophagosome number. To determine the role for Atg27 in autophagosome biogenesis,

we used electron microscopy to examine the ultrastructure of the autophagic bodies that

accumulated in the absence of Atg27 (Fig. 2.3A). Autophagosomes are double-membrane

vesicles. After the outer membrane of an autophagosome fuses with the vacuole limiting

membrane, the single-membrane inner vesicle, now termed an autophagic body, is

released into the vacuolar lumen where it is degraded in a Pep4-dependent manner. In

pep4Δ cells, which lack vacuolar proteinase A activity, the breakdown of autophagic bodies is blocked, allowing them to be visualized by electron microscopy. To eliminate the background vesicles that are delivered into the vacuole through the multivesicular body pathway, we deleted the *VPS4* gene (187). Wild-type, *atg1Δ*, and *atg27Δ* strains additionally harboring *pep4Δ vps4Δ* double mutations were grown in YPD to early log phase and then shifted to SD-N for 5 h and prepared for electron microscopy.
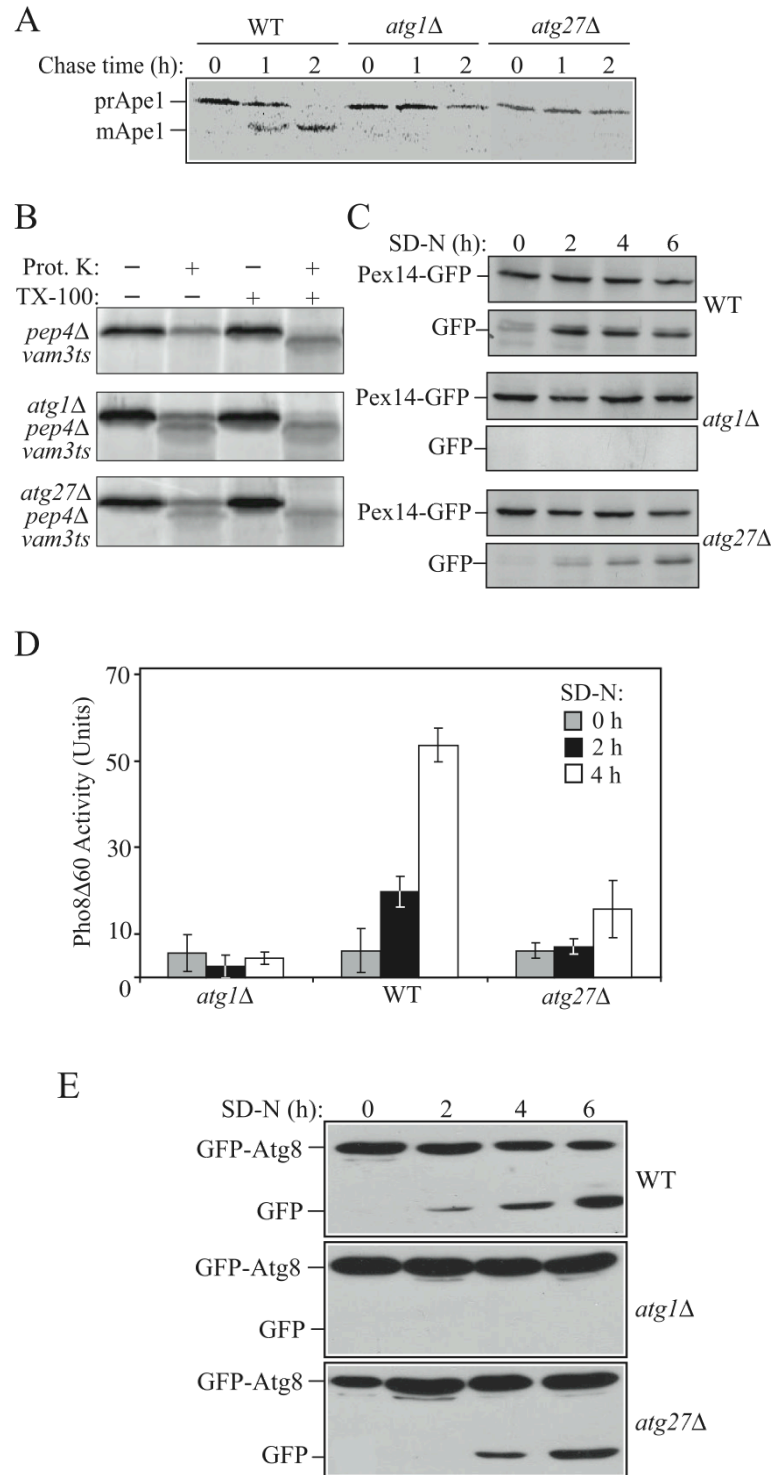
Figure 2.2. The *atg27Δ* mutant is defective for autophagy-related pathways. (A) *atg27Δ* cells are defective in the Cvt pathway. Wild-type (WT; SEY6210), *atg1Δ* (WHY001), and *atg27Δ* (WLY002) cells were pulse-labeled for 10 min and subjected to a nonradioactive chase for 2 h. At the indicated time points cells were collected and TCA-precipitated. The cell lysates were immunoprecipitated with anti-Ape1 serum, resolved by SDS-PAGE, and then subjected to autoradiography. The positions of prApe1 and mApe1 are indicated. (B) Atg27 functions in the vesicle formation and/or completion step. Spheroplasts from the wild-

type (*pep4Δ vam3^{ts}*; WLY26) strain or this same strain harboring the *atg1Δ* (WLY74) or *atg27Δ* (WLY33) deletions were incubated at 37°C for 20 min, pulse-labeled with [^{35}S]methionine/cysteine for 10 min, and then subjected to a non-radioactive chase for 27 min. The spheroplasts were osmotically lysed and separated into low-speed pellet and supernatant fractions after 5,000 x g centrifugation. The pellet fractions that contained prApe1 were treated with proteinase K in the presence or absence of 0.2% Triton X-100. The resulting samples were immunoprecipitated with Ape1 antiserum and resolved by SDS-PAGE. (C) Atg27 is required for efficient pexophagy. Pex14-GFP (WT; IRA001), Pex14-GFP *atg1Δ* (IRA002), and Pex14-GFP *atg27Δ* (WLY27) strains were grown in oleic acid-containing medium to induced peroxisome proliferation and shifted to starvation medium. Protein extracts were prepared from cells at each indicated time point, resolved by SDS-PAGE, and probed with monoclonal anti-GFP antibody. The positions of Pex14-GFP and free GFP are indicated. (D) *atg27Δ* has an intermediate autophagy defect. *atg1Δ* (HAY572), wild-type (TN124), and *atg27Δ* (WLY3) cells expressing Pho8Δ60 were shifted from SMD to SD-N medium for 4 h. Samples at the indicated time points were collected, and protein extracts were assayed for alkaline phophatase activity. The resulting graph represents the mean of three separate experiments, and the error bars represent the SD. (E) Wild-type (WT; SEY6210), *atg1Δ* (WHY001), and *atg27Δ* (WLY2) strains harboring a plasmid expressing GFP-Atg8 [pGFP-Aut7(414)] were grown in SMD lacking auxotrphic amino acids and shifted to SD-N. Aliquots were removed at the indicated time points. Protein extracts were prepared and resolved at the indicated time points. After western blot, the membranes were probed with anti-GFP antibody.

Wild-type (*pep4Δ vps4Δ*) cells showed numerous autophagic bodies, with 13-15 autophagic bodies in 22% of the vacuoles and an average of 14.62±5.31 per vacuole after 5 h of starvation (Fig. 2.3A and C; n=63 vacuoles). The control *atg1Δ pep4Δ vps4Δ* cells, defective in autophagy, did not accumulate autophagic bodies as expected. The *atg27Δ pep4Δ vps4Δ* cells accumulated a reduced number of these structures, with 1-3 autophagic bodies in 44% of the vacuoles and an average of 3.13±2.63 per vacuole (n=77 vacuoles). To determine whether *atg27Δ pep4Δ vps4Δ* cells accumulated normal-sized autophagic bodies, we quantified their size in wild-type and *atg27Δ pep4Δ vps4Δ* cells by measuring the diameter (Fig. 2.3B). We found that the autophagic bodies that accumulated in wild-type and *atg27Δ pep4Δ vps4Δ* cells were similar in diameter, suggesting that *atg27Δ pep4Δ vps4Δ* cells produced normal-sized autophagosomes. Taken together, the reduction of the autophagic body number in addition to the biochemical data indicate that the decreased efficiency of nonspecific autophagy in the *atg27Δ* mutant was not due to a structural defect in autophagosome formation but rather a kinetic delay in the process.
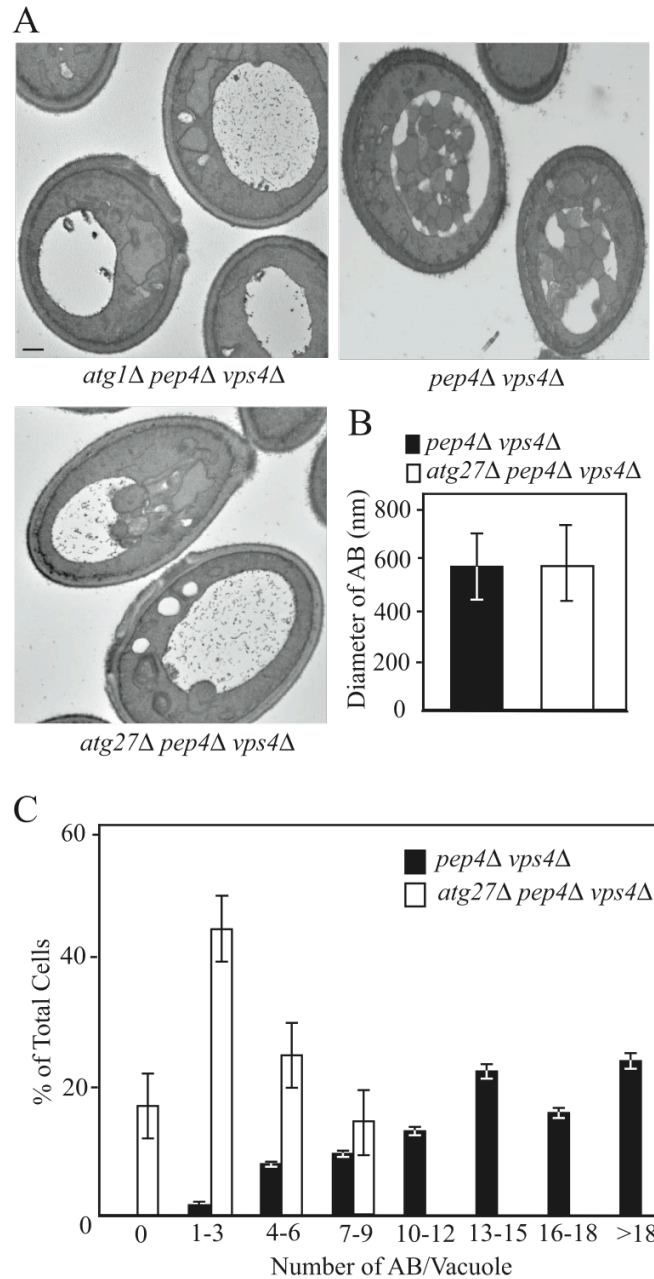
Figure 2.3. The *atg27Δ* mutant generates fewer autophagosome. (A) The wild-type (*pep4Δ vps4Δ*; FRY143), *atg1Δ* (JHY28), and *atg27Δ* (WLY002) cells are defective in the Cvt pathway. Wild-type (WT; SEY6210), *atg1Δ* (WHY001), and *atg27Δ* (WLY8) strains were grown to early log phase in YPD, shifted to SD-N for 5 h to induce autophagy, and examined by electron microscopy as described in Materials and Methods. Bar, 0.5 μm. (B) Quantification of the diameter of autophagic bodies (AB). To quantify the size of the accumulated ABs inside the vacuole, the diameter of ABs with a clear membrane boundary was measured. The number of ABs counted was 50 for the *atg27Δ* strain and 67 for wild type. (C) Quantification of autophagic body accumulation. To quantify the number of ABs accumulated, the number of autophagic bodies was counted in cells containing similar-sized vacuoles.

Atg27 Cycles among the PAS, Mitochondria, and Golgi complex

Atg27 localizes to multiple unidentified perivacuolar punctate structures (254). To gain insight into the function of Atg27, we decided to examine the structures at which Atg27 resides *in vivo* by using fluorescence microscopy. A common feature of Atg proteins is that they appear to transiently localize at the PAS. The function of the PAS is not clear, but it has been implicated in the formation of Cvt vesicles and autophagosomes (101, 222). We hypothesized that Atg27 may have the same subcellular distribution as most other Atg proteins. To monitor the PAS localization of Atg27, we generated a functional C-terminal GFP fusion at the *ATG27* chromosomal locus. An Atg27-GFP strain harboring an RFP-Ape1 plasmid was grown to the early log phase and then visualized by fluorescence microscopy (Fig. 2.4A top panel). Atg27-GFP was distributed in several subcellular punctate structures, only one of which colocalized with the PAS marker RFP-Ape1. Next, we extended our study by examining the colocalization of organelle markers with the non-PAS population of Atg27. Among the organelle markers that we examined, Atg27-GFP partially localized with the mitochondria (MitoFluor Red) and Golgi complex marker (Vrg4-RFP; middle and bottom panels of Fig. 2.4A). Atg27-GFP was found to not colocalize with the ER or peroxisomes (data not shown).

Most Atg proteins can only be detected at the PAS. Two exceptions, Atg9 and Atg23, show unique localization in multiple punctate structures other than the PAS (186, 230), similar to the Atg27 distribution. Both Atg9 and Atg23 cycle between the PAS and mitochondria (186). This cycling is dependent on the Atg1-Atg13 complex (186). Atg1 is a serine/threonine kinase, which may play an important role in regulating the switch between the Cvt pathway and autophagy. In *atg1Δ* cells, both Atg9 and Atg23 are

restricted to the PAS (186). We visualized Atg27-GFP distribution in *atg1Δ* cells to see if

Atg27 showed a similar trafficking pattern (Fig. 2.4B). The majority of Atg27 was

restricted to the PAS in the absence of Atg1, as indicated by colocalization with RFP-

Ape1 in both growing and starvation conditions, but occasionally with some additional

very faint punctate structures in the cytosol. This PAS restriction could be reversed and

the wild-type localization restored by expressing a plasmid encoding wild-type Atg1

(data not shown). Moreover, a recent study showed that Atg1 kinase activity is required

for Atg23 cycling in growing conditions, but not for Atg9 cycling (186). A plasmid

containing an *ATG1* mutant with reduced kinase activity (*Atg1^{K54A}*) was introduced into

the Atg27-GFP *atg1Δ* strain. Similar to Atg9, Atg27 distribution was not affected when

the Atg1 kinase activity was reduced in both growing and starvation conditions (Fig.

2.4C). The regulatory function of Atg1 is regulated through protein-protein interactions

with several other Atg proteins (90). Therefore, we examined the effect on Atg27

localization of mutants deleted for Atg1-interacting proteins. With the exception of Atg13,

deletion of other Atg proteins we screened had no effect on Atg27 distribution (Fig. 2.4A

and data not shown). Similar to *atg1Δ*, most of the Atg27-GFP was restricted to the PAS

in *atg13Δ* cells under both growing and starvation conditions. Taken together, these data

show that Atg27 cycles between the PAS and the non-PAS pool in an Atg1-Atg13

complex-dependent manner, but normal Atg1 kinase activity is not required for Atg27

trafficking.

The results with the *atg1Δ* and *atg13Δ* strains indicated that Atg27 cycling was

dependent on the Atg1-Atg13 complex, similar to Atg9. To further examine the cycling

pattern of Atg27, we tested the effect on Atg27 movement of other factors that are

required for Atg9 trafficking. In the absence of either Atg2 or Atg18, Atg9 is restricted to the PAS (186). Atg27 distribution in the *atg2Δ* and *atg18Δ* strains was also confined to one strong dot, although additional faint dots could also be detected (Fig. 2.4E). Thus, Atg27 appears to have a less stringent requirement for components involved in retrograde cycling. Along these lines, Atg27 cycling was independent of Atg14 (See Fig. 2.7B) in contrast to Atg9. The actin cytoskeleton is required for Atg9 anterograde movement; Atg9 does not accumulate at the PAS in the *atg1^{ts}* strain treated with latrunculin A at the nonpermissive temperature (183). We were unable to determine the requirement of actin filaments in Atg27 cycling, however, because of a delayed PAS accumulation phenotype seen with Atg27-GFP in the *atg1^{ts}* strain; *atg27Δ* cells lost viability after treatment with latrunculin A before we could assay the movement of Atg27-GFP.

Finally, we extended our analysis of Atg27 localization. A P13 pellet fraction from the Atg27-HA strain was separated on a sucrose density gradient as described in Materials and Methods (Fig. 2.5). After centrifugation at 176,000 x g for 18 h at 4°C, 13 fractions were collected from the top to bottom and subjected to immunoblot analysis. The vacuole membrane marker Pho8 was concentrated in the top fractions, whereas the plasma membrane marker, Pma1, was in the bottom fractions. In agreement with a previous report (185), the P13 population of Atg9 cofractionated with mitochondria (Por1). Atg27-HA was distributed through several fractions with the peak concentration in fraction 7. A population of Atg27 cofractionated with mitochondria (Por1) and the Golgi complex (Mnn1), supporting the fluorescence data suggesting that Atg27 resides in these membrane compartments.
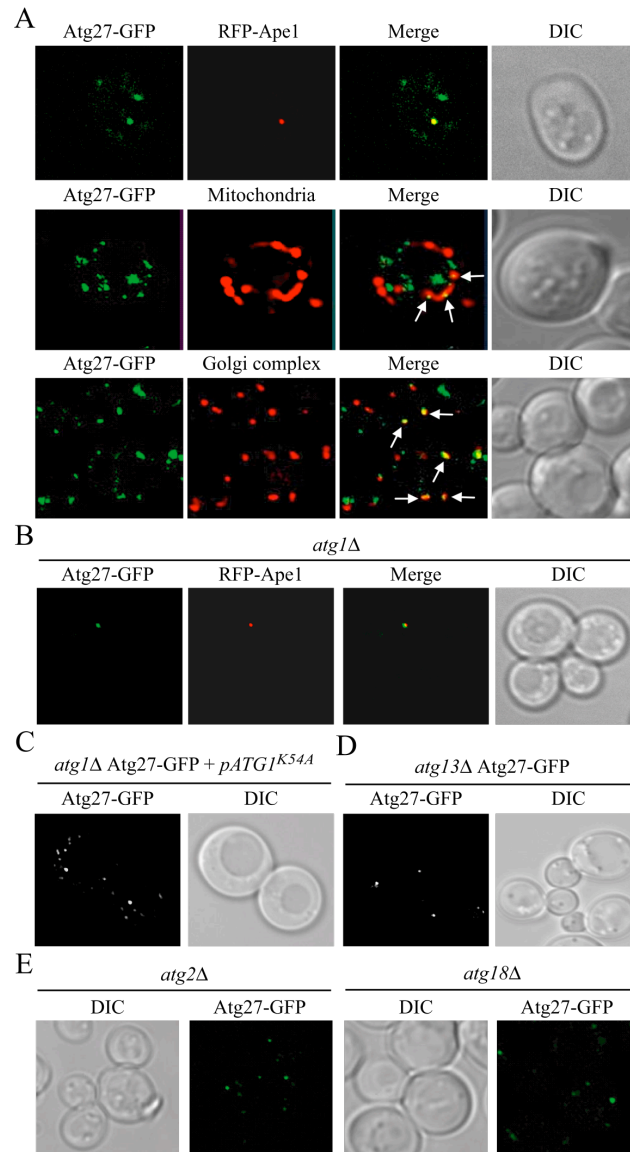
Figure 2.4. Atg27 cycles among the PAS, mitochondria, and Golgi complex. (A) Atg27 localizes to the PAS and partially to the mitochondria and Golgi. The strain expressing chromosomally tagged Atg27-GFP (WLY5) carrying either a PAS marker [pRFP-APE1(414)] or expressing chromosomally tagged Vrg4-RFP (Golgi complex marker; WLY6) were grown to early log phase or subjected to nitrogen starvation for 3 h before imaging. For mitochondrial staining, the Atg27-GFP culture was incubated for 30 min in the presence of 1 μM MitoFluor Red 589 (Molecular Probes, Eugene, OR). The arrows indicate the colocalization of Atg27-GFP with mitochondria or the Golgi complex. (B) Atg27 is restricted to the PAS in *atg1Δ*. The chromosomally tagged Atg27-GFP *atg1Δ* strain (WLY11) carrying a PAS marker [pRFP-APE1(414)] was grown in selective medium to early log phase and then visualized by fluorescence microscopy. (C and D) The absence of Atg13, but not the reduced Atg1 kinase activity, affected Atg27 localization. (C) The chromosomally tagged Atg27-GFP atg1D strain carrying an Atg1 kinase mutant (*ATG1^{K54A}*) plasmid and (D) the Atg27-GFP *atg13Δ* strain (WLY18) were grown in selective SMD medium to OD$_{600}$=0.8 and analyzed by fluorescence microscopy. Essentially identical results were obtained when cells were incubated in starvation medium. (E) Atg2 and Atg18 are required for efficient Atg27 retrograde cycling from the PAS. The chromosomally tagged Atg27-GFP *atg2Δ* (WLY78) and Atg27-GFP *atg18Δ* (WLY70) strains were grown in SMD medium and fixed with 1.5% formaldehyde in 50 mM potassium phosphate buffer (pH 8) for 30 min before imaging. DIC, differential interference contrast.
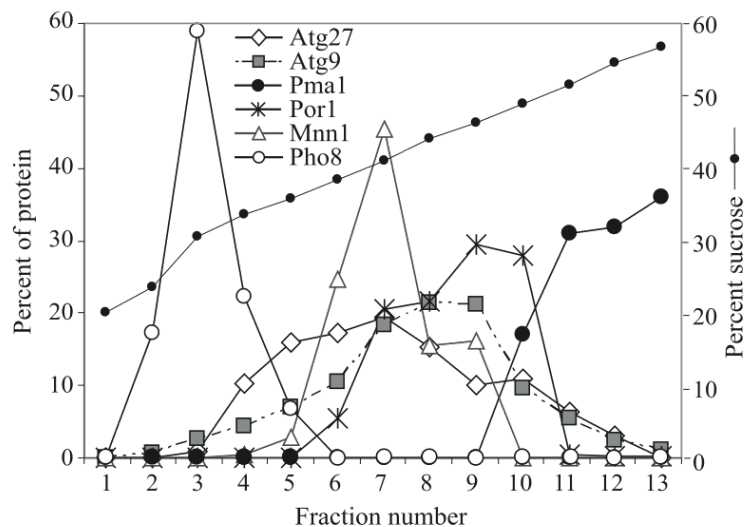
Figure 2.5. Atg27 localizes to mitochondria and the Golgi complex. The Atg27-HA (WLY1) strain was grown in YPD to OD_{600}=1.0 and converted into spheroplasts. The spheroplasts were osmotically lysed and separated into pellet (P13) and supernatant (S13) fractions after a 13,000 x g centrifugation. The P13 pellet fraction was separated on a sucrose density gradient (18-54%) and centrifuged for 18 h at 176,000 x g as described in Materials and Methods. A total of 13 fractions were collected from the top to the bottom of the gradient and were subjected to immunoblot analysis with antiserum against Atg27-HA, Atg9, Pma1 (plasma membrane), Por1 (mitochondria), Mnn1 (Golgi complex), and Pho8 (vacuole).

Atg27 Is Required for Atg9 Cycling from the Mitochondria to the PAS

Atg9, Atg23, and Atg27 have a common phenotype involving the PAS and multiple additional punctate dots. Atg23 is needed for delivery of Atg9 to the PAS (J. E. Legakis, W.-L. Yen, and D. J. Klionsky, unpublished results). To examine whether Atg27 is required for Atg9 localization before Atg1 function, we performed an epistasis analysis termed the transport of Atg9 after knocking out Atg1 (TAKA) assay (30). In wild-type cells Atg9 displays multiple punctate dots, one of which localized to the PAS, indicated by colocalization with the PAS marker RFP-Atg8 (Fig. 2.6A). In an *atg1Δ* strain, Atg9 was restricted to the PAS, as previously shown (186). In both *atg27Δ* and *atg1Δ atg27Δ* double mutant cells, Atg9 localized to multiple punctate dots, with none of the dots corresponding to the PAS. The colocalization of Atg9 with MitoFluor Red confirmed that a population of Atg9 was restricted to the mitochondria in the *atg27Δ* and *atg1Δ atg27Δ* double mutants (Fig. 2.6B). This result suggested that Atg27 functions before Atg1 in Atg9 cycling and is required for Atg9 movement from the mitochondria to the PAS.

The type I topology suggested that the majority of Atg27 is localized on the lumenal side of the membrane, whereas Atg23 is a cytosolic protein. To determine whether the cytosolic tail of Atg27 is required for the movement of Atg9, we tested the effect of an Atg27 truncation on Atg9 cycling. We generated a version of Atg27 lacking the C-terminal cytosolic tail, *Atg27ΔC*. In *atg1Δ atg27ΔC* cells, Atg9 was restricted in one dot similar to the localization in the *atg1Δ* strain (Fig. 2.6C). This result indicates that the cytosolic C terminus of Atg27 is not required for anterograde movement of Atg9 to the PAS.

In the light of the data that Atg27 is required for Atg9 cycling, we decided to test the requirement of Atg9 for Atg27 movement. In *atg9Δ* and *atg1Δ atg9Δ* cells, Atg27 localized to multiple punctate structure similar to the wild-type Atg27 distribution except that none of the dots corresponded with the PAS marker (Fig. 2.6D and data not shown). This result indicated that Atg9 functions in Atg27 cycling before Atg1 and is required for Atg27 movement from the non-PAS structures (mitochondria and Golgi complex) to the PAS.
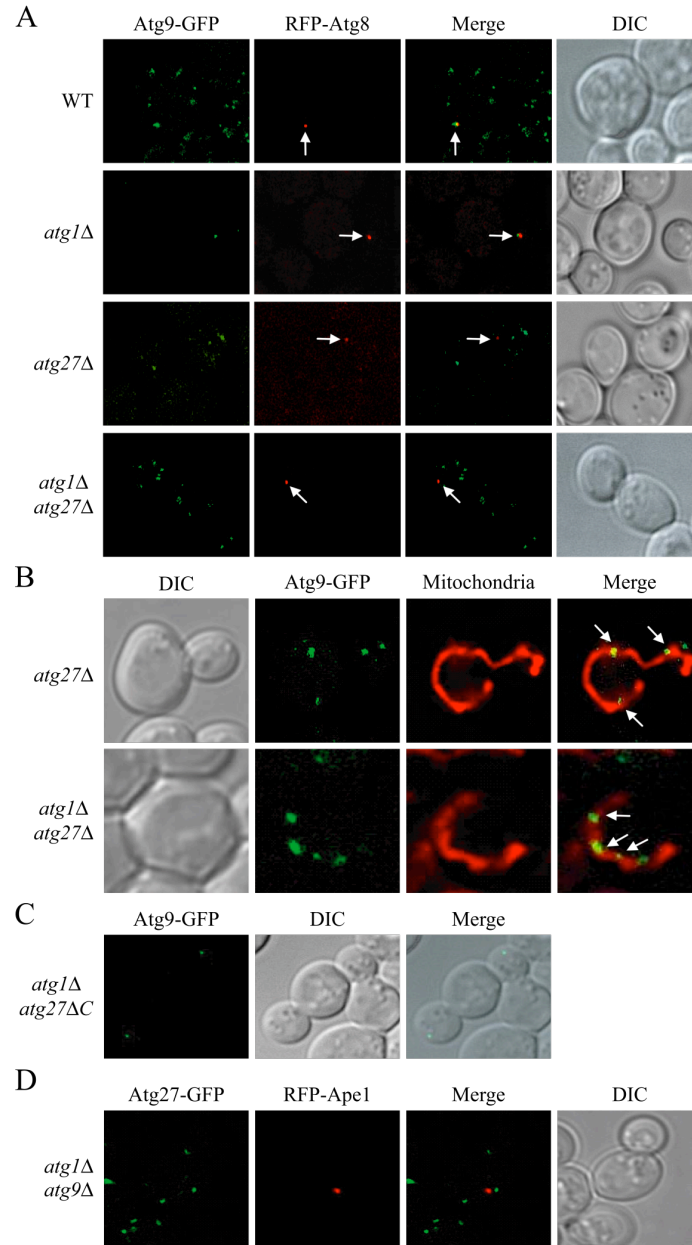
Figure 2.6. Atg27 functions before Atg1 and is required for Atg9 cycling. (A) Atg27 is required for Atg9 anterograde trafficking. The chromosomally tagged Atg9-GFP (WT; JLY44), Atg9-GFP *atg1Δ* (JY45), and Atg9-GFP *atg27Δ* (JLY47) strains expressing plasmid-based RFP-Atg8 were grown to OD_{600}=0.8 in selective SMD medium and visualized by fluorescence microscopy. Arrows locate the PAS marker RFP-Atg8. (B) Atg9 localizes to mitochondria in the *atg27Δ* and *atg1Δ atg27Δ* mutants. The chromosomally tagged Atg9-GFP *atg27Δ* (JLY43) and Atg9-GFP *atg1Δ atg27Δ* (JLY47) strains were grown in SMD complete medium, and mitochondria were stained by incubating for 30 min in the presence of 1 μM MitoFluor Red 589. (C) The C-terminal cytosolic portion of Atg27 is not required for Atg9 cycling. Chromosomally tagged Atg9-GFP *atg1Δ atg27ΔC* (WLY49) cells were grown to early-log phase and collected for fluorescence microscopy. (D) Atg9 is required for Atg27 cycling from the non-PAS structures to the PAS. The chromosomally tagged Atg27-GFP *atg1Δ atg9Δ* strain (WLY41) expressing chromosomally tagged RFP-Ape1 was grown to early-log phase in selective medium before imaging. DIC, differential interference contrast.

Atg27 Localization Does Not Require Vps34 Function

In the yeast *S. cerevisiae*, Vps34 is the only PtdIns 3-kinase. Vps34 is found in two distinct tetrameric complexes named complex I and complex II (97). Vps34 kinase complex I generates PtdIns(3)P at the PAS and is essential for both the Cvt pathway and autophagy (97, 101, 160). Etf1 was originally identified as a PtdIns(3)P binding protein, which functions as a Vps34 downstream effector specifically involved in the Cvt pathway (254). Given the type I membrane protein topology that we demonstrated (Fig. 2.1), the proposed PtdIns(3)P-binding site in Etf1/Atg27 would not be exposed to the cytosol, yet PtdIns(3)P is generally limited to the cytosolic face of membranes. To examine the requirement for PtdIns(3)P in Atg27 localization, we analyzed a temperature-sensitive Vps34 (*vps34^{ts}*) mutant (Fig. 2.7A). Atg20, a phox homology domain-containing protein required for Cvt pathway function, binds to PtdIns(3)P and requires Vps34 for its localization (160) and served as a control. In *vps34^{ts}* cells grown at permissive temperature (26°C), Atg20-GFP showed one strong dot localized at the PAS indicated by colocalization with RFP-Ape1. After shifting to 38°C, a nonpermissive temperature, for 12 min, Atg20-GFP dissociated from the membrane and was dispersed throughout the cytosol. In contrast, Atg27-GFP distribution was similar in both wild-type and *vps34^{ts}* mutant cells at permissive as well as nonpermissive temperatures. Moreover, Atg27 still localized to the PAS even after Vps34 was inactivated. To further confirm that the PAS localization of Atg27 does not requires binding to PtdIns(3)P, we examined the localization of Atg27 in the *atg14Δ* background. Atg14, one of the components in Vps34 complex I, is required to localize the Vps34 complex to the PAS (164). In the *atg14Δ* mutant, Atg27-GFP distribution was not affected, and the chimera still localized to the

PAS (Fig.2.7B). Because Atg27 localization was not affected by inactivation of Vps34 or deletion of *ATG14*, we concluded that Atg27 does not bind PtdIns(3)P or at least does not require binding for its localization.

To further test our conclusion, we mutated the previously proposed putative PtdIns(3)P binding site on Etf1/Atg27 (residues 188-193) and tested the function of the mutant Atg27$^{K188-193A}$. First, we examined the complementation of the plasmid-based Atg27$^{K188-193A}$ by pulse-chase analysis of prApe1 import in the *atg27Δ* background. Both wild-type Atg27 and Atg27$^{K188-193A}$ constructs driven by the endogenous promoter showed ~85% complementation of the prApe1 import defect of *atg27Δ* cells after a 2 h chase (data not shown), indicating that this construct was functional for the Cvt pathway. We also tested the complementation of the Atg27$^{K188-193A}$ mutant by the TAKA assay (Fig. 2.8A). Plasmids encoding either wild-type Atg27 or Atg27$^{K188-193A}$ but not the empty vector allowed Atg9 cycling from the non-PAS pool to the PAS in the *atg1Δ atg27Δ* background under both growing (Fig. 2.8A) and starvation conditions (data not shown). To test the function of Atg27$^{K188-193A}$ mutant in autophagy, we examined nonspecific uptake of the cytosolic marker Pho8Δ60. We transformed the *atg27Δ* Pho8Δ60 strain with a plasmid encoding either wild-type Atg27 or Atg27$^{K188-193A}$. The Pho8Δ60 activity of the strains expressing Atg27 and Atg27$^{K188-193A}$ were essentially identical to that of the wild-type strain (Fig. 2.8B). This result supports the conclusion that PtdIns(3)P binding by Atg27 is not required for Atg27 function.
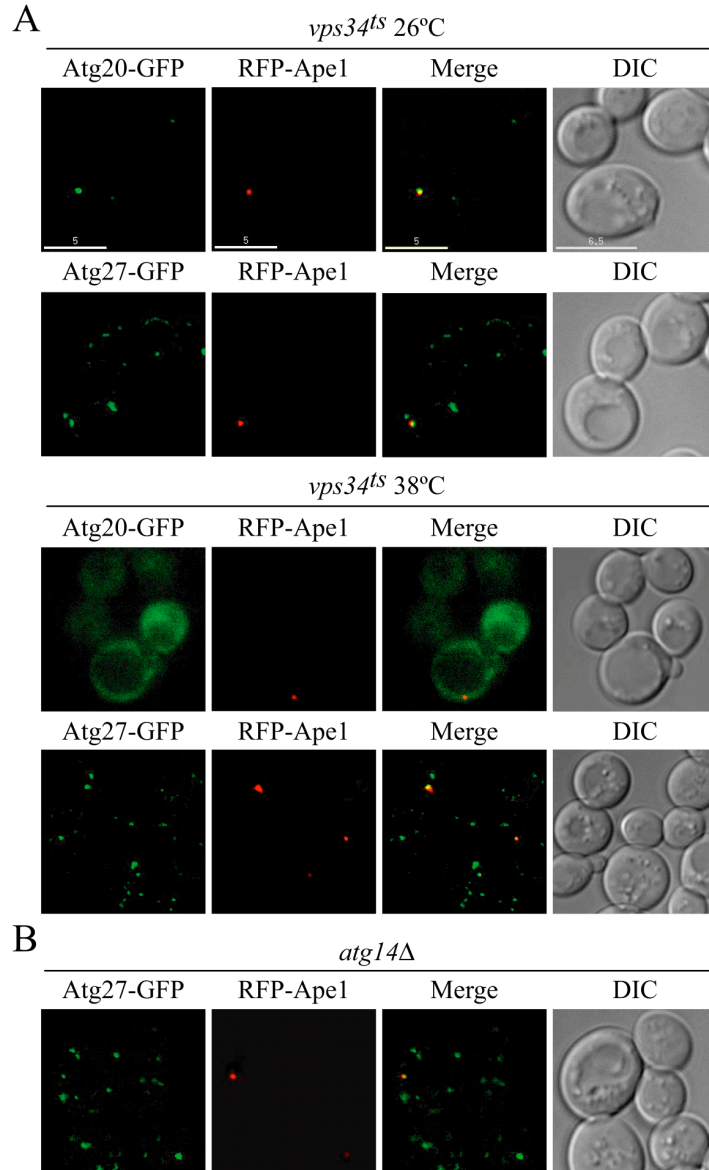
Figure 2.7. Binding to PtdIns(3)P is not required for Atg27 function. (A) Atg27 localization is not affected by Vps34. Chromosomally tagged Atg20-GFP and Atg27-GFP strains expressing plasmid-based *vps34^{ts}* and RFP-Ape1 (WLY50 and WLY51, respectively) were grown in selective SMD medium to OD_{600}=0.8 at 26°C or shifted to 38°C for 12 min before imaging. (B) Atg14 does not affect Atg27 PAS localization. The Atg27-GFP *atg14Δ* strain (WLY52) expressing RFP-Ape1 was grown in selective SMD medium and visualized by fluorescence microscopy. Bar, 5 μm.

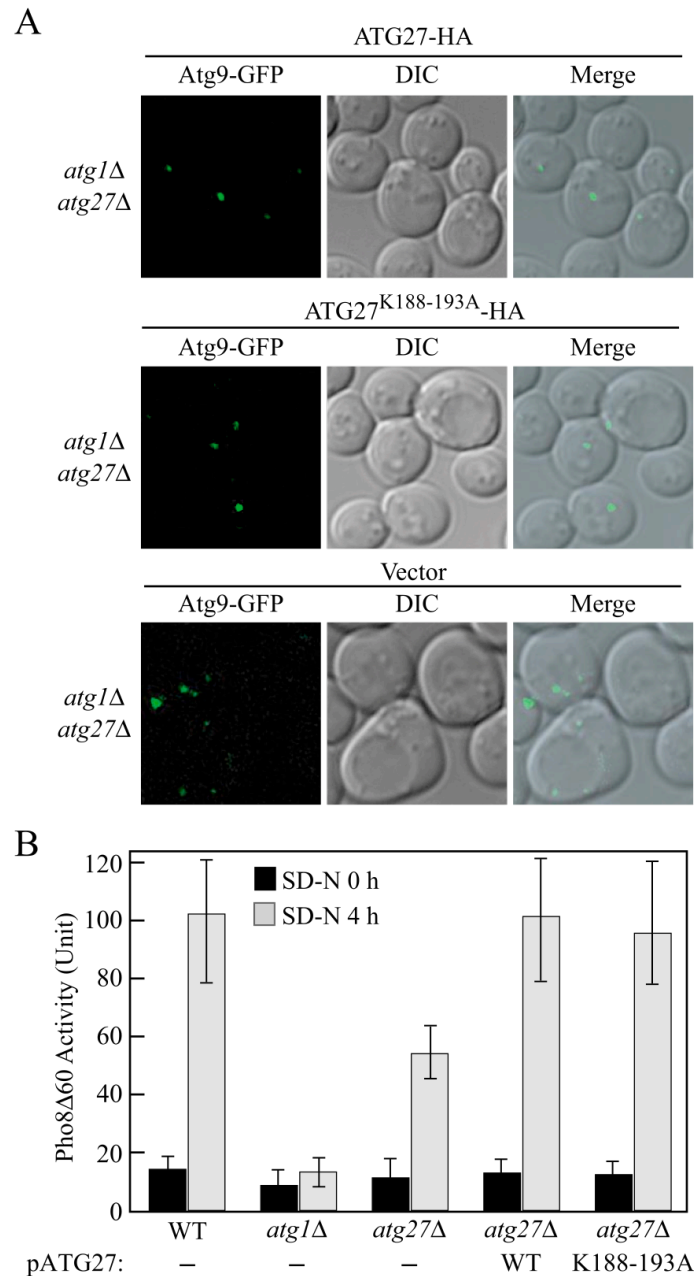**Figure 2.8. Mutation of the Atg27 putative PtdIns(3)P binding site has no effect on function**. (A) The Atg27[K188-193A] mutant does not affect Atg9 cycling to the PAS. The chromosomally tagged Atg9-GFP *atg1Δ atg27Δ* strain (JLY47) expressing either plasmid-based Atg27-3xHA, Atg27[K188-193A]-3xHA or vector were grown in selective SMD medium and visualized by fluorescence microscopy. DIC, differential interference contrast. (B) Wild-type (TN124), *atg1Δ* (HAY572), and *atg27Δ* (WLY40) strains and the *atg27Δ* strain expressing plasmid-based wild-type Atg27-HA or Atg27[K188-193A]-HA were shifted from SMD to SD-N medium for 4 h. Samples were collected at the indicated time points, and protein extracts were assayed for Pho8Δ60-dependent alkaline phosphatase activity. The results represent the mean of three separate experiments and the error bars represent the SD.

69

Discussion

Atg27 was characterized as a type II transmembrane protein (254); however, this assessment was based on an incorrect sequence that had been present in the *Saccharomyces* Genome Database. The corrected full-length Atg27 includes an N-terminal extension that contains a signal sequence, which would typically result in an orientation opposite to the one reported. In the present study we showed that Atg27 is in fact a type I transmembrane protein (Fig. 2.1). Also in the original description, Atg27 was reported to be required for the Cvt pathway but not autophagy. That conclusion was based solely on an analysis of prApe1 processing in conditions that induce autophagy (254); however, more recent studies have shown that monitoring prApe1 is not sufficient to assess autophagic capacity (30). Our analysis of the *atg27Δ* mutant phenotype demonstrated that Atg27 is required for efficient autophagy and pexophagy (Fig. 2.2 and 2.3).

One of the major questions about the process of autophagy is the source of the lipid that is used for formation of autophagosomes and the mechanism used for lipid movement to the vesicle assembly site. Unlike most endomembrane trafficking processes in which the vesicles bud from a pre-existing membrane surface, the double-membrane of the autophagosome is though to form *de novo* and likely involves an expansion process that necessitates multiple membrane delivery events. Until now, Atg9 was the only potential candidate to help us understand the mechanism and the source of the membrane for autophagosome formation. Recent studies show that Atg9 cycles between the PAS an the mitochondria (185). This characteristic, coupled with it being an integral membrane

protein, make Atg9 a potential carrier bringing membrane to the autophagosome formation site. These studies also suggest that the mitochondria are part of the membrane source for the double-membrane vesicles. Here, we show that Atg27 is the second transmembrane protein that is involved in vesicle formation in the Cvt pathway and autophagy. We found that Atg27 localizes to the mitochondria and the Golgi complex, and possibly other unknown structures. These characteristics of Atg27 lead us to suggest that Atg27 may also mark the membrane source that is donated to the forming vesicles. The localization of Atg27 to the Golgi complex fits with previous studies implicating this organelle as another source of membrane for the forming vesicles (187).

To gain insight on how lipid is recruited to the sequestering vesicles, we investigated the mechanisms that regulate Atg9 cycling. This is a complex process and several components have been shown to be required for Atg9 cycling between the PAS and the mitochondria, including the Atg1-Atg13 complex, Atg2, Atg18, and the PtdIns 3-kinase complex I (186). In contrast, the Atg components that are required for Atg9 anterograde transport form the mitochondria to the PAS have not yet been identified; however, we have shown that actin cytoskeleton is involved in this step (183). We have recently discovered that Atg27, Atg23, and Atg11 are all required for Atg9 anterograde trafficking (Fig. 2.6). The requirement for Atg27 in Atg9 cycling suggests that these two proteins may interact with each other. The finding that Atg9 interacts with Atg27 by yeast two-hybrid analysis, and affinity isolation supports this idea (126).

Etf1/Atg27 was originally identified as a PtdIns(3)P-binding protein, and a putative PtdIns(3)P-binding site was proposed in the previous study; upon mutation of the proposed site, the mutant lost the ability to bind this phophoinositide (254). From the

detailed topological characterization, we found that this putative binding site resides in the lumenal potion of the protein. Because PtdIns(3)P is present on the cytosolic face of the membrane, it is highly unlikely that a physiologically relevant binding site is in the lumen. Our studies suggest that Atg27 does not bind to PtdIns(3)P via this lumenal domain and that the presence of PtdIns(3)P does not influence the localization of Atg27 (Fig. 2.7 and 2.8). Moreover, mutation of this site did not affect the function of Atg27 in either the Cvt pathway or autophagy (Fig. 2.8B). Therefore, we concluded that Atg27 is probably not a PtdIns(3)P-binding protein and that, at any rate, binding to this phosphoinositide does not play a role in its function.

Atg27 is the second transmembrane Atg protein that is required for the formation of the sequestering vesicle in autophagy-related pathways. The topology of Atg27 indicates that the majority of the protein would be present within the intermembrane space between the autophagosome inner and outer vesicle membrane or in the lumenal space during autophagosome formation. The specific function of this domain is not known. Further analysis of Atg27 may provide more information regarding the membrane sources in autophagy and the cycling of proteins that are proposed to deliver membrane to the site of autophagosome formation.

Materials and Methods

Yeast strains and media

The *S. cerevisiae* strain (BY4742) knockout library was purchased from ResGen (Invitrogen, Carlsbad, CA). The yeast strains used in this study are listed in Table 2.1. For gene disruptions, the entire coding regions were replaced by the *Saccharomyces cerevisiae TRP1*, the *Kluyveromyces lactis LEU2* or *URA3*, the *S. kluyveri HIS3*, or the *Escherichia coli kan^r* gene using PCR primers containing ~50 bases of identity to the regions flanking the open reading frame. For PCR-based integrations of the 3xHA, RFP and GFP tags at the 3' end of *ATG9*, *ATG27*, *VRG4*, *PEX14* and *ATG20* genes, pFA6a-3HA-TRP1, pFA6a-GFP-HIS3, pFA6a-GFP-KanMX, and pFA6a-mRFP-TRP1 were used as templates to generate strains expressing fusion proteins under the control of their own promoters (24, 138). PCR verification and prApe1 processing were used to verify the functionality of all the fusion proteins.

Yeast cells were grown in rich medium (YPD; 1% yeast extract, 2% peptone, 2% glucose) or synthetic minimal medium (SMD; 0.67% yeast nitrogen base, 2% glucose, amino acids, and vitamins as needed). Starvation experiments were conducted in synthetic medium lacking nitrogen (SD-N; 0.17% yeast nitrogen base without amino acids, 2% glucose).

Plasmids

The carboxyl-terminal HA fusion of Atg27 (pATG27-3xHA(416)) was made by PCR amplification of the *ATG27* ORF and upstream 500 base pairs of genomic DNA,

followed by ligation into the pRS416-3xHA plasmid. The plasmid pATG27$^{K188-193A}$-3xHA(416), pATG27^{G105N}-3HA(416), pATG27^{V17P}-3HA(416), pATG27^{Q155N}-3HA(416), and pATG27^{D176TD181T}-3HA(416) were made using the QuikChange™ Site-directed Mutagenesis Kit (Stratagene). The vectors for the gene fusion to *SUC2* have been described previously (110). To make the *ATG27-SUC2* fusion construct, the *ATG27* gene was amplified from *S. cerevisiae* genomic DNA by PCR and cloned as a *BamH*I fragment. This procedure was used to generate an Atg27 N-terminal 28 amino acids-invertase fusion. The pP4I- 23 and pP4I-137 (110), pCuGFP-AUT7(416) (100), pATG1^{K54A} (1), and pRFP-APE1(414) [pPS130; (218)] plasmids have been described previously. Two plasmids, pAtg27-HA(424) and pATG27$^{K188-193A}$-HA(424) used for the Pho8Δ60 assay, were cloned from the pATG27-3xHA(416) and pATG27$^{K188-193A}$-3xHA(416) plasmids, respectively, into the pRS424 empty vector using *Sac*I and *Sal*I sites.

Protein extraction and immunoblot analysis

 S. cerevisiae strains were generally grown at 30°C to the early mid-log phase in YPD or SMD media. Cells were harvested and treated with 10% trichloroacetic acid (TCA) on ice for 20 min. After centrifugation at 16,000 x g for 5 min, cell pellets were washed with 100% acetone and air dried. The dry cell pellets were resuspended in MURB buffer (50 mM Na_2HPO_4, 25 mM MES, pH 7.0, 1% SDS, 3 M urea, 0.5% β-mecaptoethanol, 1 mM NaN_3, and 0.05% bromophenol blue) and disrupted by vortex with an equal volume of glass beads for 5 min, then heated at 70°C for 10 min. Aliquots (OD_{600} = 0.2) were resolved by SDS-PAGE and probed with appropriate antiserum.

Invertase assay

Cells expressing the Atg27 signal sequence-invertase hybrid protein were grown to early mid-log phase in SMD-URA medium then washed in 10 mM NaN_3. Cultures were divided into two aliquots, one for measuring the total activity and the other for secreted activity. Cell lysate preparation was performed as described previously (110). The invertase enzyme assay was done as described previously (54), with minor modifications: we used μM glucose/minute/OD_{600} for the unit of invertase activity, instead of using μM glucose/minute/mg.

Endoglycosidase H treatment

WLY2 cells harboring 3xHA-tagged Atg27^{G105N} were grown to late mid-log phase (OD_{600} = 5.0), TCA precipitated, subjected to centrifugation at 16,000 x g and washed once with acetone. The pellet was air dried, then glass beads and 100 μl elution buffer (1% SDS, 0.1 M Tric-HCl, pH 7.5, 1% 2-mercaptoethanol) were added and the pellet was resuspended by sonication, followed by heating at 95°C for 5 min. After cooling, 900 μl of Endo H buffer (0.15 M citric acid, pH 5.5) were added, and the resuspension was subjected to centrifugation at 15,000 x g for 30 sec. The lysate was then split into two equal portions and 10 μl of 100 mM PMSF and protease inhibitor cocktail were added to each tube. Endo H (10 mU) was then added to the mixture, which was incubated at 37°C overnight, boiled for 3 min, and subjected to immunoblotting.

Cell labeling and the immunoprecipitation

Cells were grown to early mid-log phase in SMD medium. 10 ml of cells were harvested and were labeled in 200 μl SMD with 20 μCi Trans[^{35}S]-label for 10 min at 30°C. For a non-radioactive chase, 1 ml SMD containing 0.2% yeast extract, 2 mM cysteine and methionine was added. At each indicated time point, samples were collected and precipitated with 10% TCA for 20 min on ice, then spun down at 16,000 x g for 5 min at 4°C. The pellets were washed twice with 1 ml acetone, and the cell extracts were prepared and immunoprecipitated as described previously (64).

Fluorescence microscopy

Cells expressing fusion proteins with fluorescence tags were grown in SMD medium to OD_{600} = 0.8. For mitochondrial fluorescent labeling, MitoFluor Red 589 (Molecular Probes/Invitrogen, Eugene, OR) was added to the growing culture at a final concentration of 1 μM, and the culture incubated at 30°C for 30 min. Cells were then washed with the same culture medium before imaging to remove the excess dye. For rapamycin treatment, cells were cultured with 0.2 μg/ml rapamycin at 30°C for 1.5 h. Fluorescence signals were visualized on an Olympus IX71 fluorescence microscope (Olympus, Mellville, NY). The images were captured by a Photometrics CoolSNAP HQ camera (Roper Scientific, Inc., Tucson, AZ) and deconvolved with DeltaVision software (Applied Precision, Issaquah, WA). Electron microscopy was performed as described previously (89).

Additional assays

For the GFP-Atg8 processing assay, yeast strains harboring the GFP-Atg8

plasmid (pGFP-Aut7(414)) were grown to early mid-log phase in SMD medium lacking

auxotrophic amino acids, then shifted to SD-N medium for 4 h. At each indicated time

point, 1 ml of cell culture was removed and TCA precipitated. The protein extracts were

resolved by SDS-PAGE and probed with anti-GFP monoclonal antibody (Covance

Research Products, Berkeley, CA).

The alkaline phosphatase assay to measure Pho8Δ60 activity, Pex14-GFP

processing to monitor pexophagy, the protease protection assay, and the subcellular

fractionation have been described previously (64, 102, 162, 183, 201, 230). The sucrose

density gradient used to fractionate Atg27 was generated as described previously (185)

with minor modifications (1 ml each of 18%, 22%, 26%, 30%, 34%, 38%, 42%, 46%,

50%, and 54% sucrose).

CHAPTER 3

A Cycling Protein Complex Required for Selective Autophagy

Abstract

Survival of environmental stress conditions requires the maintenance of cellular homeostasis. To preserve this balance, cells utilize a degradative mechanism known as autophagy. During this process, in response to starvation or other stresses, bulk cytoplasm is non-specifically sequestered within double-membrane vesicles and delivered to the lysosome/vacuole for subsequent degradation and recycling. The cytoplasm to vacuole targeting (Cvt) pathway is a type of specific autophagy, which occurs constitutively during growing conditions. Here, we examine three autophagy-related (Atg) proteins, Atg9, Atg23, and Atg27, which exhibit a unique localization pattern, residing both at the phagophore assembly site (PAS) and other peripheral sites. These proteins localize, interact with one another *in vivo*, and form a functional complex. Furthermore, all three proteins cycle between the PAS and the other sites, and depend upon one another for this movement. Our data suggested that Atg9, Atg23, and Atg27 play an important role in Atg protein retrieval from the PAS. In addition, Atg9 and Atg27 are the only known integral membrane Atg proteins involved in vesicle formation; a

better understanding of their function may offer insight into the mechanism of membrane

delivery to the PAS, the site of double-membrane vesicle assembly.

Introduction

An essential aspect of cellular physiology is the ability of cells to adapt to a changing environment. Included in these changes are variations in the extracellular milieu, such as nutrient availability, in conjunction with intracellular signals that trigger modifications in cellular metabolism. Part of this adaptation involves regulation and modification of the cell's biosynthetic and degradative pathways, maintaining a proper equilibrium that is essential for growth and development. One cellular process that plays an important role in maintaining this equilibrium is autophagy (132), and defects in autophagic capacity may result in diseases such as certain cancers, neurodegeneration and cardiomyopathies (208).

Autophagy is a general term for an evolutionarily conserved process involving the sequestration of cytoplasmic materials and its subsequent delivery to, and breakdown by, the lysosome/vacuole. Different types of autophagy are defined in part by the material that is sequestered, and the subcellular location of the sequestration process. Among these pathways are macroautophagy (hereafter referred to as autophagy) and the Cvt pathway. Autophagy is an inducible process, which is active under starvation conditions and is the primary vacuole-mediated degradative pathway. It involves formation of a double-membrane vesicle, termed an autophagosome, which sequesters bulk cytoplasm (109). Following completion of the autophagosome, the outer membrane fuses with the lysosome/vacuole, releasing the inner vesicle that is termed an autophagic body. Subsequently, the autophagic body is lysed, allowing access to its contents, which are degraded, released back into the cytosol and reused in metabolic processes (261, 264).

The Cvt pathway is a specific and constitutive biosynthetic process and in

Saccharomyces cerevisiae is responsible for the delivery of at least two vacuolar

hydrolases, aminopeptidase I (Ape1), and α-mannosidase (Ams1) (76, 112, 200). This

pathway involves the enclosure of precursor Ape1 (prApe1) in a double-membrane Cvt

vesicle (analogous to an autophagosome) that appears to exclude bulk cytoplasm,

followed by its delivery to and fusion with the yeast vacuole. The resulting single-

membrane Cvt body is then lysed within the vacuole lumen, and the propeptide of

prApe1 is cleaved to generate the mature, active enzyme (264). Although the pathways

serve distinct functions and respond to unique cellular cues, the machinery utilized by

both the Cvt pathway and autophagy is largely the same. Consequently, both pathways

can be similarly divided into a number of steps: (1) induction; (2) cargo selection and

packaging (this step is essentially restricted to specific autophagy-related processes such

as the Cvt pathway); (3) vesicle nucleation; (4) vesicle expansion and completion; (5)

Atg protein retrieval; (6) targeting, docking and fusion with the lysosome/vacuole; (7)

breakdown of the vesicle and its contents; and (8) subsequent recycling of the resulting

macromolecules (93, 111, 217). To date, more than 30 gene products have been identified

in yeast as essential to at least one of the various types of autophagy, and the

corresponding genes are called autophagy-related (*ATG*) genes (93, 111, 217).

One aspect of these pathways that is unknown is the source of the lipid bilayer

used for cargo sequestration. Contradictory data have been published, including studies

suggesting that the endoplasmic reticulum (ER), Golgi complex, and/or the plasma

membrane are the membrane sources for these vesicles (50). However, autophagosomes

appear to be different from both ER and Golgi complex membranes in lipid and protein

concentration (50, 182). Speculations have been made that the reason the identity of these donor membranes has been so elusive is that they are either derived from an unidentified compartment(s), or discrete domains of organelles, which are devoid of marker proteins that may be rapidly retrieved back to the donor sites (186). Our laboratory recently determined that one of the two characterized transmembrane Atg proteins involved in vesicle formation, Atg9, resides on or near mitochondria (185).

Atg9 is required for both autophagy and the Cvt pathway. As an integral membrane protein, it is a potential candidate to reside at least transiently at the membrane source for the nascent sequestering vesicles. In addition, Atg9 is involved in one of the earliest steps of autophagosome/Cvt vesicle formation (222). Under normal growth conditions, Atg9 is localized to the PAS, the organizing center for vesicle formation, and distinct sites on/near mitochondrial membrane (185, 186), as well as other peripheral punctate structures, and it cycles between the PAS and these other compartments (185, 186). Two other Atg proteins, Atg23 and Atg27, share a similar localization pattern (230), although the identities of all the structures where they reside remains unknown. Atg23 and Atg27 also cycle to and from the PAS, similar to Atg9 (186, 263). Atg23 is a peripheral membrane protein required for the Cvt pathway and efficient autophagy, which localizes to multiple subcellular locations including the cytosol, the PAS, and other unidentified punctate structures (186, 230). Our laboratory recently discovered that Atg27 is also a transmembrane protein that is localized to the PAS, mitochondria, and the Golgi complex, and is required for the Cvt pathway and efficient autophagy (263). Given the similarity of the subcellular localization of these three Atg proteins, we decided to dissect their relationship to one another. In this study, we examined the localization and

interaction of Atg9, Atg23, and Atg27, and factors required for their association, proper

cellular positioning and cycling. We demonstrated that all these three proteins cycle, and

that they colocalized at distinct subcellular compartments. We found that proper

movement of each of these proteins required the other two, in addition to other factors.

All of these proteins interacted at multiple cellular sites, with Atg9 mediating the

interaction between Atg23 and Atg27.

Results

Atg9, Atg23, and Atg27 colocalize

The vast majority of characterized Atg proteins localize at least partially and/or transiently at the PAS; however, three Atg proteins exhibit a unique localization at multiple punctate structures dispersed throughout the cytosol, in addition to the PAS. These are Atg9, Atg23, and Atg27 (161, 186, 230, 263). Atg9 localizes to the PAS (185), distinct sites on or near the mitochondrial membrane, and to other unidentified structures. Aside from the PAS, the other Atg23-containing sites have not yet been identified (186).

Because of the similar subcellular distributions of these three proteins, we decided to investigate the interrelationships among them. Accordingly, we first determined whether these three proteins colocalize, and if so, where in the cell they co-reside. We expressed chromosomally tagged fluorescent chimeras of Atg9, Atg23, and Atg27 and examined their localization in a pair wise fashion. Examination of Atg23-GFP together with Atg9-RFP in cells grown to mid-log phase and subjected to mild fixation revealed that these two proteins partially colocalized, with approximately 50% (based on visual analysis) of Atg9 puncta corresponding to both Atg9 and Atg23 (Fig. 3.1 top panel). Examination of GFP-tagged Atg27 along with Atg9-RFP yielded similar results, with again approximately half of the Atg9 puncta representing both Atg9 and Atg27 (Fig. 3.1 middle panel). The same situation was seen with Atg23 and Atg27 (Fig. 3.1 bottom panel). Attempts to simultaneously visualize all three of these proteins were unsuccessful due to the low signal intensity of the endogenous proteins.

Table 3.1. Yeast strains used in this study.

Strain	Genotype	Source or reference
SEY6210	*MATα ura3-52 leu2-3,112 his3-Δ200 trp1-Δ901 lys2-801 suc2-Δ9 mel GAL*	(190)
PJ69-4A	*MATα leu2-3,112 trp1-Δ901 ura3-52 his3-Δ200 gal4Δ gal80Δ LYS2::GAL1-HIS3 GAL2-ADE2 met2::GAL7-lacZ*	(80)
FRY162	SEY6210 ATG9-GFP::HIS5 S.p.	
FRY241	SEY6210 ATG23-GFP::TRP1 VRG4-RFP::HIS5 S.p.	This study
FRY244	SEY6210 ATG23-GFP::TRP1 ATG9-RFP::HIS5 S.p.	This study
JLY44	SEY6210 ATG9-GFP::HIS5 S.p.	This study
JLY45	SEY6210 ATG9-GFP::HIS5 S.p. *atg1Δ::URA3*	This study
JLY46	SEY6210 ATG9-GFP::HIS5 S.p. *atg1Δ::URA3 atg23Δ::KAN*	This study
JLY49	SEY6210 ATG9-GFP::HIS5 S.p. *atg23Δ::KAN*	This study
JLY65	SEY6210 ATG23-GFP::KAN	This study
JLY67	SEY6210 ATG23-PA:: HIS5 S.p. *atg27Δ::TRP1*	This study
JLY68	SEY6210 ATG23-PA:: HIS5 S.p. ATG27-HA::TRP1	This study
JLY73	SEY6210 ATG23-PA:: TRP1 *atg9Δ::HIS3 S.k. atg1Δ::URA3*	This study
JLY74	SEY6210 ATG23-PA:: HIS5 S.p. ATG27-HA::TRP1 *atg9Δ::KAN*	This study
JLY76	SEY6210 ATG23-PA:: HIS5 S.p. ATG27-HA::TRP1 *atg1Δ::URA3*	This study
JLY77	SEY6210 ATG23-PA:: HIS5 S.p. ATG27-HA::TRP1 *atg11Δ::URA3*	This study
JLY94	SEY6210 ATG23-GFP::KAN *atg27Δ::HIS5 S.p.*	This study
JLY95	SEY6210 ATG23-GFP::KAN *atg27Δ::HIS5 S.p. atg1Δ::URA3*	This study
JLY100	SEY6210 ATG23-GFP::KAN ATG9-RFP:: HIS5 S.p.	This study
JLY101	SEY6210 ATG23-RFP::KAN ATG27-GFP:: HIS5 S.p.	This study
JLY105	SEY6210 ATG23-PA:: HIS5 S.p. ATG27-HA::TRP1 *atg9Δ::LEU2 atg1Δ::URA3*	This study
JLY106	SEY6210 ATG23-PA:: HIS5 S.p. ATG27-HA::TRP1 *atg9Δ::LEU2 atg11Δ::URA3*	This study
KTY14	SEY6210 *atg23Δ::KAN*	
KTY25	SEY6210 ATG23-GFP::TRP1	This study
KTY29	SEY6210 ATG23-GFP::KAN *atg1Δ::URA3*	
KTY32	SEY6210 ATG23-GFP::KAN *atg9Δ::HIS3 S.k.*	
WLY05	SEY6210 *ATG27-GFP::HIS3*	(263)
WLY11	SEY6210 *atg1Δ::URA3 ATG27-GFP::HIS3*	(263)
WLY15	SEY6210 ATG27-GFP::HIS3 *atg23Δ::KAN atg1Δ::URA3*	This study
WLY20	SEY6210 ATG27-GFP::HIS3 ATG9-RFP:: TRP1	This study

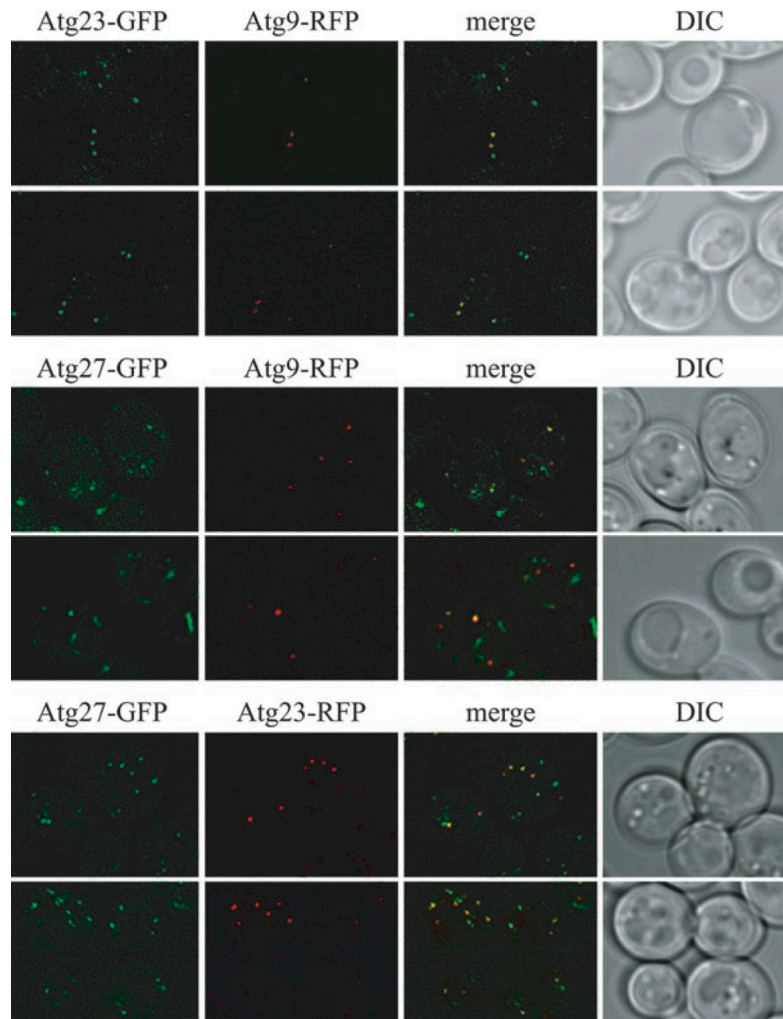**Figure 3.1. Atg9, Atg23, and Atg27 colocalize.** Strains integrated with fluorescent chimeras of Atg9-RFP and Atg23-GFP (JLY100), Atg9-RFP and Atg27-GFP (WLY20) or Atg23-RFP and Atg27-GFP (JLY101) were grown in rich medium, to mid-log phase, subjected to mild fixation with 1.5% formaldehyde, processed as described in Materials and Methods and viewed by fluorescence microscopy. DIC, differential interference contrast.

Atg9 resides on multiple punctate structures, one of which has been identified as the PAS (186). The other identified site of localization corresponds to distinct sites on or near the mitochondrial membranes (185). Because Atg23 and Atg27 partially colocalize with Atg9, we speculated that some of the structures on which these proteins are located may also correspond to mitochondrial regions. To identify the subcellular location of the Atg23 and Atg9 puncta, we examined cells expressing Atg9 or Atg23 tagged with GFP, in conjunction with a plasmid expressing blue fluorescent protein fused to a C-terminal mitochondrial matrix targeting sequence (Mito-BFP). Visualized with this plasmid, mitochondria are manifest as both tubular and somewhat punctate structures. We observed some colocalization of Atg9-GFP with mitochondria, with a population of Atg9-GFP manifest as distinct puncta on/near the mitochondrial membrane, in agreement with previous findings (Fig. 3.2A, top panel)(185). Similar results were obtained upon visualization of Atg23-GFP along with Mito-BFP, with some of the Atg23-GFP punctate structures colocalizing with the mitochondrial marker, while other Atg23-positive puncta were located in the cytosol (Fig. 3.2A, bottom panel) (185). These non-mitochondrial structures containing Atg23 were then evaluated for colocalization with other organelle markers. We found that none of the Atg23-GFP puncta colocalized with any of the other organelle markers tested, including the ER, Golgi complex, actin cables, or peroxisomes (Fig. 3.2B, top and middle panels, and data not shown).

We next wanted to determine whether the sites where Atg23 and Atg9 colocalize are at the mitochondria. When both Atg23-GFP and Atg9-RFP were observed along with Mito-BFP, it was apparent that some of the sites at which Atg9-RFP and Atg23-GFP colocalized were indeed on or in proximity to the mitochondria (Fig. 3.2B bottom panel).

Our laboratory recently found that Atg27 also localized to distinct puncta on/near the mitochondrial membrane, and partially colocalized with a Golgi marker (263). Taken together, we conclude from these data that Atg9, Atg23, and Atg27 are all located in multiple punctate structures including the PAS and distinct sites on/near the mitochondria; Atg23 is also present in a cytosolic pool.
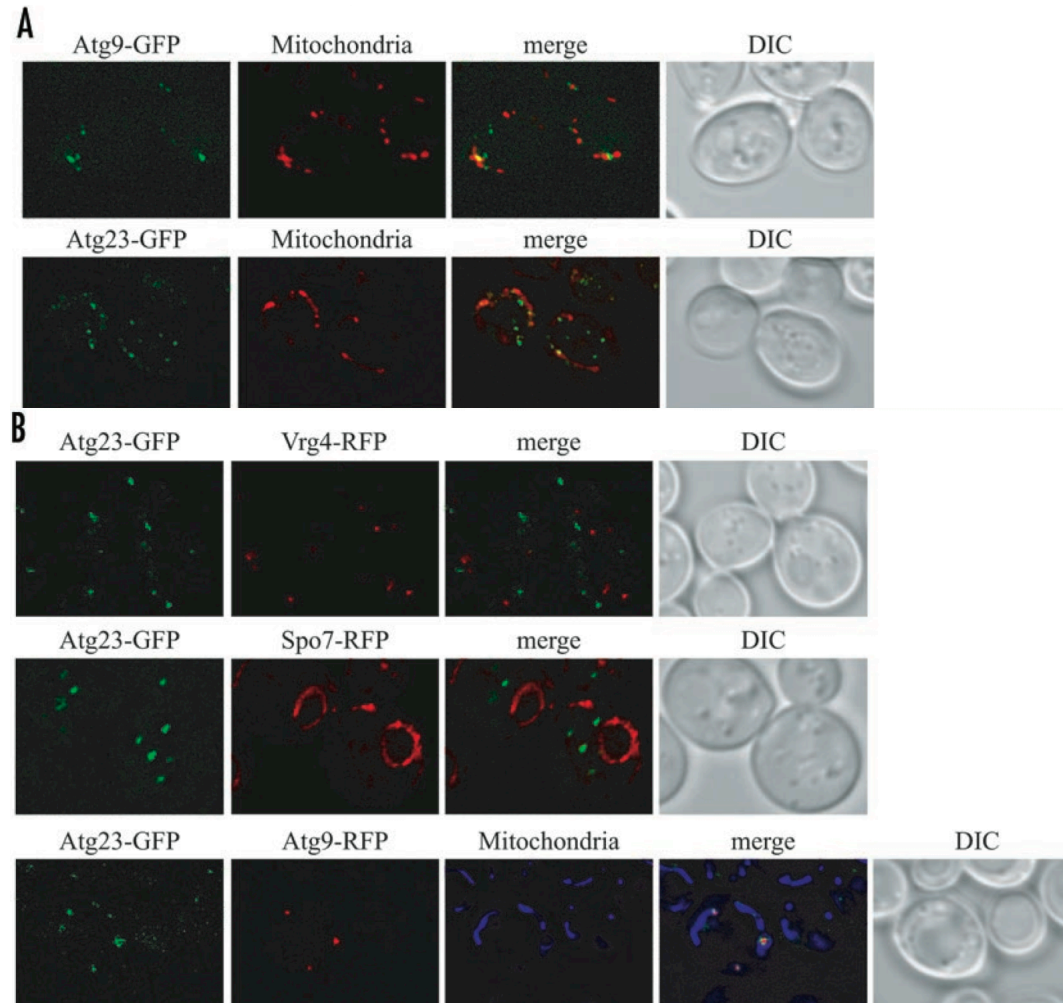
Figure 3.2. Atg9 and Atg23 colocalize at or near the mitochondria. (A) Cells chromosomally-tagged with fluorescent fusion proteins Atg23-GFP (KTY25) or Atg9-GFP (FRY162) and transformed with a plasmid encoding pYES-Mito-BFP were grown to mid-log phase, fixed as described in Materials and Methods, and examined by fluorescence microscopy. Mito-BFP is depicted in red for ease of visualization (B) Cells expressing Atg23-GFP and either Vrg4 (FRY241), a plasmid encoding Spo7-RFP or Atg9-RFP (FRY244) and plasmid-based Mito-BFP, were prepared and viewed as in (A). DIC, differential interference contrast.

Atg23 is required for anterograde movement of Atg9

Having found that these three proteins partially colocalized, we next examined

potential interdependence with regard to their subcellular localization. In particular, we

first examined the effect of eliminating any one of these proteins on the localization of

the other two. We used the Transport of Atg9 after Knocking out *ATG1* (TAKA) assay,

to investigate the effect of deleting *ATG23* on Atg9 cycling. The TAKA assay is an

epistasis analysis that takes advantage of established properties of Atg9 cycling (30). In

particular, Atg1 is needed for retrograde transport of Atg9 back to the peripheral (non-

PAS) sites; in *atg1Δ* mutants, Atg9 cycling is disrupted, and the protein is restricted to

the PAS, in contrast to its multiple punctate distribution in wild-type cells (Fig. 3.3) (186).

The effect of a second mutation is examined in the *atg1Δ* background to determine

whether the corresponding gene product acts upstream of Atg1, thus preventing

accumulation of Atg9 at the PAS (185, 208). Thus, the TAKA assay allow us to assign a

temporal order of action to factors involved in protein cycling; however, we cannot be

absolutely certain the effects are a direct result of the *ATG* gene deletion and do not

reflect in an epistatic effect due to another gene product.

Using this assay, we found that Atg9 anterograde cycling was defective in the

absence of Atg23; Atg9 was unable to move to the PAS, and was not present as a single

punctate dot with an additional deletion at the *ATG1* locus (Fig. 3.3). A similar phenotype

was seen with a deletion of *ATG27* (263). Essentially the same results were obtained

when cells were subjected to nitrogen starvation for 1 h to induce nonspecific autophagy

(data not shown). These data indicate that Atg23 and Atg27 are required for anterograde

movement of Atg9 (from peripheral sites to the PAS).

Atg9 and Atg27 are required for Atg23 trafficking.

As stated previously, Atg23 exhibits a subcellular localization similar to that of Atg9, residing in multiple punctate structures, including the PAS, distinct regions on/near the mitochondrial membrane, and other unidentified sites, in addition to a separate diffuse cytosolic population (Fig. 3.2 and 3.4) (230). Subcellular fractionation experiments support the morphological evidence that Atg23 is a peripheral membrane protein, which is both membrane-associated as well as having a significant cytosolic population (230). In addition, it has been established that Atg23 is a cycling protein similar to Atg9, and is dependent upon Atg1 and Atg13 for retrograde movement from the PAS (186).

In the light of these overall similarities, as well as the role of Atg23 in Atg9 cycling, we decided to examine the requirement for both Atg9 and Atg27 in Atg23 cycling. We observed the localization of Atg23 in wild-type cells as multiple punctate structures in addition to a diffuse cytosolic staining, whereas in *atg1Δ* cells, Atg23 was restricted to a single bright punctate structure, which corresponds to the PAS, in agreement with previous data (Fig. 3.4A and 3.4D) (186, 230). Atg23 was similarly restricted to the PAS in *atg13Δ* cells (data not shown) (230), but was dispersed in the cytosol in the absence of Atg9, apparently no longer membrane-associated (Fig. 3.4B) (230). To better understand the temporal order of factors involved in movement of Atg23 between its subcellular locations, we performed an epistasis study analyzing the localization of Atg23 in strains harboring deletions of different combinations of genes required for proper Atg23 localization.

In an *atg1Δ atg9Δ* strain, Atg23-GFP was evenly dispersed in the cytosol, similar to its localization in cells only deleted for *ATG9* (Fig. 3.4B), indicating that Atg9

90

functions before Atg1 in Atg23 localization. Similarly, in cells lacking both Atg9 and

Atg13, Atg23-GFP exhibited a cytosolic localization (data not shown). Atg23-GFP was

restricted to the PAS in *atg1Δ atg13Δ* cells (data not shown), similar to its distribution in

either of the single mutants. We did not observe the appearance of free GFP in Atg23-

GFP strains harboring *ATG9* deletions when extracts were analyzed by western blot (data

not shown), suggesting that the chimeric Atg23-GFP protein was stable and the

generation of free GFP did not account for the dispersed localization pattern. Furthermore,

we found that protein A-tagged Atg23 was stable in both *atg9Δ* and *atg1Δ atg9Δ* cells

(Fig. 3.4C), further suggesting that lack of stability did not account for the loss of

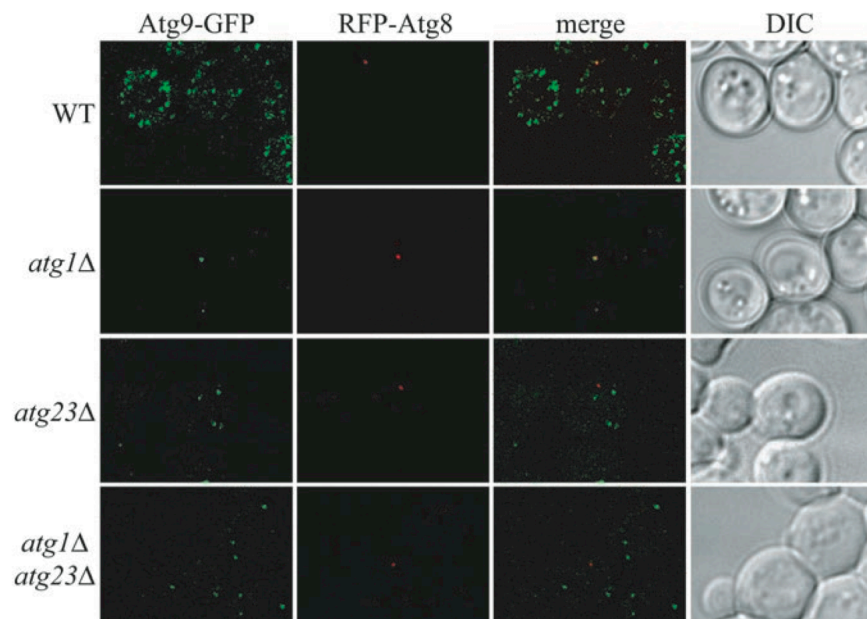punctate staining.

Figure 3.3. Atg23 is required for Atg9 localization at the PAS. The wild-type (JLY44), *atg1Δ* (JLY45), *atg23Δ* (JLY49) and *atg1Δ atg23Δ* (JLY46) strains, expressing Atg9-GFP were transformed with the plasmid encoding RFP-Atg8, grown to mid-log phase and fixed with 1.5% formaldehyde prior to examination by fluorescence microscopy. DIC, differential interference contrast.

In wild-type cells, one Atg23-GFP puncta colocalized with the PAS marker, RFP

-Atg8 (Fig. 3.4D). Finally, we observed Atg23-GFP in both *atg27Δ* and *atg1Δ*

atg27Δ cells and found that in these mutants, Atg23-GFP was seen in multiple puncta,

but was unable to move to the PAS, as detected by lack of colocalization with the PAS

marker, RFP-Atg8 (Fig. 3.4C). As a control, Atg23-GFP in *atg1Δ* cells was restricted to a

single punctate structure that corresponds to the PAS, shown by colocalization with RFP-

Atg8 (Fig. 3.4C). No difference in the localization pattern was observed upon nutrient

deprivation of the same cells (data not shown). We concluded from these results that

Atg27 function in Atg23 localization, like that of Atg9, occurs prior to that of Atg1.
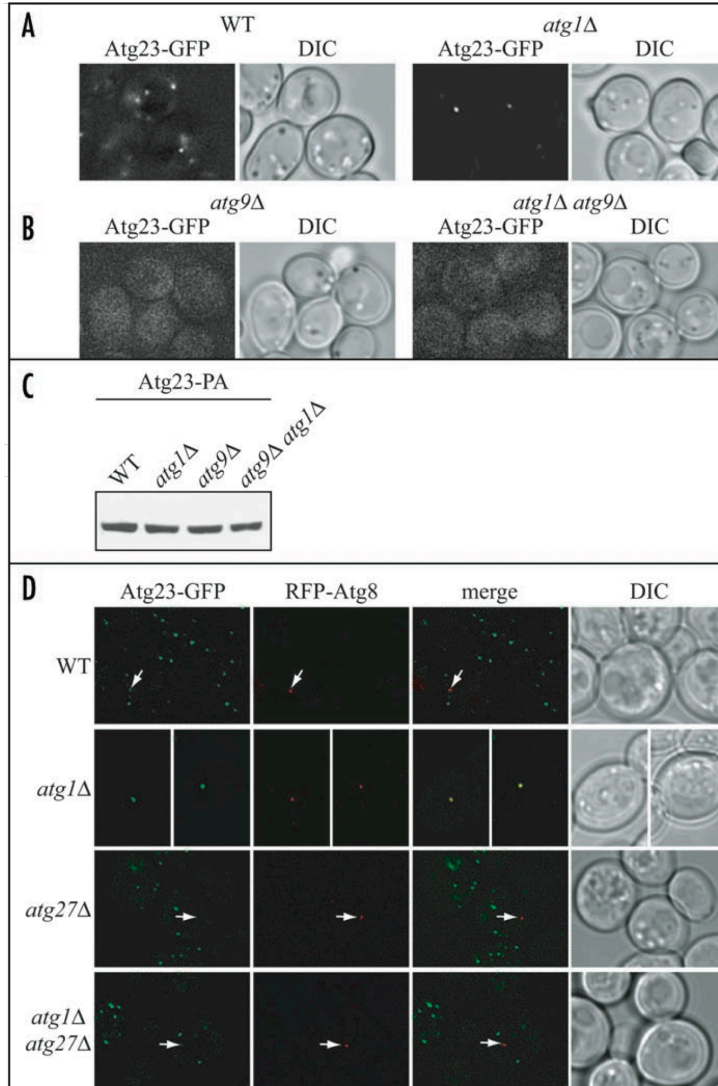
Figure 3.4. Atg23 localization required Atg1, Atg9, and Atg27. (A) Chromosomally-tagged Atg23-GFP fusion protein was examined by fluorescence microscopy in both wild-type (KTY25) and *atg1Δ* (KTY29) strains, grown to mid-log phase. (B) Integrated Atg23-GFP *atg9Δ* (KTY32) and *atg1Δ atg9Δ* (JLY73) cells were prepared as described for (A). (C) Cell extracts from strains expressing Atg23 chromosomally tagged with protein A (Atg23-PA) in wild-type (JLY68), *atg1Δ* (JLY76), *atg9Δ* (JLY74), and *atg1Δ atg9Δ* (JLY98) backgrounds were resolved by SDS-PAGE, and the Atg23-PA fusion protein was visualized by immunoblotting with antibodies against protein A. (D) The wild-type (JLY65), *atg1Δ* (KTY29), *atg27Δ* (JLY94), and *atg1Δ atg27Δ* (JLY95) strains additionally harboring Atg23-GFP were transformed with an RFP-Atg8 plasmid, fixed and processed as described in Materials and Methods, and imaged by fluorescence microscopy. The arrows mark the position, or relative position, of RFP-Atg8. DIC, differential interference contrast.

93

Atg27 localization is dependent upon Atg23.

Atg27 shares a localization pattern similar to Atg9 and Atg23, and was required for movement of both proteins to the PAS (Fig. 3.4D) (263). We next determined whether Atg27 has a similar requirement for its localization. In wild-type cells, Atg27 was localized to multiple punctate structures, one of which is the PAS (Fig. 3.5) (263). Similar to Atg9 and Atg23, Atg27 was restricted to a single dot, which has been identified as the PAS (263), in an *atg1Δ* strain (Fig. 3.5). In the absence of Atg23, Atg27 was unable to localize to the PAS; this phenotype was most evident in the *atg1Δ atg23Δ* double mutant where Atg27-GFP did not colocalize with the PAS marker protein RFP-Atg8 (Fig. 3.5). Furthermore, Atg9 was also required for Atg27 retrograde movement at the PAS, whereas Atg13 was required for Atg27 retrograde movement from the PAS to the mitochondria (263). Observation of the cells after starvation yielded a similar distribution of Atg27 (data not shown). Therefore, we concluded that Atg23 and Atg9 are required for Atg27 anterograde movement to the PAS, whereas the Atg1-Atg13 protein complex is needed for its transport from the PAS to the peripheral sites.
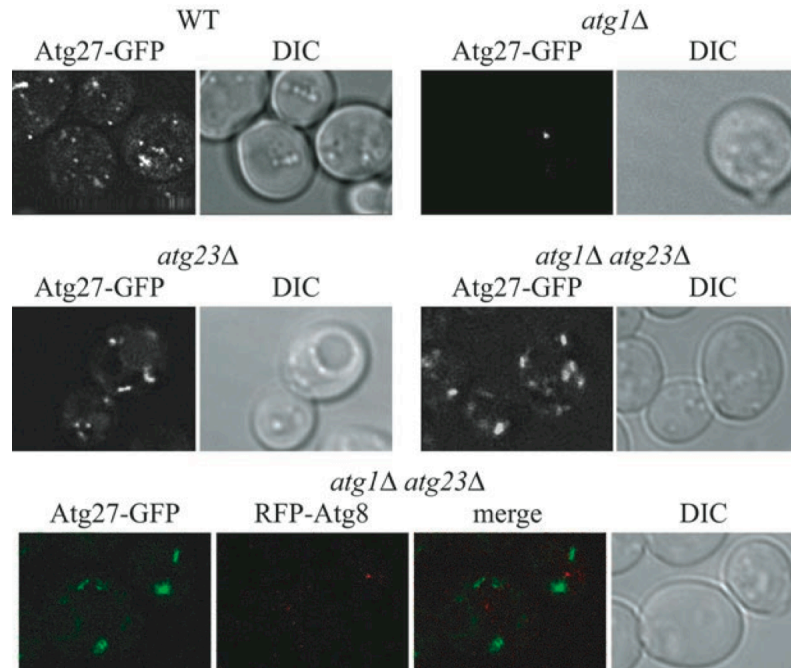
Figure 3.5. Atg1 and Atg23 are necessary for proper localization of Atg27. (A) The wild-type (WLY5), *atg1Δ* (WLY11), and *atg1Δ atg23Δ* (WLY15) strains expressing chromosomally-tagged Atg27-GFP, and *atg23Δ* (KTY14) cells transformed with a plasmid encoding Atg27-GFP were prepared for, and viewed by fluorescence microscopy as outlined in Materials and Methods. For colocalization analysis, *atg1Δ atg23Δ* cells expressing RFP-Atg8 underwent mild fixation before imaging. DIC, differential interference contrast.

Atg9, Atg23, and Atg27 interact with one another

The fact that Atg9, Atg23, and Atg27 exhibit a similar localization and that each play a role in both of the other proteins' movement suggests that these proteins directly interact. Accordingly, we examined potential interactions through a yeast two-hybrid analysis. A yeast two-hybrid strain transformed with various combinations of plasmids encoding either full-length or truncated Atg9, Atg23, or Atg27 was grown on selective plates lacking either histidine or adenine. We detected interactions between all three of the full-length versions of these proteins (Table 3.2). In addition, full-length Atg9 self-interacted, in agreement with previous data (185), whereas we did not detect a self-interaction of Atg23 or Atg27 (Table 3.2). Evaluation of interactions with truncated Atg9 constructs revealed that Atg23 interacted with both the amino-and carboxy-termini of Atg9 and had a barely detectable interaction with the carboxy terminus. Neither protein interacted with a truncated Atg9 consisting of only the transmembrane region (Table. 3.2). Plasmids encoding truncated Atg27 demonstrated that both the amino- and carboxy-terminal ends of Atg27 interacted with Atg9 and Atg23. Atg27 lacking only the carboxy-terminal cytosolic tail also interacted with full-length Atg9 and Atg23.

To further dissect these interactions, we performed a similar analysis in strains that lacked Atg9, Atg23 or Atg27. These experiments showed that the Atg9-Atg23 and the Atg9-Atg27 interactions were unaffected by the absence of Atg27 and Atg23, respectively (Table 3.2). In contrast, a strong interaction between Atg23 and Atg27 required the presence of Atg9. These data suggested that the Atg9-Atg23 and Atg9-Atg27 interactions were direct, whereas the interaction between Atg23 and Atg27 was largely indirect, and may be mediated by Atg9.

Table 3.2 Atg23, Atg27, and Atg9 interaction by yeast two-hybrid assay

Strain	Interactions	Atg23	Atg27	Atg9
WT	Atg9FL	++++	+++	++++
WT	Atg9TM	−	−	n.d.
WT	Atg9N	++	+	n.d.[b]
WT	Atg9C	++	+/−	n.d.[c]
WT	Atg23	−	++	++
WT	Atg27	++	−	+++
WT	Atg27N	++	n.d.	++
WT	Atg27C	++	n.d.	++
WT	Atg27ΔC	++	n.d.	++
atg9Δ	Atg27	+/−	n.d.	n.d.
atg23Δ	Atg9	n.d.	+++	n.d.
atg27Δ	Atg9	+++	n.d.	n.d.

Table 3.2. The wild-type (PJ69-4A), *atg9Δ* (JLY86), *atg23Δ* (JLY87), or *atg9Δ* (JLY88) yeast two-hybrid strains were transformed with vectors containing full-length or truncated Atg9, Atg23, or Atg27, as indicated. All transformations were performed along with a negative control using the empty AD or BD vectors, as appropriate. Cells were first grown on plates selective for the plasmids, lacking leucine and uracil. Subsequently, transformants were restreaked onto plates also lacking histidine or adenine. The strength of interaction is indicated by the number of pluses, as follows: "+" indicates a very week interaction (e.g., growth only after three or more days, and only on plates lacking histidine), "++" designates a weak interaction, "+++" denotes a strong interaction, and "++++" represents a very strong interaction (e.g., growth after one or two days on plates lacking adenine). ""+/−" indicates a barely detectable interaction, and "−" means no interaction was detected. Thus, the strength of interaction was determined by the time needed for, and robustness of, growth and the plates on which they were grown. The proteins expressed were full-length unless otherwise stated. Atg9FL indicates the full-length protein, Atg9N or Atg27N and Atg9C or Atg27C represent only the cytosolic amino and carboxy termini of each portion of this protein. The exact lengths of each of the above-mentioned truncation mutants are described in Materials and Methods. N.d., not determined.; [b]Atg9N self-interacts (unpublished results); [c]Atg9C self-interacts (unpublished results).

To verify the results from the yeast two hybrid analysis, we performed affinity isolation and immunoprecipitation experiments using cells in which Atg23 was chromosomally-tagged with carboxy-terminal protein A (Atg23-PA). Lysates expressing Atg23-PA in addition to hemagglutinin-tagged Atg27 (Atg27-HA) were prepared and Atg23-PA, along with any associated proteins, was isolated with IgG sepharose. The affinity isolates were eluted from the IgG sepharose beads, and the eluate was evaluated by SDS-PAGE and western blotting, as described in Materials and Methods.

We found that both Atg9 (detected with antisera to the endogenous protein) and Atg27-HA were coisolated with Atg23-PA (Fig. 3.6A). Furthermore, the interaction between Atg9 and Atg23-PA did not depend upon Atg27, as Atg9 was present in the affinity eluate from *atg27Δ* cells. Supporting the yeast two-hybrid data, Atg23-PA did not interact with Atg27 in the absence of Atg9 (Fig. 3.6A). Similar results were obtained from immunoprecipitation experiments in which Atg27-HA was isolated from cell lysates and the eluates were examined for the presence of Atg23-PA and Atg9; these anti-HA immunoprecipitation data also supported a direct interaction between Atg27 and Atg9, and an indirect Atg27-Atg23 interaction mediated by Atg9 (data not shown). There was a slight discrepancy in that we detected a minimal Atg23-Atg27 interaction in *atg9Δ* cells by the two-hybrid assay (Table. 3.2), whereas the same interaction was not detected by affinity isolation and immunoprecipitation. However, we think this simply represents the differences in the experimental conditions employed in the two sets of assays. The affinity isolation experiments examined proteins expressed at physiological levels and the interactions presumably occur at the normal subcellular site. In contrast, in the two-hybrid assay, the proteins were overexpressed, and the interactions occurred in the

nucleus. We conclude from the yeast two-hybrid assay and the affinity isolation results that Atg23 interacts directly with Atg9 both at the amino and carboxy termini, and Atg7 interacts directly with the amino terminus of Atg9, whereas the interaction between Atg23 and Atg27 is not direct, but is mediated by Atg9 (Table 3.2, Fig. 3.6).

We next asked where in the cell these interactions occur. Atg1 and Atg11 are proteins that are critical for proper assembly and localization of factors required for the Cvt pathway and autophagy. In *atg1Δ* cells, most of the Atg proteins are localized to the PAS (101, 222), perhaps unable to dissociate from this location. Moreover, in the absence of Atg11, there is no identifiable PAS, suggesting that proteins can no longer assemble at this structure (209). Taking advantage of these properties, we examined the ability of Atg23 to interact with Atg9 and Atg27 at different subcellular locations. Atg23-PA affinity isolates contained Atg9 and Atg27-HA in both *atg1Δ* and *atg11Δ* cells. As negative controls, the aforementioned strains with *ATG9* additionally deleted were utilized. The results indicated that Atg23 resides at the PAS and non-PAS locations within the cell, but the association between Atg23 and Atg27 at both subcellular locations requires Atg9.
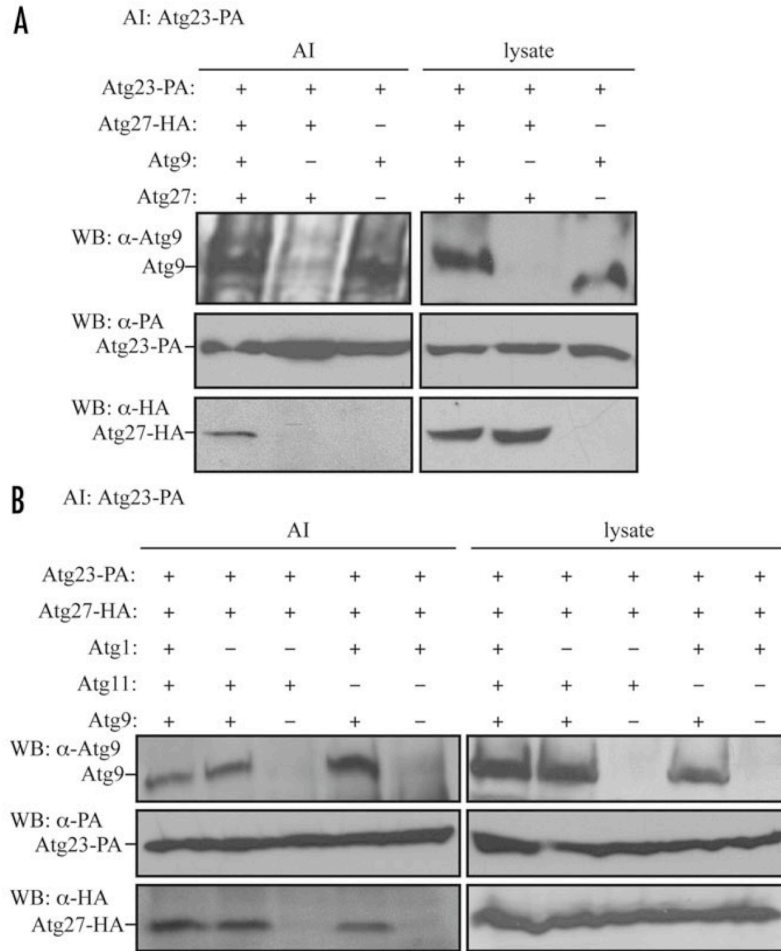
A AI: Atg23-PA

	AI			lysate		
Atg23-PA:	+	+	+	+	+	+
Atg27-HA:	+	+	−	+	+	−
Atg9:	+	−	+	+	−	+
Atg27:	+	+	−	+	+	−

WB: α-Atg9 Atg9

WB: α-PA Atg23-PA

WB: α-HA Atg27-HA

B AI: Atg23-PA

	AI					lysate				
Atg23-PA:	+	+	+	+	+	+	+	+	+	+
Atg27-HA:	+	+	+	+	+	+	+	+	+	+
Atg1:	+	−	−	+	+	+	−	−	+	+
Atg11:	+	+	+	−	−	+	+	+	−	−
Atg9:	+	+	−	+	−	+	+	−	+	−

WB: α-Atg9 Atg9

WB: α-PA Atg23-PA

WB: α-HA Atg27-HA

Figure 3.6. Atg23 interacts with Atg9 and Atg27 by affinity isolation. Extracts were prepared from Atg23-PA Atg27-HA (JLY68), Atg23-PA Atg27-HA *atg9Δ* (JY74), Atg23-PA *atg27Δ* (JLY67), Atg23-PA Atg27-HA *atg1Δ* (JLY76), Atg23-PA Atg27-HA *atg1Δ atg9Δ* (JLY105), Atg23-PA Atg27-HA *atg11Δ* (JLY77) and Atg23-PA Atg27-HA *atg9Δ atg11Δ* (JLY106) strains as outlined in Materials and Methods. Atg23-PA-containing fractions were extracted using IgG-sepharose beads and affinity isolates were resolved by SDS-PAGE. Western blots with anti-Atg9, anti-PA and anti-HA antisera were performed by standard procedures. For each lane, 2% of cell lysate or 20% of affinity isolates was loaded. Strains deleted for the protein of interest served as negative controls. AI, affinity isolate; WB, Western blot.

Discussion

During the initial identification and characterization of the 29 gene products now denoted as the Atg proteins, Atg9, Atg23, and Atg27 were all separately examined and described (161, 230, 263). Along with these characterizations, the proteins' functions were assigned to a discrete step within the Cvt pathway and/or autophagy. Accordingly, Atg9, Atg23, and Atg27 were all found to be required for completion of the forming autophagosome/Cvt vesicle (161, 230, 263). Furthermore, it was discovered that these three components exhibit an unusual localization pattern, residing in multiple punctate perivacuolar and cytosolic compartments. A more recent investigation revealed that both Atg9 and Atg23 are cycling proteins, which move between the PAS and other structures (186). Our laboratory ultimately identified a portion of these other Atg9-harboring structures as discrete sites on or near the mitochondrial membrane (185). Here we show that Atg23 is similarly distributed in part among the PAS, sites at or near the mitochondria, and at other unidentified punctate structures. Recently, mammalian Atg9 was found to localize to the Golgi complex and late endosomes (267), but did not show localization near the mitochondria. Atg9 in *Pichia pastoris* showed either a reduced (185) or a complete lack of localization with mitochondria (26); however, although the *S. cerevisiae* and *P. pastoris* proteins both show a cycling phenotype, there are distinct differences with regard to the specific requirements (26).

One of the intriguing questions regarding the field of autophagy concerns the source of the membrane for the nascent sequestering vesicles (84, 109, 203). Until recently, Atg9 was the only known integral membrane Atg protein involved in vesicle

formation; accordingly, it has been the focus of studies attempting to indentify the membrane source for nascent autophagosome and Cvt vesicles (185). Additionally, our laboratory recently characterized another transmembrane protein, Atg27, which localizes to the PAS, sites at or near the mitochondrial membrane and to the Golgi complex, in addition to other punctate sites (263). Considering these data and the fact that the PAS marker protein Atg8 may localize to the Golgi complex (127, 187), we proposed that the mitochondria and Golgi complex are both potential membrane sources for autophagy and the Cvt pathway, however, we note that no direct data yet demonstrate that any of these sources directly provide membrane during autophagy-related processes.

In the Cvt pathway, only two Atg proteins remain associated with the completed vesicles, Atg8 and the Cvt pathway cargo receptor Atg19 (105, 201). Thus, another unresolved aspect of autophagy is the mechanism by which proteins are retrieved from the vesicle prior to or following completion. A recent study identified factors required for retrograde trafficking of both Atg9 and Atg23, revealing that the Atg1-Atg13 kinase complex is needed for release of both of these factors from the PAS, although normal Atg1 kinase activity is required only for Atg23 movement (186). To complement this analysis, we sought to identify protein components that participate in anterograde traffic (movement to the PAS) of these cycling proteins. We showed that Atg23 and Atg27 are needed for anterograde movement of Atg9. Similarly, movement of Atg27 to the PAS required Atg9 and Atg23, and Atg23 PAS transport required Atg27.

Given the codependence of these three proteins for proper cycling, it was not surprising to find that they interacted, both by yeast two-hybrid and affinity isolation experiments (Table 3.2 and Fig. 3.6). We found that these proteins likely formed a

hetero-trimeric complex and we speculatively place Atg9 oligomers positioned in the center, and Atg23 and Atg27 flanking these clusters based on analysis of truncated protein interactions (Table 3.2 and Fig. 3.7). It seems also that this complex exists both at the PAS and distinct regions at non-PAS sites. These biochemical data are supported by fluorescence microscopy showing that Atg9, Atg23, and Atg27 all colocalize with one another, both at peripheral sites and at the PAS (Fig. 3.1 and 3.2) (263).

The role of these three proteins in membrane recruitment and/or Atg protein retrieval is still not known. We propose that Atg9, Atg23, and Atg27 are all involved in bringing membrane to the forming vesicles, with Atg9 absolutely required for this process during both vegetative and starvation conditions, whereas Atg23 and Atg27 are needed for efficient Cvt vesicle formation and to recruit membrane or recycle protein components in order to form a larger number of autophagosomes. The cycling of these proteins is required for their proper function, because mutants defective in cycling are also defective in autophagy or the Cvt pathway. Further studies will doubtless increase our understanding of the movement of these proteins, and their role in autophagosome formation, and give us insight into the mechanism of the same process in higher eukaryotes.
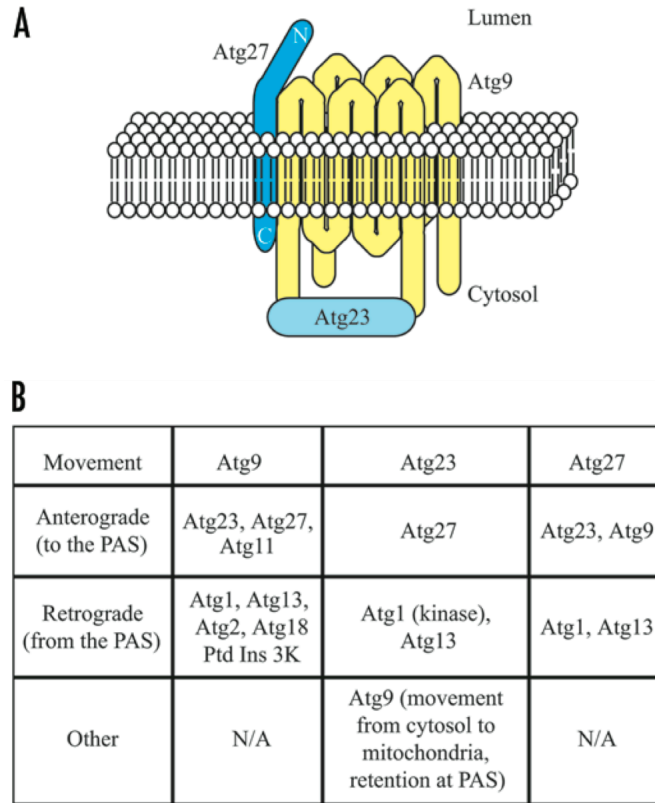
A

B

Movement	Atg9	Atg23	Atg27
Anterograde (to the PAS)	Atg23, Atg27, Atg11	Atg27	Atg23, Atg9
Retrograde (from the PAS)	Atg1, Atg13, Atg2, Atg18 Ptd Ins 3K	Atg1 (kinase), Atg13	Atg1, Atg13
Other	N/A	Atg9 (movement from cytosol to mitochondria, retention at PAS)	N/A

Figure 3.7. Summary of Atg9, Atg23, and Atg27 interactions and requirements for proper cycling.
These data are compiled from results presented throughout this paper, and from previous studies (68, 186, 263). Although these three proteins interact, their movement is not necessarily coincident, given that the requirements for movement are not identical for all three. (A) Schematic representation of Atg9, Atg23, and Atg27 and their regions of interaction. (B) Chart indicating factors required for anterograde and retrograde cycling of Atg9, Atg23, and Atg27.

Materials and Methods

Yeast strains and media

The *S. cerevisiae* strains used in this study are listed in Table 3.1. Gene disruptions were accomplished by replacing the entire coding region with either the *Kluyveromyces lactis HIS3, Schizoaccharomyces pombe HIS5, Escherichia coli kan^r,* or *Saccharomyces cerevisiae TRP1, LEU2,* or *URA3* genes using PCR primers containing ~45 bases of identity to the regions flanking the open reading frame. For PCR-based integration of the protein A (PA), GFP, RFP or triple HA tag at the 3' ends of *ATG23, ATG27*, and *ATG9* genes were used to generate strains expressiong fusion proteins under th control of their native promoters. The templates for integration were pFA6a-PA-HIS3, pFA6a-HA-TRP1, pFA6a-GFP-TRP1, pFA6a-GFP-KAN, pFA6a-RFP-TRP1 or pFA6a-RFP-HIS5 *S.p.* (1, 24, 42, 138).

Yeast cells were grown in rich medium (YPD; 1% yeast extract, 2% peptone, 2% glucose) or synthetic minimal medium (SMD; 0.67% yeast nitrogen base, 2% glucose, amino acids, and vitamins as needed). Starvation experiments were conducted in synthetic medium lacking nitrogen (SD-N; 0.17% yeast nitrogen base without amino acids, 2% glucose).

Plasmids

To generate the plasmid pTPI1-Atg27-GFP(416), the *ATG27* gene was amplified from *S. cerevisiae* genomic DNA by PCR and cloned as a *Hind*III-*Age*I fragment into the same sites in the pSNA3(416) plasmid (184). PpGAD-Atg9, pGBDU-Atg9, RFP-Ape1

(pRS305-RFP-Ape1), pSpo7-RFP (425), and pYESmtBFP have been described elsewhere (1, 161, 185, 218, 246).

The RFP-Atg8 plasmid was constructed as follows: The DNA fragment encoding mRFP with *BamH*I sites on both ends was ligated to the *Bgl*II site of pAUT7*Bgl*II (414) (1), in which the *Bgl*II site was introduced just after the initiation codon of the *ATG8* ORF by site-directed mutagenesis, to generate pRFP-Atg8 (414). Yeast two-hybrid plasmids pGAD-Atg27, pGBDU-Atg27, pGAD-Atg27N (amino acids 1-199), pGBDU-Atg27N, pGAD-Atg27C (amino acids 222-271), pGBDU-Atg27C, pGAD-Atg27ΔC (amino acids 1-221), and pGBDU-Atg27ΔC were created by PCR amplifying either the full-length gene or the truncated ORFs and ligating into the *BamH*I/*Sal*I sites of the pGAD-C3 and pGBDU-C1 vectors.

The plasmids pGAD-Atg9N (amino acids 1-320), pGBDU-Atg9N, pGAD-Atg9TM (amino acids 321-665), pGBDU-Atg9TM, pGAD-Atg9C (amino acids 666-998), pGBDU-Atg9C, were created by PCR-amplifying the full-length gene or truncated ORFs and ligating into the *BamH*I/*Sal*I sites of the pGAD-C1 and the pGBDU-C3 vectors for yeast two-hybrid analysis.

Protein A affinity isolation

Cells were grown in YPD to $OD_{600} = 1.0$, and 100 OD_{600} units of cells were harvested. Cells were then resuspended in ice-cold lysis/IP buffer (140 mM NaCl, 27 mM KCl, 10 mM Na_2HPO_4, 1.8 mM KH_2PO_4, pH 7.2, 200 mM sorbitol, 1 mM $MgCl_2$, 0.1% Tween-20, 2 mM PMSF and protease inhibitor cocktail (Roche Diagnostics, Mannheim, Germany)), and extracts were generated by glass beads lysis. The lysates were then

incubated with IgG sepharose beads or rabbit anti-HA antibodies and protein-A

sepharose for 1 h at 4 °C, and washed 6 times with 1 ml of lysis/IP buffer. Proteins were

eluted by resuspending in cold sample buffer with 2 mM PMSF and incubating at 55°C

for 15 min. They were then resolved by SDS-PAGE and visualized by western blot using

antibodies or antiserum against HA, PA, or Atg9 (161).

Fluorescence microscopy

Cells expressing fluorescently tagged fusion proteins were grown to mid-log

phase in rich or selective media, as appropriate. For nitrogen starvation, cells were

transfer to SD-N for 1 h. For all colocalization studies, cells were subjected to mild

fixation conditions, as follows: Cultures were grown as stated, harvested and resuspended

in fixation buffer (50 mM KH_2PO_4, pH 8.0, 1.5% formaldehyde, 1 μM $MgCl_2$) and

incubated at room temperature for 30 min with gentle mixing. After fixation, cells were

washed once with wash buffer (50 mM KH_2PO_4, pH 8.0, 1μM $MgCl_2$), resuspended in a

small volume of wash buffer and visualized. Fluorescence microscopy was performed on

an Olympus IX71 fluorescence microscope (Olympus, Mellville, NY). The images were

documented by a Photometrics CoolSNAP HQ camera (Roper Scientific, Inc., Tucson,

AZ) and deconvolved using DeltaVision software (Applied Precision, Issaquah, WA).

CHAPTER 4

The Conserved Oligomeric Golgi Complex Functions as a Tethering Factor in Autophagy

Abstract

Autophagy is a catabolic pathway for the turnover of long-lived proteins and organelles in eukaryotic cells. In the yeast *Saccharomyces cerevisiae,* the biosynthetic cytoplasm to vacuole targeting (Cvt) pathway that targets a subset of resident hydrolases to the vacuole shares a similar morphology and uses many of the same molecular components as autophagy. In both pathways, the cargos that have to be delivered to the vacuole are sequestered into double-membrane vesicles. The mechanism of vesicle formation and completion are the most complex steps and remain unclear. Here, we characterize the role of the conserved oligomeric Golgi (COG) complex in the Cvt and autophagy pathways. The lobe A subunits (Cog2 to Cog4) are involved in both the Cvt pathway and autophagy, whereas the lobe B components (Cog5 to Cog8) are Cvt-specific. The localization of this complex to the phagophore assembly site (PAS) and its interaction with autophagy-related proteins suggests a role in the membrane tethering and fusion events during formation of the double-membrane vesicle.

Introduction

Macroautophagy (hereafter autophagy), an evolutionarily conserved catabolic pathway in eukaryotic cells, is involved in the degradation of long-lived proteins, organelles, and a large portion of the cytoplasm in response to internal and external stresses, such as nutrient starvation (132, 182). In addition, autophagy is involved in development and cellular remodeling, and plays a cytoprotective role by removing protein aggregates, and damaged or superfluous organelles, which may contribute to a role in life span extension (113, 208, 262). Defects in autophagy are associated with various diseases, such as cancer, gastrointestinal disorders and neurodegeneration (73, 165, 208). The hallmark of autophagy is the sequestration of bulk cytoplasm into a double-membrane vesicle, termed an autophagosome, which then fuses with the lysosome/vacuole releasing the inner vesicle for degradation (113). Genetic screens in *Saccharomyces cerevisiae* and other fungi have identified more than 30 AuTophaGy-related (*ATG*) genes that are involved in autophagy (111), and orthologues of many of the yeast *ATG* genes have been identified in higher eukaryotes.

Although autophagy is generally considered to be a non-selective process, several selective autophagic pathways for specific cargo delivery have been reported in both fungi and mammalian cells. One example in the yeast *S. cerevisiae* is a constitutive biosynthetic pathway that occurs under vegetative conditions, termed the cytoplasm to vacuole targeting (Cvt) pathway, in which certain vacuolar hydrolases such as precursor aminopeptidase I (prApe1) is enwrapped in double-membrane vesicles, called Cvt vesicles, which fuse with the vacuole (103, 112, 200). The Cvt pathway shares similar

morphological and mechanistic features with bulk autophagy and requires most of the same Atg proteins. In addition, other specific autophagy pathways such as the degradation of excess peroxisomes or mitochondria, termed pexophagy and mitophagy, respectively, use the same Atg components as the Cvt pathway (43, 91). Therefore, the study of the Cvt pathway and the analysis of the roles of the various Atg proteins have provided important information for understanding the molecular basis of autophagy; however, many questions remain to be addressed.

One of the unsolved mysteries with regard to autophagy is the origin of the membrane used to form the double-membrane sequestering vesicles, and the mechanism of vesicle expansion (182). The autophagosome and Cvt vesicle are thought to form *de novo*, meaning they do not bud off intact from pre-existing organelles as occurs with transport vesicles that function in the secretory pathway. Instead, the double-membrane vesicles appear to expand via the addition of membrane through vesicular fusion; this mode of formation is critical in allowing these sequestering vesicles to accommodate essentially any sized cargo. Recent data from studies monitoring Atg9 in yeast suggest that mitochondria may be one of the membrane sources for autophagic vesicles. Atg9 is an integral membrane protein that is essential for both the Cvt and autophagy pathways. Unlike most of the Atg proteins, Atg9 is present in multiple puncta in the cell, and it cycles between peripheral sites that appear to include mitochondria, and the phagophore assembly site (PAS), the putative site for Cvt vesicle and autophagosome assembly (101, 185, 222). Thus, Atg9 has been suggested to mark the membrane that is donated to the expanding double-membrane phagophore, the initial membrane structure that ultimately forms the autophagosome (161, 185, 186). In addition to the mitochondria, proper

110

membrane flow from the endoplasmic reticulum (ER) and Golgi complex is required for

normal progression of both the Cvt pathway and autophagy, and also for proper Atg9

sorting (78, 187). Even with the characterization of several Atg proteins and the

relationship between the secretory pathway and autophagy, it is still not clear how the

double-membrane vesicles are being produced. Moreover, very little information is

available regarding the presumed tethering and fusion components that are involved in

this process. In this report, we screened the yeast deletion library, and a set of

temperature sensitive mutants and found that mutants of the conserved oligomeric Golgi

(COG) complex subunits were defective in the Cvt pathway. In *S. cerevisiae*, the COG

complex contains 8 subunits (Cog1 to Cog8) and Cog1 is a central subunit that connects

two lobes: lobe A (Cog2 to Cog4) and lobe B (Cog5 to Cog8)(98, 179, 221, 235, 236,

247). Although only six of the yeast COG subunits show high sequence homology with

their corresponding mammalian counterparts, the COG complex is structurally and

functionally conserved (231). The current evidence suggests that COG is mainly

important for retrograde trafficking within the Golgi complex, and possibly for ER-to-

Golgi and endosome-to-Golgi transport, as a tethering factor (18, 98, 166, 179, 221, 235,

236, 247). Moreover, several pieces of evidence indicate that lobe A may be involved in

different and more essential processes than lobe B; defects in any of the COG subunits in

lobe A have more severe effects on cell growth than those in lobe B (18, 166, 215, 241,

247, 251). Here, we discovered that the lobe A, but not the lobe B, subunits are essential

for autophagy. Additionally, the COG complex is involved in autophagosome formation

and is required for correct sorting of various Atg membrane-associated proteins to the

phagophore assembly site (PAS). COG subunits localize to the PAS, and interact with

Atg proteins. This is the first evidence showing that a tethering complex functions in the

formation of double-membrane sequestering vesicles during autophagy.

Results

The COG complex is involved in the Cvt pathway and autophagy

Previously we screened the yeast deletion library to obtain mutants defective in the Cvt pathway (160, 188, 218). Of the mutants we identified, the *cog1*Δ strain exhibited a relatively strong block in prApe1 maturation (Fig. 4.1A). In rich medium in a wild-type strain, most of the Ape1 is present in the mature form as a result of delivery to the vacuole through the Cvt pathway. In the *cog1*Δ mutant, all of the Ape1 was present in the precursor form in rich medium conditions, indicating a block in the Cvt pathway.

Cog1 is one of the components of the conserved oligomeric Golgi complex Therefore, we examined whether the other components of this complex were also involved in the Cvt pathway. Deletion of *COG5*, *COG6*, *COG7* or *COG8* caused an incomplete, but substantial block in prApe1 maturation in rich medium (Fig. 4.1A). Treatment of yeast cells with the Tor inhibitor rapamycin induces autophagy, and causes an increase in prApe1 synthesis, and this cargo protein is now transported to the vacuole through autophagy. In wild-type cells treated with rapamycin, the majority of Ape1 is still detected as the mature form despite the substantial increase in synthesis. Rapamycin treatment of the *COG* deletion strains, particularly those of lobe B, largely rescued the defect in prApe1 transport to the vacuole, suggesting that the selective uptake of prApe1 via autophagy occurred in these strains (Fig. 4.1A); the *cog1*Δ strain showed an approximately 50% block in prApe1 maturation, suggesting a significant block in nonspecific autophagy.

Table 4.1. Yeast strains used in this study.

Strain	Genotype	Source or reference
BCR29	*MATa his3Δ1 leu2Δ0 lys2Δ0 ura3Δ0 cog4Δ::KAN* pBCR115	This study
BCR47	*MATa his3Δ1 leu2Δ0 lys2Δ0 ura3Δ0 cog4Δ::KAN* pBCR137	This study
BY4742	*MATα his3Δ1 leu2Δ lys2Δ ura3Δ*	ResGen™
cog1Δ	BY4742 *cog1Δ::KAN*	ResGen™
cog5Δ	BY4742 *cog5Δ::KAN*	ResGen™
cog6Δ	BY4742 *cog6Δ::KAN*	ResGen™
cog7Δ	BY4742 *cog7Δ::KAN*	ResGen™
cog8Δ	BY4742 *cog8Δ::KAN*	ResGen™
GWY93	*MATα ura3-52 leu2-3 his- cog2-1*	(253)
GWY95	*MATα ura3-52 leu2-3 his- cog3-2*	(253)
IRA001	BY4742 *PEX14-GFP:: HIS3*	(183)
IRA002	BY4742 *PEX14-GFP:: HIS3 atg1Δ::URA3*	(183)
IRA030	DDY1797 *ATG9-3GFP::URA3*	(154)
IRA031	DDY1797 *ATG9-3GFP:: URA3 atg1Δ::HIS5*	(154)
PJ69-4A	*MATα leu2-3,112 trp1-Δ901 ura3-52 his3-Δ200 gal4Δ gal80Δ LYS2::GAL1-HIS3 GAL2-ADE2 met2::GAL7-lacZ*	(80)
RSY250	*MATα ura3-52*	Randy Scheckman
SEY6210	*MATα ura3-52 leu2-3,112 his3-Δ200 trp1-Δ901 lys2-801 suc2-Δ9 mel GAL*	(190)
WLY05	SEY6210 *ATG27-GFP::HIS3*	(263)
WLY11	SEY6210 *atg1Δ::URA3 ATG27-GFP::HIS3*	(263)
WLY88	BY4742 *cog1Δ::KAN ATG27-GFP::HIS3*	This study
WLY90	BY4742 *cog2-1::KAN PEX14-GFP::HIS3*	This study
WLY91	BY4742 *cog3-2::KAN PEX14-GFP::HIS3*	This study
WLY94	BY4742 *atg1Δ::URA3 cog1Δ::KAN ATG27-GFP::HIS3*	This study
WLY96	BY4742 *cog1Δ::KAN ATG27-GFP::HIS3 RFP-APE1::LEU2*	This study
WLY97	BY4742 *cog6Δ::KAN ATG27-GFP*::HIS3 *RFP-APE1::LEU2*	This study
WLY98	BY4742 *atg1Δ::URA3 cog6Δ::KAN ATG27-GFP*::HIS3 *RFP-APE1::LEU2*	This study
WLY100	SEY6210 *ATG27-GFP::HIS3 VRG4-RFP::TRP1 cog6Δ::URA3*	This study
WLY101	SEY6210 *ATG27-GFP::HIS3 VRG4-RFP::TRP1 cog1Δ::LEU2*	This study
WLY103	SEY6210 *ATG27-GFP::HIS3 VRG4-RFP::TRP1 cog1Δ::LEU2 atg1Δ::URA3*	This study
WLY153	SEY6210 *atg1Δ::HIS3 COG1-GFP::TRP1 RFP-APE1::LEU2*	This study
WLY154	SEY6210 *COG1-GFP::TRP1 RFP-APE1::LEU2*	This study

WLY155	SEY6210 *atg1Δ::HIS3 COG6-GFP::TRP1 RFP-APE1::LEU2*	This study
WLY156	SEY6210 *COG6-GFP::TRP1 RFP-APE1::LEU2*	This study
WLY166	BY4742 *cog2-1::KAN vam3Δ::ble*	This study
WLY174	BY4742 *cog6Δ::KAN PEX14-GFP::HIS3*	This study
WLY175	BY4742 *cog1Δ::KAN PEX14-GFP::HIS3*	This study
WLY188	SEY6210 *cog2-1-GFP::KAN RFP-APE1::LEU2*	This study
WLY190	BY4742 *COG2-GFP::KAN RFP-APE1::LEU2*	This study
WLY198	SEY6210 *COG1-GFP::HIS3 VRG4-RFP::KAN*	This study
WLY201	SEY6210 *COG2-GFP::TRP1 VRG4-RFP::HIS3*	This study
WLY203	SEY6210 *COG6-GFP::TRP1 VRG4-RFP::KAN*	This study
WLY205	YCY139 *COG2-GFP::TRP1*	This study
WLY206	SEY6210 *KanMX6::pGAL1-3HA-COG1*	This study
WLY207	SEY6210 *KanMX6::pGAL1-3HA-COG3*	This study
WLY208	SEY6210 *KanMX6::pGAL1-3HA-COG4*	This study
WLY209	SEY6210 *KanMX6::pGAL1-3HA-COG2*	This study
YCY67	BY4742 *cog1Δ::KAN ATG9-3GFP::URA3*	This study
YCY68	BY4742 *cog6Δ::KAN ATG9-3GFP::URA3*	This study
YCY69	BY4742 *cog1Δ::KAN atg1Δ::HIS5 ATG9-3GFP::URA3*	This study
YCY70	BY4742 *cog6Δ::KAN atg1Δ::HIS5 ATG9-3GFP::URA3*	This study
YCY71	BY4742 *cog1Δ::KAN RFP-APE1::LEU2 ATG9-3GFP::URA3*	This study
YCY72	BY4742 *cog6Δ::KAN RFP-APE1::LEU2 ATG9-3GFP::URA3*	This study
YCY73	BY4742 *cog1Δ::KAN atg1Δ::HIS5 RFP-APE1::LEU2 ATG9-3GFP::URA3*	This study
YCY74	BY4742 *cog6Δ::KAN atg1Δ::HIS5 RFP-APE1::LEU2 ATG9-3GFP::URA3*	This study
YCY139	SEY6210 *atg1Δ, 2Δ, 3Δ, 4Δ, 5Δ, 6Δ, 7Δ, 8Δ, 9Δ, 10Δ, 11Δ, 12Δ, 13Δ, 14Δ, 16Δ, 17Δ, 18Δ, 20Δ, 21Δ, 23Δ, 24Δ, 27Δ, 29Δ, ATG11::LYS2*	This study
YTS223	BY4742 *pho8Δ60::HIS3*	This study
YTS224	BY4742 *pho8Δ60::HIS3 cog1Δ::KAN*	This study
YTS225	BY4742 *pho8Δ60::HIS3 cog5Δ::KAN*	This study
YTS226	BY4742 *pho8Δ60::HIS3 cog6Δ::KAN*	This study
YTS227	BY4742 *pho8Δ60::HIS3 cog7Δ::KAN*	This study
YTS228	BY4742 *pho8Δ60::HIS3 cog8Δ::KAN*	This study
YTS243	BY4742 *pho8Δ60::HIS3 atg1Δ::KAN*	This study
YTS229	RSY250 *pho8Δ60::URA3*	This study
YTS230	*MATα ura3-52 leu2-3 his- cog2-1 pho8Δ60::URA3*	This study
YTS231	*MATα ura3-52 leu2-3 his- cog3-2 pho8Δ60::URA3*	This study

Because import of prApe1 is a selective process, it is not an adequate measure of nonspecific autophagy. Therefore, we measured nonspecific autophagy in the *COG* deletion cells by two established biochemical analyses; GPF-Atg8 processing and Pho8Δ60 activity assays. Atg8 is a ubiquitin-like protein, which remains associated with completed autophagosomes following phosphatidylenthanolamine conjugation (75, 105, 106). After GFP-tagged Atg8 is delivered into the vacuole, Atg8 is degraded while the GFP moiety remains relatively stable. Thus, autophagy progression can be monitored by free GFP accumulation (30). As shown in Figure 4.1A, there was essentially no detectable free GFP in rich conditions in the wild-type strain (the level from the Cvt pathway is typically too low to detect), but there was a clear band following rapamycin treatment. All of the *cog* mutants displayed some level of GFP-Atg8 processing, with the *cog1Δ* mutant showing the strongest block, suggesting that nonspecific autophagy is severely impaired in this mutant, in agreement with the prApe1 processing phenotype. To quantitatively measure autophagy activity, we utilized Pho8Δ60, a mutant form of the vacuolar alkaline phosphatase in which the N-terminal 60 amino acids including the transmembrane domain are deleted. Pho8Δ60 localizes in the cytoplasm and its activation by proteolytic removal of a C-terminal propeptide via a vacuolar protease depends on autophagy (162). To monitor Pho8Δ60-dependent alkaline phosphatase activity, cells were grown in a rich medium and then incubated in a nitrogen-starvation medium for 3 h to induce autophagy. Wild-type cells showed a low level of activity in rich medium and a substantial increase after autophagy induction (Fig. 4.1B). The negative control *atg1Δ* cells that are defective in autophagy showed a basal level of Pho8Δ60 activity even after autophagy was induced for 3 hours. Autophagic activity in the *cog5Δ*, *cog6Δ*, *cog7Δ* and

116

cog8Δ cells was comparable to that in the wild-type cells, whereas in the *cog1Δ* cells it was significantly decreased and did not show a substantial change from rich-medium conditions, similar to the *atg1Δ* cells.

The COG complex is proposed to be composed of two lobes, lobe A containing the Cog2 to Cog4 subunits, and lobe B the Cog5 to Cog8 subunits (51, 232). In yeast, of the lobe A components, Cog2 to Cog4 are essential for cell growth. Therefore, we used temperature-sensitive *cog2-1* and *cog3-2* mutants (253) to assess their requirement in the Cvt pathway and autophagy. The Cvt pathway was measured by monitoring prApe1 maturation by a pulse-chase experiment. Cells were incubated at a non-permissive temperature for 30 min before labeling and then subjected to a nonradioactive chase at the same temperature for 2 h. The prApe1 processing was significantly affected in these mutants at the non-permissive temperature, although no obvious delay in processing was seen in these mutants compared with the wild type at a permissive temperature (Fig. 4.1C). These results suggested at least a kinetic defect in the Cvt pathway.

Next, autophagic activities of the *cog* temperature-sensitive mutants were measured by both GFP-Atg8 processing and the Pho8Δ60 assay. Cells were transformed with plasmid-based GFP-Atg8 and grown in a rich medium at permissive temperature to early log phase. Cell cultures were split into two aliquots: one aliquot was incubated at a permissive temperature, and the other at a non-permissive temperature for 30 min; rapamycin was then added to induce autophagy for 2 h. Cell lysates were collected and prepared at the indicated time points and then subjected to western blot using anti-GFP antibody. In the wild-type strain, GFP-Atg8 processing occurred at both temperatures (Fig. 4.1D). In contrast, in the *cog2-1* and *cog3-2* temperature-sensitive mutants, GFP-

Atg8 processing was blocked at the non-permissive temperature, suggesting that these mutants had autophagy defects. To extend our analysis to Cog4, we tested two temperature sensitive mutants in the *COG4* gene that were designed based on structural studies of human Cog4 (B.C.R. and F.M.H., unpublished results) to disrupt binding of Cog4 to other proteins. Similar to the results with *cog2-1* and *cog3-2*, the *cog4-1* and *cog4-2* mutants displayed defects in GFP-Atg8 processing at the nonpermissive temperature (Fig. 4.1D).

To make a quantitative measurement of autophagy in these mutants, we performed the Pho8Δ60 assay. Wild-type cells showed the expected increase in Pho8Δ60-dependent alkaline phosphatase activity after autophagy induction, but they displayed a slight decrease in activity at the elevated temperature (Fig. 4.1E). When the *cog* mutant cells were incubated at a non-permissive temperature, autophagic activity was severely compromised, whereas the level of activity was essentially normal at permissive temperature. These data further suggest that the lobe A COG subunits are needed for nonspecific autophagy.

Considering the effect on prApe1 delivery through the Cvt pathway, we decided to extend our study to test if COG subunits are required for the specific degradation of peroxisomes. To do this, we monitored the vacuolar delivery of the peroxisomal integral membrane protein Pex14 that was tagged with GFP at the C terminus (2, 183). Similar to GFP-Atg8, delivery of Pex14-GFP-tagged peroxisomes into the vacuole would result in the cleavage of the GFP moiety, allowing us to monitor pexophagy progression through the appearance of free GFP (183). Pexophagy was induced as described in Materials and Methods. Free GFP was detected in the wild-type cells after being transferred to SD-N

medium, whereas no free GFP was seen in the *atg1Δ* strain (Fig. 4.1F). In contrast to the wild-type cells, no free GFP was observed in the *cog2-1* or *cog3-2* mutant at nonpermissive temperature, even though processing was normal at the permissive temperature. We also tested Pex14-GFP degradation in *COG1* and *COG6* deletion strains. There was a strong kinetic delay in Pex14-GFP processing in the *cog1Δ* strain, but only a slight delay in pexophagy in *cog6Δ*. These results indicated that lobe A, but not lobe B, of the COG complex was essential for autophagy and pexophagy, although all of the components were required for an efficient Cvt pathway.

Atg9 and Atg27 cycling is affected in COG mutants

Golgi complex structure and function are defective in COG mutants (179, 221, 247). Because the sorting of Atg9 is affected in mutants defective in ER-to-Golgi trafficking, and those mutants have previously been shown to block the Cvt pathway and autophagy (59, 78, 187), it is possible that Golgi structure abnormality in COG mutants may result in an Atg9 sorting defect, thus affecting both the Cvt and autophagy pathways. Atg9 is the only transmembrane protein that is required for double-membrane vesicle formation; Atg27 is also a membrane protein, but the *atg27Δ* mutant still retains a decreased level of autophagy (263). Atg9 is also required for the organization of the PAS and recruitment of certain Atg proteins to this specialized site (222). We hypothesized that COG mutants may affect Atg9 movement similar to those mutants defective in ER-to-Golgi trafficking. To assess if Atg9 localization is affected in COG mutants we examined Atg9 localization in the *cog1Δ* and *cog6Δ* strains. In the wild-type strain in rich
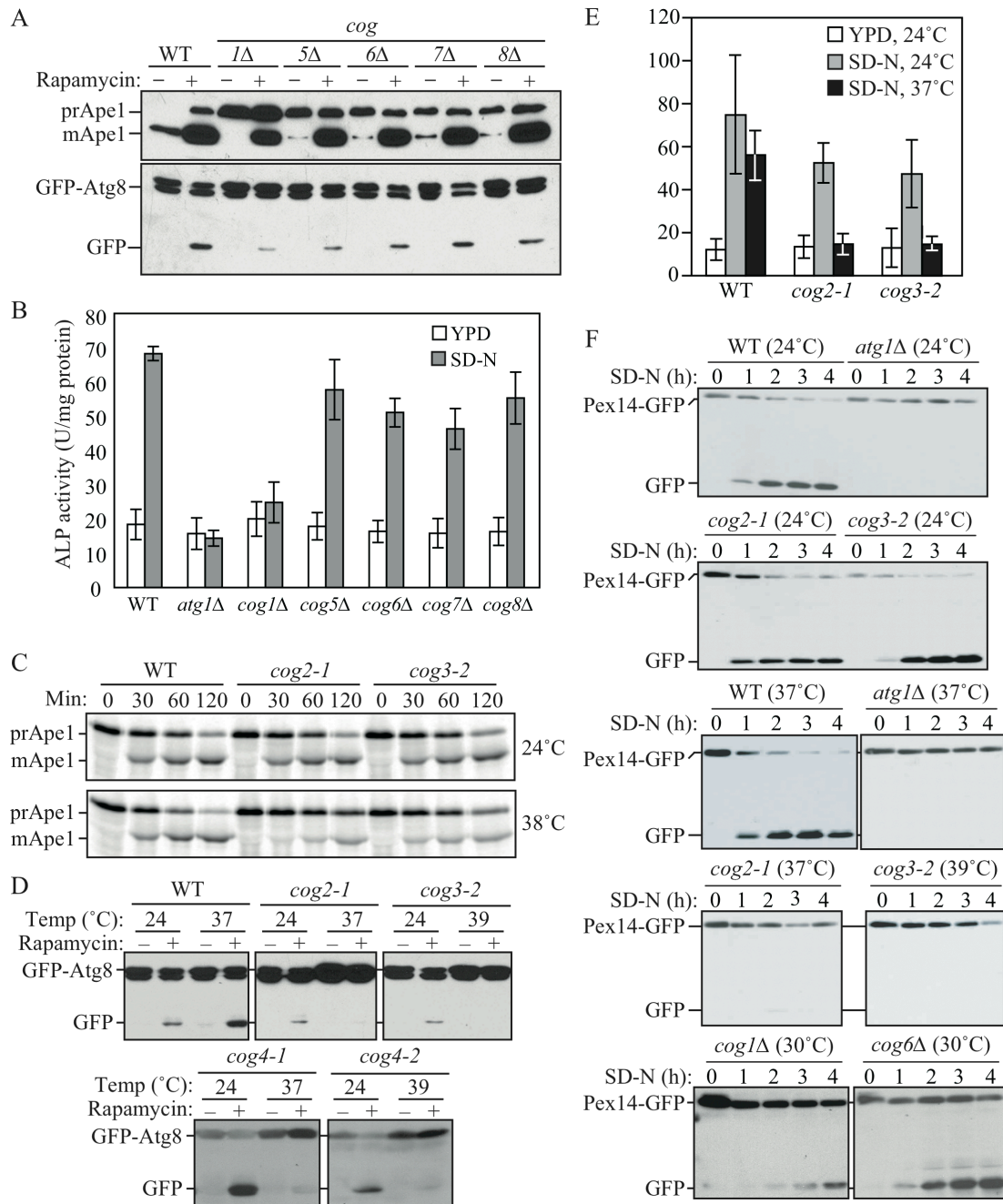
Figure 4.1. The Cvt, autophagy, and pexophagy pathways are defective in *cog* mutants. (A) The Cvt pathway is defective in *COG* deletion mutants. The wild-type (WT, BY4742), *cog1*Δ, *cog5*Δ, *cog6*Δ, *cog7*Δ and *cog8*Δ cells were grown in SMD + CA medium and then rapamycin was added to the culture at a final concentration of 0.2 μg/ml. After incubation for 2 h, cell extracts were prepared and subjected to immunoblot analysis with anti-Ape1 and anti-YFP antisera. (B) Autophagic activity in the *cog* deletion mutants. The wild-type (YTS223), *cog1*Δ (YTS224), *cog5*Δ (YTS225), *cog6*Δ (YTS226)*, cog7*Δ (YTS227), *cog8*Δ (YTS228) and *atg1*Δ (YTS243) cells expressing Pho8Δ60 were grown in YPD medium and then incubated in SD-N for 3 h to induce autophagy. Cell extracts were used to measure the enzymatic activity of Pho8Δ60-dependent alkaline phosphatase. (C) The Cvt pathway is defective in *cog2-1* and *cog3-2* mutants. The wild-type (RSY250), *cog2-1* (GWY93) and *cog3-2* (GWY95) cells were grown in SMD +

CA medium at 24°C and shifted to SMD medium. After incubation at either 24°C or 38°C for 30 min, cells were labeled with [^{35}S]-methionine/cysteine and then subjected to a nonradioactive chase at the same temperature for 2 h. Ape1 was immunoprecipitated and subjected to SDS-PAGE. (D) GFP-Atg8 processing is defective in *cog* temperature-sensitive mutants. WT (BY4742), *cog2-1*, *cog3-2*, *cog4-1* (BCR29) and *cog4-2* (BCR47) mutants were grown at permissive temperature until OD$_{600}$=0.8. After incubation at either 24°C or nonpermissive temperatures (37 or 39°C) for 30 min, rapamycin was added. Aliquots were collected at the indicated time points, and protein extracts were subjected to immunoblotting analysis. (E) Autophagic activity in temperature-sensitive *cog* mutants. WT (YTS223), *cog2-1* (YTS230), and *cog3-2* (YTS231) cells expressing Pho8Δ60 were grown in YPD medium and then incubated in SD-N at either 24°C or 37°C for 3 h. Cell lysates were used to measure Pho8Δ60 activity. (F) COG complex subunits are required for pexophagy. The wild-type (IRA001), *atg1Δ* (IRA002), *cog2-1* (WLY90), and *cog3-2* (WLY91) cells expressing Pex14-GFP were grown under conditions where peroxisome proliferation was induced as described in Materials and Methods. After incubation at either 24°C or nonpermissive temperature for 30 min, the cultures were shifted to SD-N. For *cog1Δ* (WLY175) and *cog6Δ* (WLY174) strains, the cells were grown at 30°C and after being induced for peroxisome proliferation, were shifted to SD-N at the same temperature. Protein extracts were prepared at the indicated time points and resolved by SDS-PAGE.

or starvation conditions, Atg9-3GFP is present in multiple puncta, one of which corresponds to the PAS as marked with RFP-Ape1 (Fig. 4.2A). Atg9 localizes and cycles between the PAS and mitochondria in a process dependent on the serine/threonine kinase Atg1 (186). When the retrograde transport of Atg9 from the PAS is blocked in *atg1Δ* cells, Atg9 becomes restricted to the PAS (186). In both *cog1Δ* and *cog6Δ* strains, Atg9-3GFP localized to multiple dots with one of the puncta colocalizing with the PAS under both growing and starvation conditions (Fig. 4.2A and 4.2B). To test if the COG complex is required for Atg9 localization before the function of Atg1, we performed an epistasis analysis termed the transport of Atg9 after knocking out *ATG1* (TAKA) assay. Additional deletion of *ATG1* in the *cog1Δ* or *cog6Δ* strain did not restrict Atg9 to a single punctum at the PAS suggesting that the forward movement of Atg9 to the PAS was defective. However, a portion of Atg9 did reach the PAS as shown by its colocalization with RFP-Ape1 (Fig. 4.2A). These data suggest that the anterograde movement of Atg9 to the PAS is partially defective in both *cog1Δ* and *cog6Δ* strains under growing conditions. In contrast, under starvation conditions Atg9-3GFP was detected primarily as a single PAS dot with many faint dots in *cog1Δ atg1Δ* and *cog6Δ atg1Δ* cells similar to an *atg1Δ* phenotype (Fig. 4.2B). These results indicate that Cog1 and Cog6 are required for Atg9 anterograde transport to the PAS under vegetative conditions (the Cvt pathway), but are less important during starvation (nonspecific autophagy). Of note, a population of RFP-Ape1 was inside the vacuole in *cog6Δ* cells, but not in *cog1Δ* cells, which agrees with the observation that the *COG1* deletion had a stronger block in prApe1 maturation (Fig. 4.1A). In addition, we examined the mitochondrial localization of Atg9 in *cog1Δ*, *cog6Δ*, *cog1Δ atg1Δ* and *cog6Δ atg1Δ* cells. A portion of Atg9 localizes to mitochondria and the

morphology of mitochondria in these mutants was similar to that of wild-type cells (data not shown).

Atg27 also localizes to and cycles between the PAS, mitochondria, and the Golgi complex (263). Moreover, Atg27 is required for Atg9 anterograde movement to the PAS. Since Atg27 localizes to the Golgi complex, we hypothesized that Atg27 localization and cycling may be affected in COG mutants. First we monitored the Atg27 PAS localization by generating functional GFP and RFP fusions at the *ATG27* and *APE1* chromosomal loci, respectively, in the *cog1Δ* and *cog6Δ* backgrounds. Similar to Atg9-3GFP, Atg27-GFP was dispersed in several puncta in wild-type cells, and a single punctum colocalizing with RFP-Ape1 in *atg1Δ* cells (Fig. 4.S1). In the *cog1Δ* and *cog6Δ* strains, Atg27-GFP was also present in several puncta in rich conditions, and in addition we detected continuous ring-like structures. One of the Atg27-GFP puncta colocalized with the PAS marker, RFP-Ape1; however, the percentage of PAS localization was much lower than in the wild-type background (<10% in the *cog1Δ* mutant and 15% in the *cog6Δ* mutant, versus 50% in wild-type). To test if COG components are required for Atg27 cycling prior to Atg1 function, we repeated the TAKA assay. The additional deletion of Atg1 in the *cog1Δ* and *cog6Δ* mutants did not alter Atg27 localization in growing conditions. Atg27 remained in multiple puncta and ring-like structures with one of the dots colocalizing with RFP-Ape1, suggesting that these two mutations are epistatic to *atg1Δ*. In contrast, when shifted to starvation medium, Atg27 became restricted to the PAS in both *cog1Δ atg1Δ* and *cog6Δ atg1Δ* cells, and a portion of RFP-Ape1 could again be seen in the vacuole lumen only in the *cog6Δ* strain. Similar to Atg9, Cog1 and Cog6

are required for Atg27 transport to the PAS in growing conditions, but are less important during starvation (Fig. 4.S1).
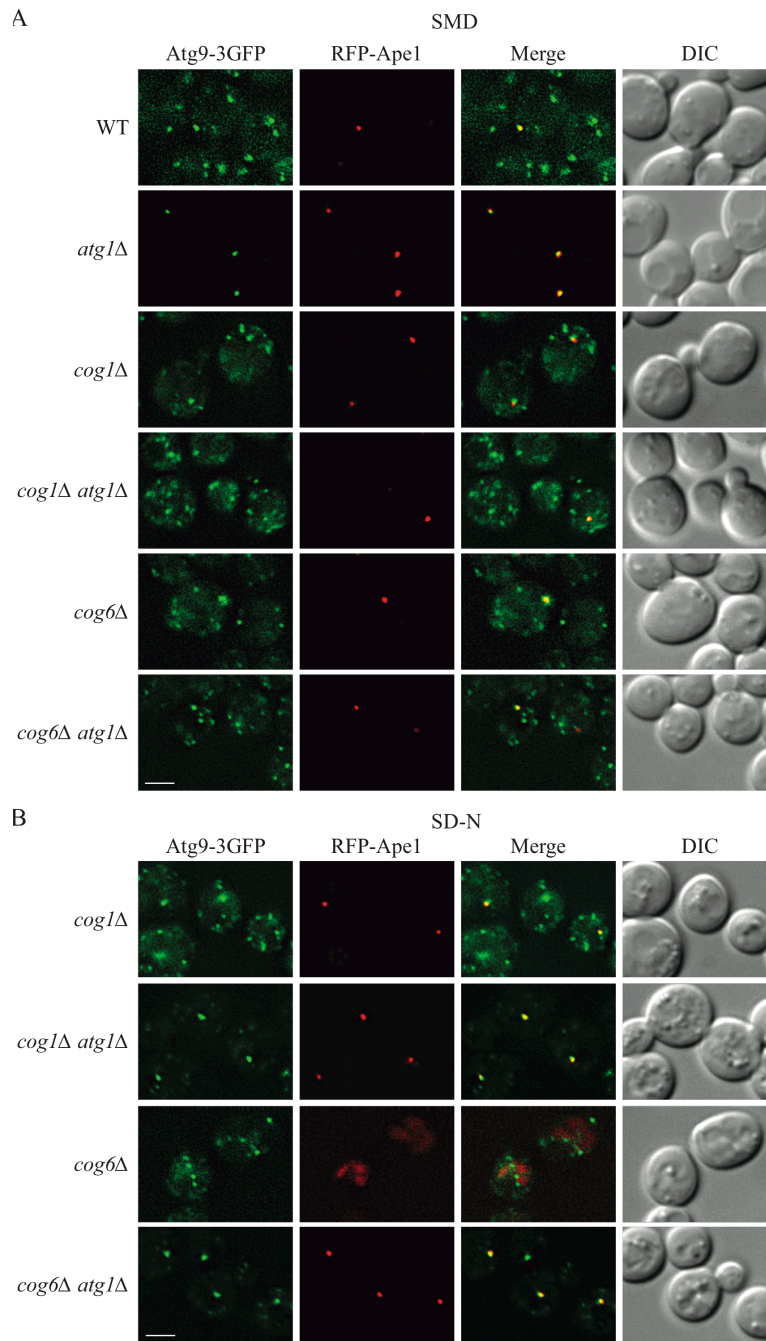

Figure 4.2. Anterograde movement of Atg9 is partially blocked in the *cog1Δ* and *cog6Δ* strains.
Analysis of Atg9 anterograde movement in growing (A) and starvation (B) conditions. The WT (IRA030), *atg1Δ* (IRA3), *cog1Δ* (YCY70), *cog1Δ atg1Δ* (YCY73), *cog6Δ* (YCY72) and *cog6Δ atg1Δ* (YCY74) strains expressing Atg9-3GFP and RFP-Ape1 were grown to mid-log phase at 30°C (A) or shifted to starvation conditions for 2 h before imaging (b), and analyzed by fluorescence microscopy. DIC, differential interference contrast. Bar, 5 μm.

The Atg27-GFP ring-like structures observed in the *cog* mutants were similar to the morphology of the ER. Since the COG complex is reported to be involved in ER-to-Golgi and intra-Golgi trafficking, when these routes are blocked Atg27 may accumulate at the ER. To determine whether the ring-like structures are ER-localized Atg27-GFP, we examined ER localization by comparing it with the ER marker Spo7-RFP. Spo7-RFP colocalized with the Atg27-GFP ring structures in *cog1Δ* and *cog6Δ* cells (data not shown). In addition, Atg27-GFP remained associated with the Golgi complex (marked with Vrg4-RFP), and mitochondria (stained with MitoFluor Red), although the Golgi complex structures in *cog1Δ* and *cog6Δ* cells were smeared and enlarged (data not shown). Taken together, these data indicate that both Atg9 and Atg27 transport to the PAS were partially blocked under growing conditions, whereas deletion of COG complex components did not alter the association with the organelles where these proteins normally reside.
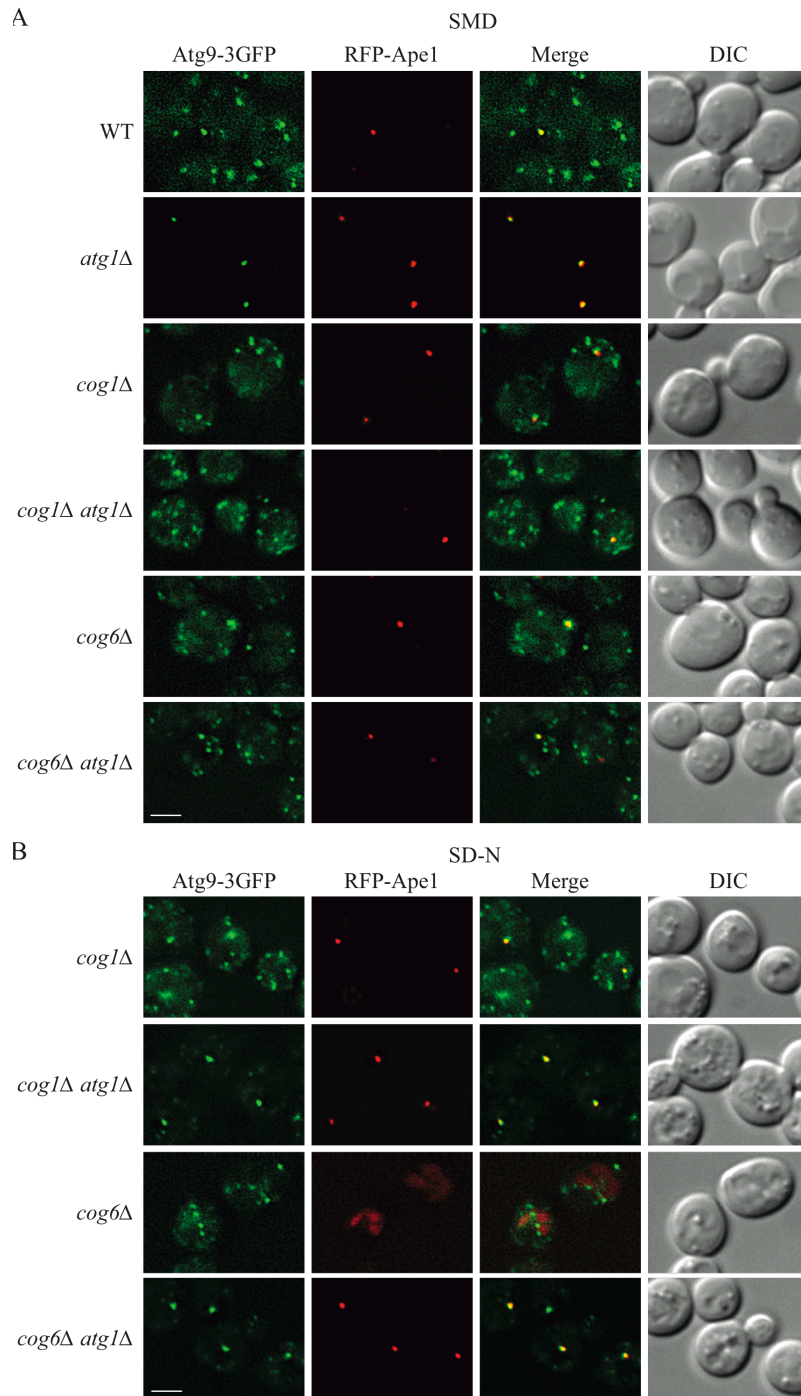
A   SMD

B   SD-N

Figure 4.S1. Anterograde movement of Atg27 is partially blocked in the *cog1Δ* and *cog6Δ* strains. (A) The anterograde movement of Atg27 in growing conditions was analyzed by the TAKA assay. The WT (WLY5), *atg1Δ* (WLY11), *cog1Δ* (WLY96), *cog1Δ atg1Δ* (WLY103), *cog6Δ* (WLY97) and *cog6Δ atg1Δ* (WLY98) strains expressing Atg27-GFP and RFP-Ape1 were grown to OD_{600}=0.8 at 30°C, and visualized by fluorescence microscopy. (B) The *cog1Δ*, *cog1Δ atg1Δ*, *cog6Δ* and *cog6Δ atg1Δ* strains expressing Atg27-GFP and RFP-Ape1 were grown to early-log phase at 30°C, then shifted to starvation conditions for 2 h before imaging. DIC, differential interference contrast. Bar, 5 μm.

COG may be involved in double-membrane vesicle formation

The inefficient transport of Atg9 and Atg27 to the PAS may be due to indirect defects in the secretory pathway in COG mutants. In other words, correct membrane flow from the early secretory pathway is required for efficient PAS localization of Atg9 and Atg27. Indeed, in yeast, early secretion (*sec*) mutants or mutations that affect protein exit from the ER or trafficking through the Golgi complex have an indirect negative effect on both the Cvt and autophagy pathways (59, 78, 187). Thus, the transport defect seen with the two transmembrane Atg proteins, Atg9 and Atg27, in *COG* mutants may be due to the defect in intra-Golgi transport. Therefore, we next extended our study to test Atg8 PAS localization in *COG* mutants. Atg8 is a synthesized in the cytosol and its membrane association is through lipid conjugation (75, 105, 106); Atg8 does not transit through the secretory pathway. Because Atg8 forms a punctum at the putative Cvt vesicle and phagophore assembly site and remains associated with the complete double-membrane vesicles, it serves as a marker for both Cvt vesicles and autophagosomes. Two mutant strains, *cog2-1* and *cog3-2*, were transformed with a plasmid expressing GFP-Atg8, and were incubated at 24°C, then shifted to a non-permissive temperature for 60 min. When the cells were grown at permissive temperature, the GFP-Atg8 localization in the *cog2-1* and *cog3-2* mutants was similar to the wild-type pattern, being diffuse in the cytosol and having one prominent PAS punctum (Fig. 4.3A and data not shown). After one hour of the temperature shift, abnormal GFP-Atg8 fluorescent structures started to appear. To examine the GFP-Atg8 localization during starvation in *cog2-1* and *cog3-2*, the same strains were grown at permissive temperature then either shifted to non-permissive temperature or maintained at permissive temperature for 1 h, then autophagy was induced

by adding rapamycin for 30 min before imaging the cells. When grown at permissive temperature after autophagy had been induced for 30 min, the localization pattern of the GFP-Atg8 chimera was one single perivacuolar dot (Fig. 4.3A). In contrasts to cells incubated at non-permissive temperature in rich medium, during autophagy a mixture of phenotypes was observed: some cells showed abnormal GFP-Atg8 localization, while some had one single GFP-Atg8 punctum. Following a shift back to the permissive temperature, GFP-Atg8 regained its normal localization pattern within 30 min for growing conditions, and 60-90 min in starvation conditions, implying that the aberrant GFP-Atg8 structures observed during incubation at the non-permissive temperature are not terminal structures. Thus, lobe A *cog* mutants affect the normal localization of GFP-Atg8 during autophagy-inducing conditions.

The aberrant GFP-Atg8 localization in two temperature-sensitive *COG* mutants suggests that COG may be involved in Cvt vesicle and autophagosome formation. To test this hypothesis, we performed a prApe1 proteinase-sensitivity assay to examine the role of the COG complex during vesicle formation. When prApe1 is enwrapped in a completed double-membrane vesicle, it is protected from exogenously added proteinase following lysis of spheroplasts in osmotic conditions that retain the integrity of the vacuole and other subcellular compartments including autophagosomes and Cvt vesicles. In contrast, when there are defects in vesicle formation and/or completion, the proteinase-sensitive propeptide domain of prApe1 would be cleaved off, resulting in a molecular mass shift and/or partial degradation. We used the *vam3Δ* strain background, because this deletion prevents fusion of the vesicle with the vacuole; in *vam3Δ* cells, prApe1 accumulates in cytosolic vesicles and the prApe1 propeptide cannot be processed in the

vacuolar lumen. Spheroplasts generated from *vam3Δ*, *atg1Δ vam3Δ*, and *cog2-1 vam3Δ*

cells were incubated at non-permissive temperature for 20 min. Spheroplasts were pulse-

labeled with [^{35}S]methionine/cysteine for 10 min, then subjected to a non-radioactive

chase for 30 min at non-permissive temperature. The prApe1-containing low-speed pellet

fractions from cell lysates were prepared and subjected to proteinase K treatment with or

without detergent as described in Materials and Methods. In *vam3Δ* cells, prApe1 was

protected from proteinase K and was only digested in the presence of detergent (Fig. 4.3B,

compare lane 2 and lane 4). In contrast, in the *atg1Δ* strain, which is defective in vesicle

formation, a portion of prApe1 was sensitive to the proteinase K digestion independent of

detergent (Fig. 4.3B, lane 6). A similar phenotype was observed in the *cog2-1* mutant; the

prApe1 was partially sensitive to exogenously added proteinase K (Fig. 4.3B, lane 10),

indicating that the prApe1 was not completely enclosed by the membrane. Taken together,

these results suggest that the COG complex is required for double-membrane vesicle

biogenesis.

We extended this analysis by examining Atg8 localization through

immunoelectron microscopy. In wild-type cells, Atg8 is detected primarily at the

phagophore/PAS and on completed autophagosomes. In contrast, in the *cog2-1* mutant at

the nonpermissive temperature Atg8 was dispersed throughout the cytosol in multiple

clusters and dots (Fig. 4.3C). Thus, lobe A *cog* mutants affect the normal localization of

GFP-Atg8 during autophagy-inducing conditions.

A
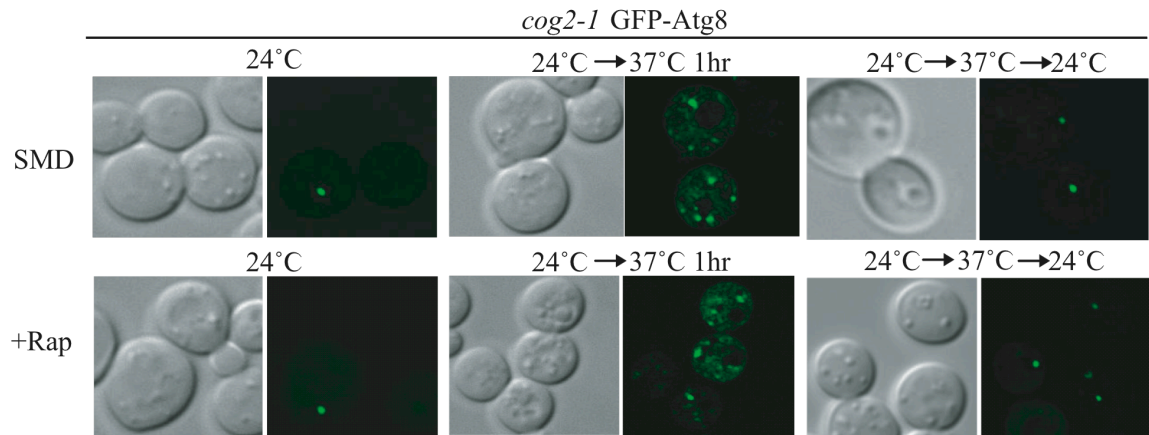
B
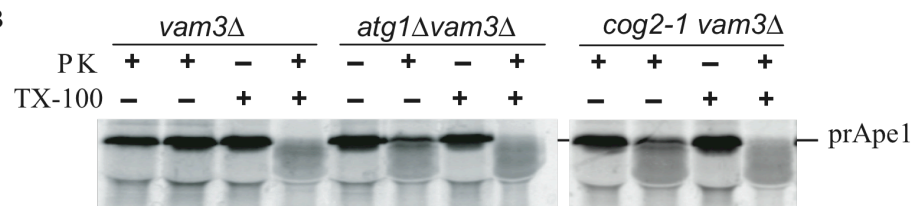
C
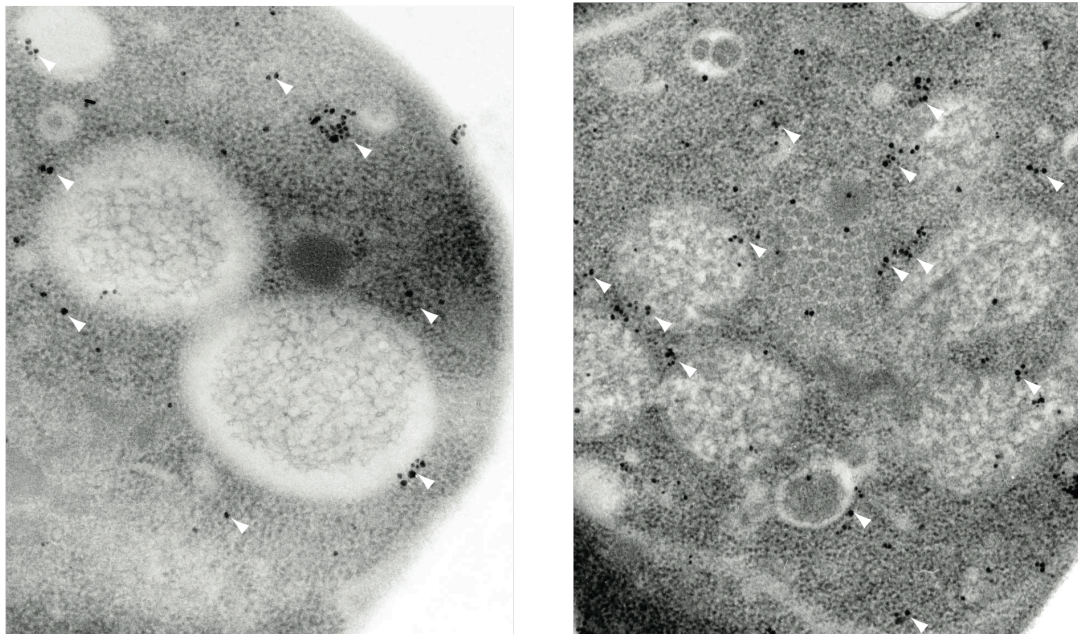
Figure 4.3. The *cog* mutants affect sequestering vesicle formation. (A) GFP-Atg8 localization is defective in *cog2-1* and *cog3-2* mutants. The *cog2-1* strain carrying a plasmid expressing GFP-Atg8 [pGFP-AUT7(416)] was grown in SMD at 24°C to OD_{600}=0.8 or shifted to non-permissive temperature for 60 min before imaging. For starvation conditions, the cells were incubated at either 24°C or a non-permissive temperature for 60 min, then rapamycin (final concentration 0.2 μg/ml) was added and the

culture was incubated for another 30 min before imaging. To reverse the temperature, the cultures were shifted back to 24°C for 30 min in growing conditions, or 60 min when rapamycin was added. DIC, differential interference contrast. Essentially identical results were seen with the *cog3-2* mutant. Bar, 5 μm. (B) Cog2 is involved in Cvt vesicle formation. Spheroplasts from the wild-type (*vam3Δ*; WLY118), *cog2-1* (WLY117) and *atg1Δ* (WLY119) stains were incubated at 38°C for 20 min, pulse-labeled with [^{35}S]-methionine/cysteine for 10 min then subjected to a non-radioactive chase for 30 min. The prApel-containing pellet fractions were obtained after osmotically lysing the spheroplasts and centrifuged at 5,000 × g. The pellets were treated with proteinase K in the presence or absence of 0.2% Triton X-100 for 30 min on ice. The resulting samples were TCA precipitated and immunoprecipitated with Ape1 antiserum and resolved by SDS-PAGE. (C) The *cog2-1* mutant mislocalizes Atg8 at the nonpermissive temperature. *cog2-1* cells were grown in SMD and shifted to 38°C for 1.5 h and prepared for electron microscopy using the freeze substitution method and labeled with anti-YFP antibody followed by immunogold labeling as described in Materials and Methods. The white arrowheads indicate the GFP-Atg8 clusters.

The COG complex localizes to the PAS and interacts with Atg proteins

The requirements for COG subunits in localization of Atg8 and Atg9 suggest that the COG complex may have a direct role in the Cvt pathway and autophagy. Therefore, we decided to examine if the COG complex localizes to the PAS. The chromosomally tagged Cog1-GFP, Cog2-GFP, and Cog6-GFP were distributed in several punctate structures, one of which colocalized with RFP-Ape1, the PAS marker (Fig. 4.4 and Fig 4.S2). We further analyzed the PAS localization frequency of these COG components by quantifying the colocalization percentages from cells with both fluorescence signals. As shown in Tables 4.2 and 4.3, the PAS localization frequency of Cog1-GFP, Cog2-GFP, and Cog6-GFP were 11.1%, 12.5%, and 8% respectively. Next, we examined whether the PAS localization rate could be elevated by additional deletion of *ATG1*, which causes the accumulation of Atg proteins at the PAS. However, the PAS localization rates of Cog1-GFP and Cog6-GFP were not altered in the *atg1Δ* strain and were similar to that of the wild type (Table 4.2).

To further verify the PAS localization of the COG proteins, we decided to compare the PAS localization rate between Cog2-GFP and the thermosensitive mutant cog2-1-GFP. *cog2-1* bears a transversion mutation at nucleotide 584, thus encoding a truncated protein (179). To monitor cog2-1-GFP localization, we chromosomally tagged GFP at the *COG2* locus resulting in a 194 amino acid truncated protein with a C-terminal GFP fusion. At the permissive temperature, both Cog2-GFP and cog2-1-GFP were localized to several punctate dots, one of which colocalized with RFP-Ape1 under both growing and rapamycin treatment conditions (Fig. 4.4).
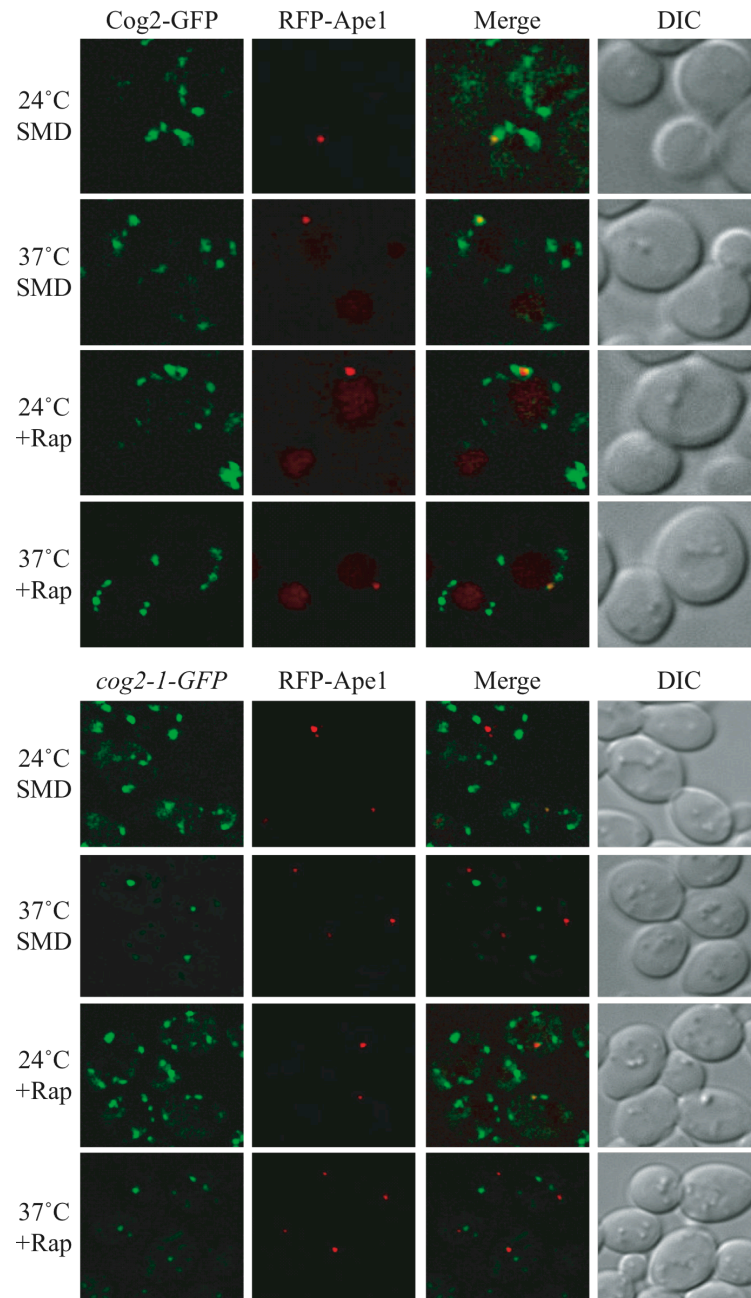
Figure 4.4. Cog2 localizes to the PAS. Cog2-GFP (WLY190) and cog2-1-GFP (WLY188) strains expressing RFP-Ape1 were grown in SMD medium at 24°C or shifted to 37°C for 30 min before being visualized under a fluorescence microscope. For starvation condition, cells were either grown at 24°C or shifted to 37°C for 30 min, then rapamycin was added for an additional 30 min. DIC, differential interference contrast. Bar, 5 μm.
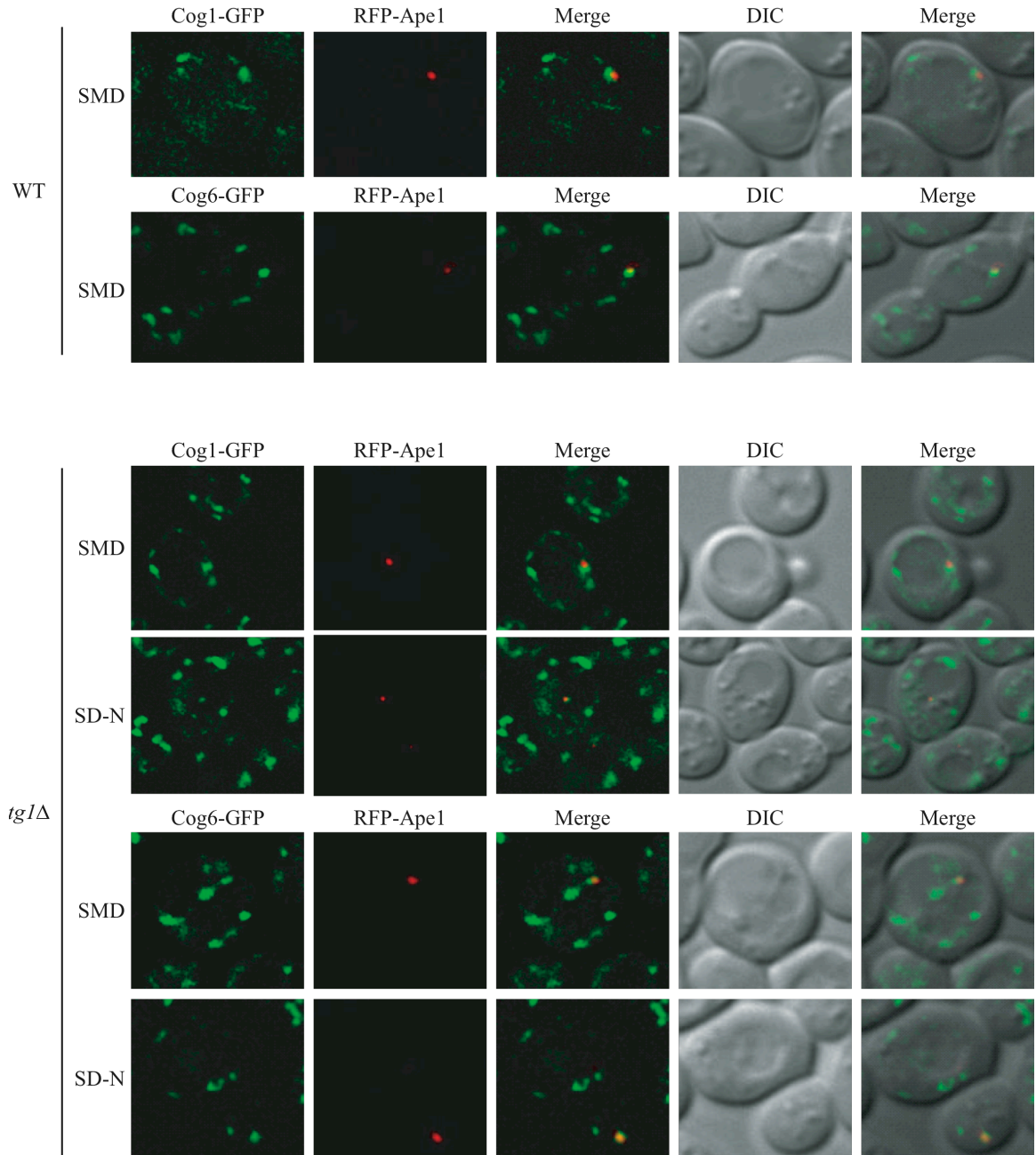
Figure 4.2S. Cog1 and Cog6 localize to the PAS. The Cog1-GFP (WLY154), *atg1*Δ Cog1-GFP (WLY153), Cog6-GFP (WLY156), and *atg1*Δ Cog6-GFP (WLY155) strains expressing RFP-Ape1 were grown in SMD medium to early-log phase then collected for analysis by fluorescence microscopy. For starvation conditions, cells were grown in SMD medium to OD_{600}=0.8 then shifted to SD-N medium for another 2 h before imaging. DIC, differential interference contrast. Bar, 5 μm.

After incubation of the cultures at nonpermissive temperature for 30 min, the cog2-1-GFP signal became one or two strong dot with several faint dots. The percentage of PAS localization of this protein dropped after the temperature shift (from 8.69% to 2.19%; Table 4.3). In contrast, the temperature shift did not dramatically change the PAS localization of wild-type Cog2-GFP. Similar results were seen when rapamycin was added to induce autophagy (Fig. 4.4). In this case, the PAS localization frequency of the mutant decreased from 11.11% to 1.14%. This result further verifies the PAS localization of COG components.

Table 4.2. PAS localization of Cog1-GFP and Cog6-GFP

Condition	Cog1-GFP	Cog6-GFP
SMD	11.1% (n = 66)	8% (n = 62)
SMD, *atg1Δ*	9.7% (n = 123)	10.1% (n = 168)
SD-N, 2 h, *atg1Δ*	5.1% (n = 68)	4.3% (n = 114)

Table 4.3. PAS localization of Cog2-GFP and *cog2-1-GFP*

Condition	Cog2-GFP	cog2-1-GFP
SMD, 24°C	12.5% (n = 152)	8.69% (n = 184)
SMD, 37°C, 30 min	8.83% (n = 164)	2.19% (n = 273)
Rapamycin, 24°C, 1 h	11.17% (n = 188)	11.11% (n = 162)
Rapamycin, 37°C, 1 h	15.65% (n = 68)	1.14% (n = 175)

To determine whether the COG-GFP chimeras were localizing normally, we tested the Golgi localization of Cog1, Cog2, and Cog6. The majority of the Cog1-GFP, Cog2-GFP, and Cog6-GFP punctate dots colocalized with the Golgi marker Vrg4-RFP (Fig. 4.S3). At least one of the puncta, however, did not localize to the Golgi suggesting that a portion of the COG complex in the cell is not localized at this site.

Although the COG complex associates with the Golgi and COPI-containing vesicles (206, 231, 237, 247), it is still not clear which vesicles it tethers with regard to its role in autophagy. The PAS localization of the COG complex suggested that in addition to maintaining correct membrane flow through the secretory pathway that is important for autophagy, the COG complex may participate in double-membrane vesicle formation, possibly functioning in the membrane tethering and fusion event. To gain more insight into the function of the COG complex in the Cvt and autophagy pathways, we extended our study to test if COG components interact with Atg proteins by yeast two-hybrid analysis.

Cog1-GFP	Vrg4-RFP	Merge	DIC

Cog2-GFP	Vrg4-RFP	Merge	DIC

Cog6-GFP	Vrg4-RFP	Merge	DIC
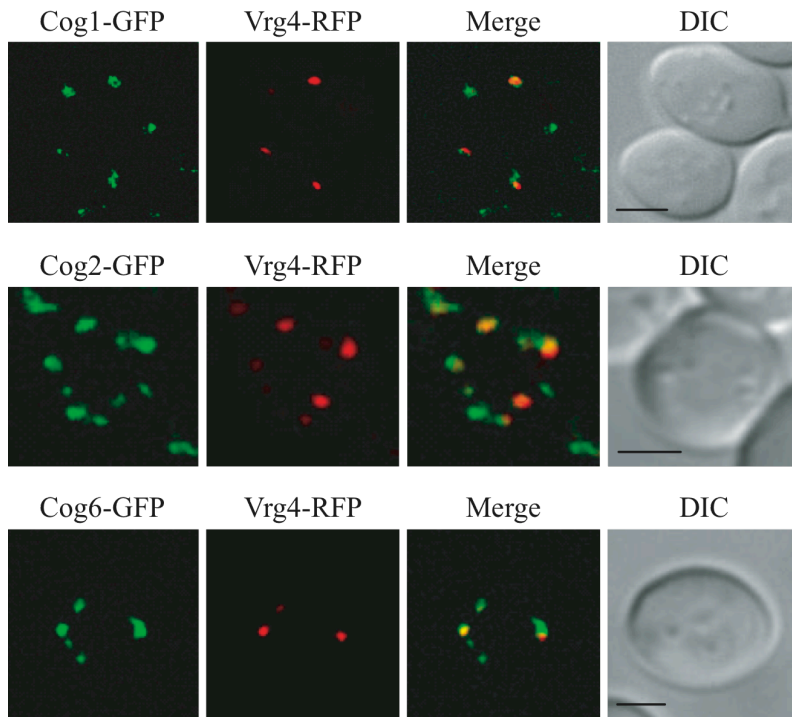
Figure 4.S3. COG partially localizes to the Golgi complex. Cog1-GFP (WLY198), Cog2-GFP (WLY201), and Cog6-GFP (WLY203) strains expressing the Golgi complex marker Vrg4-RFP were grown in SMD medium to early-log phase before imaging by fluorescence microscopy. DIC, differential interference contrast. Bar, 2.5 μm.

COG complex components showed weak interaction with Atg9, and stronger binding with Atg12, Atg17, Atg20, and Atg24 (Table 4.4); no interaction was detected with Atg5, Atg7, Atg8, Atg11, Atg13, Atg16 or Atg18. To explore the physical interactions between COG and Atg proteins, we investigated the protein interactions under physiological conditions. First, we performed the co-immunoprecipitation using endogenous COG subunits, however, we were unable to detect the endogenous COG proteins due to their low expression levels (data not shown).

Table 4.4. Yeast two-hybrid interactions between lobe A COG components and Atg proteins.

	Atg5	Atg7	Atg8	Atg9	Atg11	Atg12
Cog1	–	–	–	–	–	–
Cog2	–	–	–	–	–	+++
Cog3	–	–	–	+	–	–
Cog4	–	–	–	+	–	–

	Atg13	Atg16	Atg17	Atg18	Atg20	Atg24
Cog1	–	–	+++	–	+	++
Cog2	–	–	++	–	++	++
Cog3	–	–	+++	–	+	++
Cog4	–	–	+++	–	++	++

Table 4.4. The interaction strength is scored by the number of pluses: "+" means grown weakly on plates lacking histidine, "++" means growth on plates lacking histidine but not on plates lacking adenine, and "+++" corresponds to growth on plates lacking adenine); "–" means no growth. All the interactions were scored after growth for three days at 30°C.

To overexpress COG subunits, we chromosomally replaced their endogenous promoters with the *GAL1* promoter and a N-terminal hemagglutinin (HA) tag, and performed a series of protein A (PA)-affinity purification experiments. Either a protein A fusion or protein A alone was coexpressed in combination with HA-COG subunits. Cells were grown in galactose medium (SMG) to induce COG subunit overexpression. Cell extracts were prepared, and protein A-tagged Atg proteins and associated proteins were affinity-isolated. The recovered immunocomplex was resolved by SDS-PAGE and the presence of HA-COG subunits was analyzed by western blot using anti-HA antibody. HA-Cog1 bound to PA-Atg17 and PA-Atg20, whereas HA-Cog3 was coprecipitated with PA-Atg17 and PA-Atg24 (data not shown). HA-Cog4 was able to bind PA-Atg17, PA-Atg20, and PA-Atg24 (Fig. 4.5A). HA-COG subunits did not bind to protein A alone,

indicating that the interactions with HA-COG subunits were dependent on Atg17, Atg20, or Atg24 fused to protein A.

We also tested the interaction between Cog2 and Atg12. Lysates were prepared from yeast cells expressing HA-Cog2, Myc-Atg12 or both, and incubated with protein A-Sepharose beads and anti-HA or anti-Myc antibody. The resulting immunocomplex was subjected to western blot analysis using anti-HA or anti-Myc antibody. In the cells expressing either HA-Cog2 or Myc-Atg12 alone, no Myc-Atg12 was detected after immunoprecipitation, indicating that both proteins did not bind non-specifically to the protein A-Sepharose beads. In contrast, when both HA-Cog2 and Myc-Atg12 were coexpressed, Myc-Atg12 coimmunoprecipitated with HA-Cog2, and vice versa (Fig. 4.5B). We were unable to detect an interaction between Cog2 and Atg12–Atg5 conjugates. This could be due to either the absence of this interaction or the relatively low level of Atg12–Atg5 conjugates in our experimental conditions where Atg12 is overexpressed. Atg9 weakly interacted with Cog3 and Cog4 in the yeast two-hybrid analysis; however, we could not verify these interactions by protein A-affinity isolation. Thus, the interaction between Atg9 and Cog3/4 might be transient or too weak to detect reproducibly.

The COG complex primarily localizes to the rims and the tips of the Golgi membrane and their associated vesicles (231, 237). However, none of the COG subunits has either a transmembrane domain or lipid-binding motif. Thus, it remains unclear whether COG subunits themselves or other factors mediate this membrane association. The interactions between COG and Atg proteins raise a possibility that PAS membrane association of the COG complex is through interaction with Atg proteins. To address this

point, we utilized a multiple knockout (MKO) strain where 24 *ATG* genes that are

directly involved in autophagy and/or the Cvt pathway have been deleted. We used a

MKO strain containing Atg19, the Ape1 cargo receptor, and re-introduced Atg11, an

adaptor protein required for prApe1 cargo recruitment, to this strain allowing the Ape1

complex to be recruited to the PAS (25, 207, 223, 264). In this strain, chromosomally

tagged Cog2-GFP and plasmid based RFP-Ape1 were coexpressed, and the

colocalization was examined by fluorescence microscopy. In the MKO (*ATG11, ATG19*)

strain, the Cog2-GFP colocalized with RFP-Ape1, the PAS marker (Fig. 4.5C). We

further quantified the PAS localization frequency of Cog2-GFP in the MKO (*ATG11,*

ATG19) strain and found that the PAS localization rate was similar to that of the wild

type (MKO: 11.11%, n=225; wild-type: 12.5%, n=152). Because Atg11 was introduced

into the MKO strain, it is possible that Atg11 alone might be sufficient to recruit the

COG complex to the PAS. However, from the yeast two-hybrid analysis, no interaction

between Atg11 and Cog1-Cog4 was detected (Table 4.4), suggesting that either an

unknown factor(s) or the COG complex subunits themselves direct the complex to
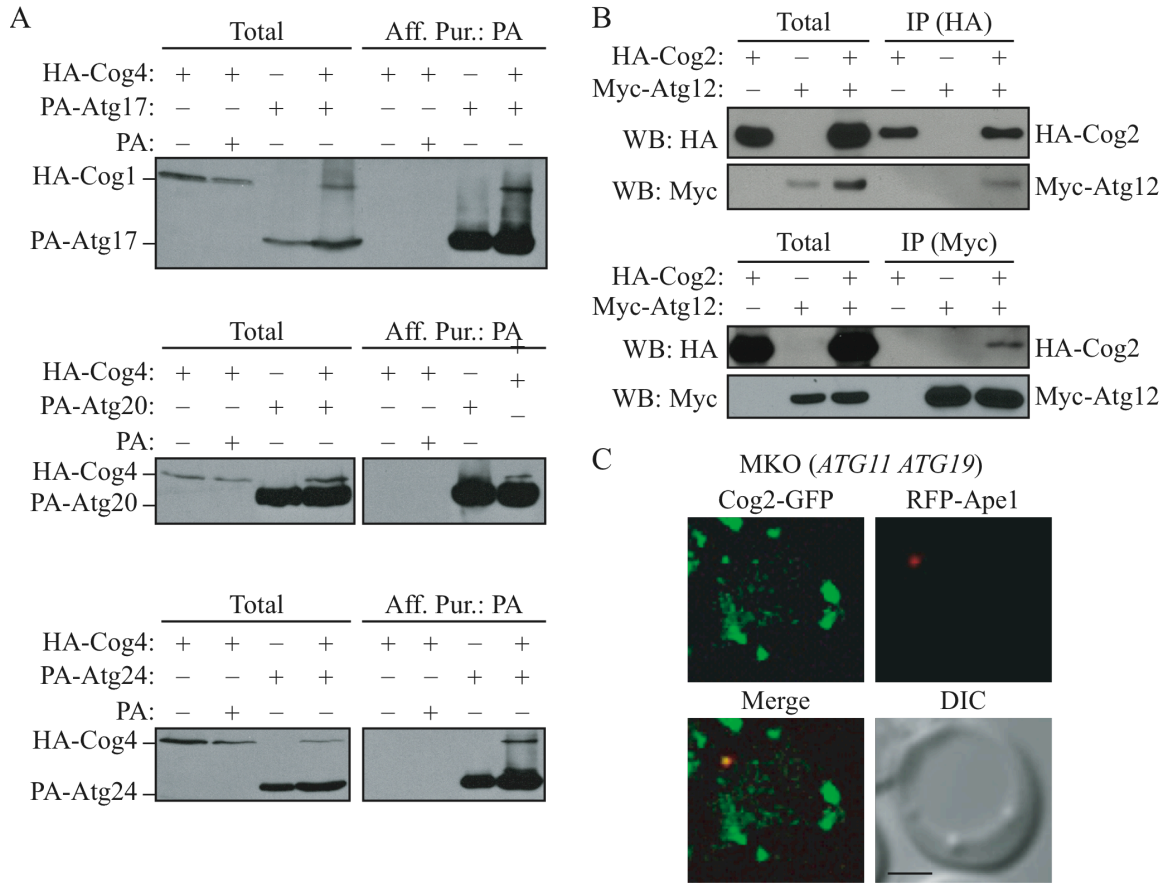
associate with the PAS.

Figure 4.5. COG subunits associate with Atg proteins. (A) HA-Cog4 (WLY208) and (B) HA-Cog2 (WLY209) cells transformed with the indicated plasmids expressing tagged-Atg proteins were grown in selective SMG medium to OD_{600}=1.0. Cell lysates were prepared and subjected to affinity isolation or immunoprecipitation with either anti-HA or anti-Myc antibody as described in Materials and Methods. Plasmids expressing protein A (pRS424-CuProtA), PA-tagged Atg17 (pProtA-Apg17(424)), PA-tagged Atg20 (pProtA-Cvt20(424)), Atg24 (pProtA-Cvt13(424)), and Myc-tagged Atg12 (pMyc-Apg12(426)) were used as indicated. The eluted proteins were separated by SDS-PAGE and detected with monoclonal anti-HA antibody (A) or immunoblotting with anti-HA and anti-Myc antibodies (B). For each experiment, ~1% of the total cell lysate or 10% of the total eluate was loaded. (C) Cog2-GFP localizes to the PAS in the MKO (*ATG11 ATG19*) strain. The MKO (*ATG11 ATG19*) (WLY205) cells expressing chromosomally tagged Cog2-GFP and a plasmid-based RFP-Ape1 were grown in selective SMD medium to OD_{600}=0.8 and observed by fluorescence microscopy. DIC, differential interference contrast. Bar, 2.5 μm.

Discussion

An autophagosome is formed through nucleation, membrane expansion and completion. Because of the similarity between autophagy and the Cvt pathway, the Cvt vesicle is considered as a variant of an autophagosome. However, the Cvt vesicle (130-150 nm in diameter) is smaller than an autophagosome (300-900 nm in diameter) in size (9, 202). Furthermore, during selective types of autophagy the membrane may form in close apposition to the cargo, utilizing receptors (e.g., Atg19) and adaptor proteins (e.g., Atg11) to link the two, whereas these types of proteins do not play a role in nonspecific autophagy. These observations suggest that the nature of Cvt vesicle and autophagosome formation may in part be different. Indeed, some components are involved in the formation of one but not the other, which may explain why lobe A subunits are required for both the Cvt and autophagy pathways, whereas the lobe B subunits of COG are Cvt-specific. This idea is supported by the normal Pho8Δ60-dependent alkaline phosphatase activity seen in lobe B, but not lobe A, mutants of the COG complex (Fig. 4.1A, 1B, 1D, and 1E). Similarly, abnormal GFP-Atg8-positive structures were detected in *cog2-1* and *cog3-2* mutants during vegetative growth and following rapamycin treatment (Fig. 4.3), indicating that the lobe A subunits of COG may play a role in autophagosome formation.

The COG complex may be directly involved in autophagy

It is proposed that during the process of double-membrane vesicle formation, there are two membrane fusion events: the condensation of transient vesicles with the phagophore at the PAS, and the fusion of the completed double-membrane vesicles with

the vacuole (187). The last event is the best characterized and relies on components that are needed for other vesicle fusion events that terminate at the vacuole, as well as homotypic vacuole fusion. In contrast, little is known about the role of SNAREs or tethering factors in the phagophore expansion step. The localization of the COG complex at the PAS (Fig. 4.4) implies that the COG complex might participate in membrane tethering events which are required for Cvt vesicle and autophagosome formation and completion. In agreement with this hypothesis, the accumulation of GFP-Atg8-positive structures in a *cog2-1* mutant at non-permissive temperature also suggests that the COG complex is required for GFP-Atg8 vesicle fusion to form a normal PAS structure (Fig. 4.3).

The interactions between COG complex and Atg proteins suggest a direct involvement of the COG complex in autophagy and the Cvt pathway, and also provides insight about the function of these Atg proteins. According to the yeast two-hybrid analysis, Atg17 showed strong interactions with many COG subunits (Table 4.4). Atg17 is an autophagy-specific protein and functions as a scaffold to recruit other Atg proteins to organize PAS formation (30, 223). Atg17 modulates the timing and the magnitude of the autophagy response, such as the size of the sequestering vesicles, through interacting with and regulating Atg1 kinase activity (30, 90). The interaction between Atg17 and COG subunits provides a link between the autophagy regulatory components and the phagophore expansion/vesicle fusion machinery. This may explain how the Atg1 kinase activity can be translated into the size of sequestering vesicles.

The significance of the interaction between Atg12 and Cog2 is not known. The finding that Atg9 interacts with COG subunits by yeast two-hybrid is intriguing.

Although we were unable to obtain consistent results from protein A-affinity isolation experiments, it is possible that the interaction between Atg9 and the COG complex is transient. Atg9 is an integral membrane protein that cycles between the PAS and peripheral sites and is directly involved in double-membrane vesicle formation (161, 185). During its cycling, it remains associated with lipid, which makes Atg9 a prime candidate for a carrier that brings membrane from a source(s) to the PAS (185). We hypothesize that the COG complex may function as a tethering factor allowing Atg9-containing vesicles to fuse with the expanding phagophore at the PAS, which might explain the transient interaction between the tether and Atg9.

In conclusion, our data provide the first evidence indicating that the COG complex may act as a tethering factor mediating the condensation of transient vesicles with the phagophore at the PAS, which is required for Cvt vesicle and autophagosome formation and completion.

Materials and Methods

Strains, Media, and Materials

The yeast strains used in this study are listed in Table 4.1. For gene disruption, the entire coding regions were replaced with the *Kluveromyces lactis URA3, LEU2*, *Saccharomyces kluyveri HIS3*, *Saccharomyces pombe HIS5*, *Saccharomyces cerevisiae TRP1*, *HIS3*, or the *Escherichia coli kan^r^*, gene using polymerase chain reaction (PCR) primers containing ~50 bases identical to the flanking regions of the open reading frames. PCR-based integrations of green fluorescent protein (GFP) at the 3' end of *PEX14*, *COG1*, *COG2*, *COG6*, and *cog2-1*, and red fluorescent protein (RFP) tags at the 3' end of *VRG4*, pFA6a-GFP-HIS3, pFA6a-GFP-KanMX, pFA6a-GFP-TRP1, pFA6a-mRFP-TRP1, pFA6a-mRFP-HIS5 *S.p.*, and pFA6a-mRFP-KanMX were used as templates to generate strains expressing fusion proteins under the control of their native promoters (24, 58, 138). For PCR-based replacement of the *GAL1* promoter with an N-terminal HA tag at the 5' end of *COG1*, *COG2*, *COG3* and *COG4*, pFA6a-KanMX6-PGAL1-3HA was used as a template (138). PCR was used to verify the fusion protein. To generate an Atg9-3GFP fusion, the integrative plasmid pAtg9-3GFP (306) was linearlized by *Stu*I digestion and integrated into the *URA3* gene locus.

Strains were grown in YPD (1% yeast extract, 2% peptone, and 2% glucose), synthetic minimal medium (SMD; 2% glucose, 0.67% yeast nitrogen base without amino acids, supplemented with vitamins and appropriate amino acids), YPG (1% yeast extract, 2% peptone, and 2% galactose), or synthetic minimal medium with galactose (SMG; 2% galactose, 0.67% yeast nitrogen base without amino acids, supplemented with vitamins

and appropriate amino acids). Nitrogen starvation experiments were carried out in synthetic medium lacking nitrogen (SD-N; 0.17% yeast nitrogen base without amino acids, ammonium sulfate and vitamins, but containing 2% glucose).

Plasmids and Constructions

The plasmids pGAD-Cog1, pGBDu-Cog1, pGAD-Cog3, and pGBDu-Cog3 were generated by PCR amplifying the full-length *COG1* or *COG3* gene, respectively, and ligated into the *BamH*I/*Pst*I sites of the pGAD-C1 and pGBDU-C1 vectors. The pGAD-Cog2 and pGBDU-Cog1 plasmids were created by ligating the DNA fragment encoding full-length Cog2 with *EcoR*I and *Bgl*II sites into the pGAD-C1 and pGBDU-C1 plasmids. The pGAD-Cog4 and pGBDU-Cog4 were generated by amplifying the *COG4* gene and cloning as *BamH*I/*Bgl*II fragments into pGAD-C1 and pGBDU-C1 vectors. The plasmids pGFP-AUT7(416) (100), pRFP-Ape1(305) (207), pAtg9-3GFP(306) (154), pSpo7-RFP(425) (185), pProtA-CVT13(424) (160), pProtA-APG17(424) (160), pProtA-CVT20(424) (160), pRS424-CuProtA (101), and pMyc-APG12(426) (152) have been described previously. Plasmids expressing mutant forms of *COG4*, pBCR115 and pBCR137, were generated by PCR amplification of genomic *COG4*, including 400 bases of genomic DNA on either side of the gene, ligating the product into the pRS415 URA CEN plasmid, and introducing site-directed mutations. Residues shown to be both surface exposed (by x-ray crystallographic analysis of human Cog4) and well conserved across multiple species were selected for mutation by alanine truncation or charge introduction as appropriate (B.C.R. and F.M.H., unpublished results). To create pBCR115, a single QuikChange (Stratagene) reaction was used to generate the double substitution mutant

N607A, T608A. To create pBCR137, six mutations were introduced using the QuikChange Multi kit (Stratagene): N787A, R788A, G795D, C798D, R805A and E806A. The corresponding residues, in human Cog4, constitute a single large conserved patch on the surface of the protein (B.C.R. and F.M.H., unpublished results). To generate an Atg11 integration plasmid, first pATG11(414) was made by cloning the PCR fragment containing the *ATG11* promoter, ORF and terminator regions into the *Xma*I site of pRS414. A *Not*I-*Sal*I fragment containing *ATG11* was cut from pAtg11(414) and inserted into the corresponding sites of pRS307 to generate pATG11(307). pATG11(307) was linearized with *Pml*I and integrated into the *LYS* locus.

Ape1 Pulse-Chase Radiolabeling

Cells were grown in SMD medium at 24˚C to OD_{600}=0.8. 20 OD_{600} units of cells were collected and converted to spheroplasts, then incubated at 38˚C for 20 min. Spheroplasts were harvested and resuspended in 200 µl of spheroplasting medium (1.2 M sorbitol, 2% glucose, 0.67% yeast nitrogen base without amino acids, supplemented with vitamins and appropriate amino acids) without methionine and cysteine for 5 min at the same temperatures. Cells then were labeled with Trans-[^{35}S] methionine/cysteine for 10 min (10 μCi/OD_{600}). Chase was initiated by adding 4 ml of chase medium (SMD containing 0.2% yeast extract, 1.2 M sorbitol, and 2 mM cysteine and methionine). At each indicated time point, samples were collected, and the total cell lysate were prepared by adding ice-cold osmotic lysis buffer (20 mM PIPES, pH 6.8, 200 mM sorbitol, 5 mM $MgCl_2$, and complete EDTA-free proteinase inhibitor cocktail) at a spheroplast density of 20 OD_{600}/ml to lyse the cells. To obtain the prApe1-containing P5 fractions, cell lysates

were subjected to a 5,000 x g centrifugation for 5 min. The P5 fractions were then resuspended in osmotic lysis buffer, split into 4 aliquots, then subjected to proteinase K (100 μg/ml) and/or triton X-100 (0.2%) treatment on ice for 30 min. 10% trichloroacetic acid (TCA) was added to precipitate the cell lysates, the precipitates were washed twice with 100% acetone, and immunoprecipitated as described previously (263).

Fluorescence Microscopy

Yeast cells expressing fusion proteins with fluorescence tags were grown to OD_{600}=0.8 in YPD or SMD selective medium or starved in SD-N before imaging. To label the mitochondria, MitoFluor Red 589 (Invitrogen) was added to the growing culture with a final concentration of 1 μM for 30 min before imaging. Starved cells were stained with MitoFluor Red for 1 h before imaging. For rapamycin treatment, 0.2 μg/ml rapamycin were added to the culture. Cells were visualized with a fluorescence microscope (IX71; Olympus) fitted with differential interference contrast optics and Photometrics CoolSNAP HQ camera (Roper Scientific, Tucson, AZ). The images were deconvolved using softWoRx software (Applied Precision, Issaquah, WA).

Protein A-Affinity Isolation and Co-Immunoprecipitation

Cells (50 ml) were grown in SMG medium to OD_{600}=1.0. Protein A (PA)-affinity isolation was carried out as described previously (29). We performed Co-immunoprecipitation experiments using the same procedure as PA-affinity isolation, with only one exception: the cell lysates were incubated with protein A-Sepharose beads (50% suspension) and 5 μl monoclonal anti-HA or anti-Myc antibody overnight at 4°C. The

resulting immunocomplex was subjected to immunoblotting with monoclonal anti-HA or anti-Myc antibodies.

Additional assays

The GFP-Atg8 processing assay, Pex14-GFP processing to monitor pexophagy progression, the alkaline phosphatase assay to measure Pho8Δ60 activity, and immunoelectron microscopy procedures were performed as previously described (9, 162, 183, 230).

CHAPTER 5

Conclusions and Contributions

In this thesis, I have described my studies contributing to our understanding of the molecular machinery of the Cvt and autophagy pathways in the yeast *Saccharomyces cerevisiae*. The advances made in the areas by these studies include: first, I have characterized the role of an autophagy-related protein, Atg27, in the Cvt, autophagy, and pexophagy pathways. These results extend the current understanding on the molecular components of these pathways. Second, my work has helped elucidate the factors that are involved in the regulation of Atg9 cycling, and in particular the anterograde transport of this protein to the PAS. Third, as a result of my work, I have identified the tethering complex, the conserved oligomeric Golgi complex (COG), as being required for double-membrane Cvt vesicle and autophagosome formation.

Chapter 1 introduced a thorough review of the autophagy pathway and the current understanding of the significant role of autophagy in the aging process. In this review, I described the role of autophagy with an emphasis on the links between signaling pathways that are involved in the regulation of autophagy induction with regard to aging. I also discussed the interpretations of our current understanding of the functions of the Atg proteins and the major questions that remain in this field.

Chapter 2 describes the characterization of *ATG27*, a previously known *ATG* gene.

Atg27 was originally identified as a PtdIns(3)P-binding protein with a putative

PtdIns(3)P binding site (254). Because of the correction of a sequencing error in the

Saccharomyces Genome Database, I first re-characterized the topology and function of

the true full-length Atg27. With 75 additional amino acids at the N terminus, Atg27 is a

type I transmembrane protein containing an N-terminal signal sequence. This finding is

important because now the putative PtdIns(3)P-binding site will be placed in the lumenal

portion of this protein, which is less likely to bind cytosolic face membrane-localized

PtdIns(3)P. Moreover, the majority of this protein would be present within the

intermembrane space between the autophagosome inner and outer membrane. What kind

of role would Atg27 play within the intermembrane space of the autophagosome? Further

work remains to be done to understand the molecular function of Atg27.

In this chapter, I also carefully analyzed the phenotype of the *atg27Δ* mutant and

revealed that it is required for both the Cvt and autophagy pathways to occur efficiently.

Atg27 is unique in its localization, showing a multiple puncta distribution, that, in

addition to the PAS, includes the Golgi complex. What is the mechanism by which Atg27

helps autophagosomes form efficiently? One possibility is that Atg27 itself directly

mediates efficient membrane delivery to the forming autophagosome. If so, it would

imply that Atg27 is a marker protein for the donating membrane. This is a very

interesting possibility. In fact, Atg27 localizes to the Golgi complex, which may indicate

the potential role of this organelle as one of the membrane sources for the forming

double-membrane vesicles. Another possibility is that Atg27 may regulate other Atg

proteins that are required for autophagosome formation. In this case, the loss of Atg27

would result in inefficient function of these factors, and thus smaller autophagosomes would be formed. This possibility is equally intriguing because Atg27 is required for Atg9 cycling, a protein that is believed to be the potential membrane carrier (see bellow). In both cases, the absence of Atg27 would result in inefficient formation of autophagosomes, which agree with the observation that a smaller number of autophagosomes were formed in the *atg27* mutant compared with wild-type cells.

Autophagosome biogenesis is considered a *de novo* process, in which small membranes are sequentially added onto the phagophore, the initial sequestering structure, leading to expansion and ultimately the formation of a completed autophagosome. How the rapid membrane remodeling that is characteristic of autophagosome biogenesis is achieved remains a fundamental open question. Atg9 is the first identified transmembrane Atg protein that is required for autophagosome formation. This protein shows unique multiple punctate structures that correspond to the PAS and other peripheral sites; Atg9 partially localizes at mitochondria and possibly at the Golgi complex, both of which may provide membranes to the forming phagophore. The multiple puncta localization of Atg27 is similar to that of Atg9, and the correct localization and transit patterns of both proteins are dependent on each other. In addition, both Atg9 and Atg27 shuttle between the PAS and peripheral sites. Thus, we hypothesized that Atg9 and Atg27 may be functionally related, possibly in membrane delivery to the PAS.

The molecular mechanism and regulation of factors involved in autophagosome formation remains unclear. Any advance made in understanding the regulation of these factors would be a major step forward. Further work needs to be done to address the

molecular function of Atg27 in regulation of Atg9 protein trafficking, as well as the meaning of their Golgi complex localization.

The function of anterograde transport of Atg9 from the peripheral sites to the PAS may be to deliver lipid or proteins to the double-membrane vesicle formation site, and retrieval of Atg9 from the PAS may recycle the protein back to the membrane sources for the next round of delivery. Several components are required for Atg9 release from the PAS, including the Atg1-Atg13 complex, Atg2, Atg18, and the phosphatidylinositol 3-kinase complex (186). However, the factors that are required for Atg9 antrograde movement to the PAS remain unclear. Chapter 3 describes the discovery of two Atg proteins, Atg23 and Atg27, that are involved in Atg9 antrograde transport to the PAS. In collaboration with Dr. Julie Legakis in our lab, we found that these two Atg proteins show a similar multiple puncta distribution to that of Atg9. These proteins interact with one another and form a complex. In addition, the proper transport of each of these proteins requires the other two. This is the first demonstration that the Atg9 complex components display an interdependency in their movement.

Our lab recently discovered that a purified Atg9 complex recovered by tandem affinity purification revealed four major protein bands at sizes of 94, 50, 28 and 25 kDa (67). This suggests that in addition to Atg23 and Atg27, additional proteins may exit in an Atg9 complex. It would be interesting to characterize these components within the Atg9 complex and their roles in regulating Atg9 trafficking during autophagosome formation.

Finally, chapter 4 describes an important discovery regarding the mechanism for double-membrane Cvt vesicle and autophagosome formation. This work has led to the

identification of the tethering factor that is involved in double-membrane vesicle formation. It has been proposed that during the process of double-membrane vesicle formation, there are two membrane fusion events: the condensation of transient vesicles with the phagophore at the PAS, and the fusion of the completed double-membrane vesicles with the vacuole. The last event is the best characterized and shares similar components that are needed for other vesicle fusion events. In contrast, little is known about the role of SNAREs or tethering factors in the phagophore expansion step. Through the screening of the yeast deletion library, Dr. Takahiro Shintani found that mutants with a deletion of non-essential conserved oligomeric Golgi (COG) complex genes, *COG1*, *COG5*, *COG6*, *COG7*, and *COG8*, blocks the Cvt pathway. In yeast, the COG complex contains 8 subunits (Cog1 to Cog8) and Cog1 is a central subunit which connects two lobes: lobe A (Cog2 to Cog4) and lobe B (Cog5 to Cog8), participating in intra-Golgi retrograde, ER-to-Golgi, and endosome-to-Golgi transport (232). We found that Cog1 and lobe A components are required for bulk autophagy, and the Cvt, and pexophagy pathways, whereas the lobe B components are only involved in the Cvt pathway. There are two possibilities to explain the autophagy defect in the COG mutants. First, the COG complex could indirectly affect the Cvt pathway and autophagy, because evidence suggests that the early secretory pathway is required to maintain the membrane flow for normal Cvt and autophagy progression (78, 187). Thus, a disrupted Golgi complex in COG mutants would block membrane flow through the secretory pathway and result in a Cvt and autophagy defect. The second possibility is particularly intriguing; it could imply that the COG complex is directly involved in the formation of double-membrane vesicles. My research has demonstrated that the COG complex not only localizes to the PAS but

also interacts with Atg17, Atg20, and Atg24. This is the first evidence supporting the idea that the COG complex may be directly involved in autophagosome formation. In addition, in the *cog2-1* mutant GFP-Atg8 was dispersed throughout the cytosol in multiple clusters and dots by both fluorescence microscopy and immunoelectron microscopy (Fig. 4.3). These results support the hypothesis that the COG complex may act as a tethering factor mediating the condensation of transient vesicles during the phagophore expension step at the PAS.

The finding of the role of the COG complex in autophagosome formation may also provide insight into the orgin of the membrane for the double-membrane vesicles. The majority of the COG complex associates with the Golgi membrane suggesting that the COG complex may reside on transient vesicles derived from the Golgi complex as well as at the PAS to mediate the fusion events. In addition to the Golgi complex, COG also functions in endosome-to-Golgi retrograde transport (70). The association with two sorting nexins, Atg24/Snx4 and Atg20/Snx42, assigns a new function to these two Atg proteins in mediating a vesicle tethering event. It also raises a question about where the interaction between COG and Atg24/Snx4 and Atg20/Snx42 takes place: the Golgi complex, endosome, and/or the PAS. Future work is needed to elucidate the function of the COG complex, Atg20 and Atg24 as well as the spatial and temporal order of the vesicle tethering event for the formation of double-membrane Cvt vesicles and autophagosomes.

REFERENCES

1.   Abeliovich H, Zhang C, Dunn WA, Jr., Shokat KM, Klionsky DJ. 2003. Chemical genetic analysis of Apg1 reveals a non-kinase role in the induction of autophagy. *Mol Biol Cell* 14: 477-90

2.   Albertini M, Rehling P, Erdmann R, Girzalsky W, Kiel JA, et al. 1997. Pex14p, a peroxisomal membrane protein binding both receptors of the two PTS-dependent import pathways. *Cell* 89: 83-92

3.   Alexeyev MF, Ledoux SP, Wilson GL. 2004. Mitochondrial DNA and aging. *Clin Sci (Lond)* 107: 355-64

4.   Andziak B, O'Connor TP, Buffenstein R. 2005. Antioxidants do not explain the disparate longevity between mice and the longest-living rodent, the naked mole-rat. *Mech Ageing Dev* 126: 1206-12

5.   Anson RM, Hansford RG. 2004. Mitochondrial influence on aging rate in *Caenorhabditis elegans*. *Aging Cell* 3: 29-34

6.   Apfeld J, O'Connor G, McDonagh T, DiStefano PS, Curtis R. 2004. The AMP-activated protein kinase AAK-2 links energy levels and insulin-like signals to lifespan in *C. elegans*. *Genes Dev* 18: 3004-9

7.   Araki T, Sasaki Y, Milbrandt J. 2004. Increased nuclear NAD biosynthesis and SIRT1 activation prevent axonal degeneration. *Science* 305: 1010-3

8.   Arden KC. 2007. FoxOs in tumor suppression and stem cell maintenance. *Cell* 128: 235-7

9.   Baba M, Osumi M, Scott SV, Klionsky DJ, Ohsumi Y. 1997. Two distinct pathways for targeting proteins from the cytoplasm to the vacuole/lysosome. *J Cell Biol* 139: 1687-95

10.   Baur JA, Pearson KJ, Price NL, Jamieson HA, Lerin C, et al. 2006. Resveratrol improves health and survival of mice on a high-calorie diet. *Nature* 444: 337-42

11.   Bayne AC, Mockett RJ, Orr WC, Sohal RS. 2005. Enhanced catabolism of mitochondrial superoxide/hydrogen peroxide and aging in transgenic Drosophila. *Biochem J* 391: 277-84

12.   Bergamini E, Cavallini G, Donati A, Gori Z. 2007. The role of autophagy in aging: its essential part in the anti-aging mechanism of caloric restriction. *Ann N Y Acad Sci* 1114: 69-78

13.   Bjørkøy G, Lamark T, Brech A, Outzen H, Perander M, et al. 2005. p62/SQSTM1 forms protein aggregates degraded by autophagy and has a protective effect on huntingtin-induced cell death. *J Cell Biol* 171: 603-14

14. Bluher M, Kahn BB, Kahn CR. 2003. Extended longevity in mice lacking the insulin receptor in adipose tissue. *Science* 299: 572-4

15. Bonawitz ND, Chatenay-Lapointe M, Pan Y, Shadel GS. 2007. Reduced TOR signaling extends chronological life span via increased respiration and upregulation of mitochondrial gene expression. *Cell Metab* 5: 265-77

16. Bonkowski MS, Rocha JS, Masternak MM, Al Regaiey KA, Bartke A. 2006. Targeted disruption of growth hormone receptor interferes with the beneficial actions of calorie restriction. *Proc Natl Acad Sci U S A* 103: 7901-5

17. Brown-Borg HM, Borg KE, Meliska CJ, Bartke A. 1996. Dwarf mice and the ageing process. *Nature* 384: 33

18. Bruinsma P, Spelbrink RG, Nothwehr SF. 2004. Retrograde transport of the mannosyltransferase Och1p to the early Golgi requires a component of the COG transport complex. *J Biol Chem* 279: 39814-23

19. Brunet A, Sweeney LB, Sturgill JF, Chua KF, Greer PL, et al. 2004. Stress-dependent regulation of FOXO transcription factors by the SIRT1 deacetylase. *Science* 303: 2011-5

20. Budovskaya YV, Stephan JS, Deminoff SJ, Herman PK. 2005. An evolutionary proteomics approach identifies substrates of the cAMP-dependent protein kinase. *Proc Natl Acad Sci U S A* 102: 13933-8

21. Budovskaya YV, Stephan JS, Reggiori F, Klionsky DJ, Herman PK. 2004. The Ras/cAMP-dependent protein kinase signaling pathway regulates an early step of the autophagy process in *Saccharomyces cerevisiae*. *J Biol Chem* 279: 20663-71

22. Buetler TM, Krauskopf A, Ruegg UT. 2004. Role of superoxide as a signaling molecule. *News Physiol Sci* 19: 120-3

23. Cameroni E, Hulo N, Roosen J, Winderickx J, De Virgilio C. 2004. The novel yeast PAS kinase Rim 15 orchestrates G0-associated antioxidant defense mechanisms. *Cell Cycle* 3: 462-8

24. Campbell TN, Choy FY. 2002. Expression of two green fluorescent protein variants in citrate-buffered media in *Pichia pastoris*. *Anal Biochem* 311: 193-5

25. Cao Y, Cheong H, Song H, Klionsky DJ. 2008. In vivo reconstitution of autophagy in *Saccharomyces cerevisiae*. *J Cell Biol* 182: 703-13

26. Chang T, Schroder LA, Thomson JM, Klocman AS, Tomasini AJ, et al. 2005. PpATG9 encodes a novel membrane protein that traffics to vacuolar membranes, which sequester peroxisomes during pexophagy in *Pichia pastoris*. *Mol Biol Cell* 16: 4941-53

27. Chen D, Steele AD, Lindquist S, Guarente L. 2005. Increase in activity during calorie restriction requires Sirt1. *Science* 310: 1641

28. Chen Y, McMillan-Ward E, Kong J, Israels SJ, Gibson SB. 2007. Mitochondrial electron-transport-chain inhibitors of complexes I and II induce autophagic cell death mediated by reactive oxygen species. *J Cell Sci* 120: 4155-66

29. Cheong H, Nair U, Geng J, Klionsky DJ. 2008. The Atg1 kinase complex is involved in the regulation of protein recruitment to initiate sequestering vesicle formation for nonspecific autophagy in *Saccharomyces cerevisiae*. *Mol Biol Cell* 19: 668-81

30. Cheong H, Yorimitsu T, Reggiori F, Legakis JE, Wang C-W, Klionsky DJ. 2005. Atg17 regulates the magnitude of the autophagic response. *Mol Biol Cell* 16: 3438-53

31. Chua KF, Mostoslavsky R, Lombard DB, Pang WW, Saito S, et al. 2005. Mammalian SIRT1 limits replicative life span in response to chronic genotoxic stress. *Cell Metab* 2: 67-76

32. Clancy DJ, Gems D, Harshman LG, Oldham S, Stocker H, et al. 2001. Extension of life-span by loss of CHICO, a Drosophila insulin receptor substrate protein. *Science* 292: 104-6

33. Corona M, Hughes KA, Weaver DB, Robinson GE. 2005. Gene expression patterns associated with queen honey bee longevity. *Mech Ageing Dev* 126: 1230-8

34. Coschigano KT, Clemmons D, Bellush LL, Kopchick JJ. 2000. Assessment of growth parameters and life span of GHR/BP gene-disrupted mice. *Endocrinology* 141: 2608-13

35. Crauwels M, Donaton MC, Pernambuco MB, Winderickx J, de Winde JH, Thevelein JM. 1997. The Sch9 protein kinase in the yeast Saccharomyces cerevisiae controls cAPK activity and is required for nitrogen activation of the fermentable-growth-medium-induced (FGM) pathway. *Microbiology* 143 (Pt 8): 2627-37

36. Cuervo AM, Bergamini E, Brunk UT, Droge W, Ffrench M, Terman A. 2005. Autophagy and aging: the importance of maintaining "clean" cells. *Autophagy* 1: 131-40

37. Cuervo AM, Dice JF. 1998. How do intracellular proteolytic systems change with age? *Front Biosci* 3: d25-43

38. Daitoku H, Hatta M, Matsuzaki H, Aratani S, Ohshima T, et al. 2004. Silent information regulator 2 potentiates Foxo1-mediated transcription through its deacetylase activity. *Proc Natl Acad Sci U S A* 101: 10042-7

39. Demarchi F, Bertoli C, Copetti T, Tanida I, Brancolini C, et al. 2006. Calpain is required for macroautophagy in mammalian cells. *J Cell Biol* 175: 595-605

40. Dillin A, Hsu AL, Arantes-Oliveira N, Lehrer-Graiwer J, Hsin H, et al. 2002. Rates of behavior and aging specified by mitochondrial function during development. *Science* 298: 2398-401

41. Dilova I, Easlon E, Lin SJ. 2007. Calorie restriction and the nutrient sensing signaling pathways. *Cell Mol Life Sci* 64: 752-67

42. Drees BL, Sundin B, Brazeau E, Caviston JP, Chen GC, et al. 2001. A protein interaction map for cell polarity development. *J Cell Biol* 154: 549-71

43. Dunn WA, Jr., Cregg JM, Kiel JAKW, van der Klei IJ, Oku M, et al. 2005. Pexophagy: the selective autophagy of peroxisomes. *Autophagy* 1: 75-83

44. Fabrizio P, Gattazzo C, Battistella L, Wei M, Cheng C, et al. 2005. Sir2 blocks extreme life-span extension. *Cell* 123: 655-67

45. Fabrizio P, Pletcher SD, Minois N, Vaupel JW, Longo VD. 2004. Chronological aging-independent replicative life span regulation by Msn2/Msn4 and Sod2 in *Saccharomyces cerevisiae*. *FEBS Lett* 557: 136-42

46. Fabrizio P, Pozza F, Pletcher SD, Gendron CM, Longo VD. 2001. Regulation of longevity and stress resistance by Sch9 in yeast. *Science* 292: 288-90

47. Farre JC, Subramani S. 2004. Peroxisome turnover by micropexophagy: an autophagy-related process. *Trends Cell Biol* 14: 515-23

48. Felkai S, Ewbank JJ, Lemieux J, Labbe JC, Brown GG, Hekimi S. 1999. CLK-1 controls respiration, behavior and aging in the nematode *Caenorhabditis elegans*. *EMBO J* 18: 1783-92

49. Feng J, Bussiere F, Hekimi S. 2001. Mitochondrial electron transport is a key determinant of life span in *Caenorhabditis elegans*. *Dev Cell* 1: 633-44

50. Fengsrud M, Erichsen ES, Berg TO, Raiborg C, Seglen PO. 2000. Ultrastructural characterization of the delimiting membranes of isolated autophagosomes and amphisomes by freeze-fracture electron microscopy. *Eur J Cell Biol* 79: 871-82

51. Fotso P, Koryakina Y, Pavliv O, Tsiomenko AB, Lupashin VV. 2005. Cog1p plays a central role in the organization of the yeast conserved oligomeric Golgi complex. *J Biol Chem* 280: 27613-23

52. Fridell YW, Sanchez-Blanco A, Silvia BA, Helfand SL. 2005. Targeted expression of the human uncoupling protein 2 (hUCP2) to adult neurons extends life span in the fly. *Cell Metab* 1: 145-52

53. Gerhardt B, Kordas TJ, Thompson CM, Patel P, Vida T. 1998. The vesicle transport protein Vps33p is an ATP-binding protein that localizes to the cytosol in an energy-dependent manner. *J Biol Chem* 273: 15818-29

54. Goldstein A, Lampen JO. 1975. Beta-D-fructofuranoside fructohydrolase from yeast. *Methods Enzymol* 42: 504-11

55. Gottlieb S, Esposito RE. 1989. A new role for a yeast transcriptional silencer gene, SIR2, in regulation of recombination in ribosomal DNA. *Cell* 56: 771-6

56. Gross L, Dreyfuss Y. 1990. Prevention of spontaneous and radiation-induced tumors in rats by reduction of food intake. *Proc Natl Acad Sci U S A* 87: 6795-7

57. Guarente L, Picard F. 2005. Calorie restriction--the SIR2 connection. *Cell* 120: 473-82

58. Gueldener U, Heinisch J, Koehler GJ, Voss D, Hegemann JH. 2002. A second set of loxP marker cassettes for Cre-mediated multiple gene knockouts in budding yeast. *Nucleic Acids Res* 30: e23

59. Hamasaki M, Noda T, Ohsumi Y. 2003. The early secretory pathway contributes to autophagy in yeast. *Cell Struct Funct* 28: 49-54

60. Hansen M, Chandra A, Mitic LL, Onken B, Driscoll M, Kenyon C. 2008. A role for autophagy in the extension of lifespan by dietary restriction in *C. elegans*. *PLoS Genet* 4: e24

61. Hansen M, Hsu AL, Dillin A, Kenyon C. 2005. New genes tied to endocrine, metabolic, and dietary regulation of lifespan from a *Caenorhabditis elegans* genomic RNAi screen. *PLoS Genet* 1: 119-28

62. Hara T, Nakamura K, Matsui M, Yamamoto A, Nakahara Y, et al. 2006. Suppression of basal autophagy in neural cells causes neurodegenerative disease in mice. *Nature* 441: 885-9

63. Hardie DG, Hawley SA. 2001. AMP-activated protein kinase: the energy charge hypothesis revisited. *Bioessays* 23: 1112-9

64. Harding TM, Morano KA, Scott SV, Klionsky DJ. 1995. Isolation and characterization of yeast mutants in the cytoplasm to vacuole protein targeting pathway. *J Cell Biol* 131: 591-602

65. Harman D. 1972. The biologic clock: the mitochondria? *J Am Geriatr Soc* 20: 145-7

66. Hars ES, Qi H, Ryazanov AG, Jin S, Cai L, et al. 2007. Autophagy regulates ageing in *C. elegans*. *Autophagy* 3: 93-5

67. He C, Baba M, Klionsky DJ. 2009. Double duty of Atg9 self-association in autophagosome biogenesis. *Autophagy* 5: 385-7

68. He C, Song H, Yorimitsu T, Monastyrska I, Yen WL, et al. 2006. Recruitment of Atg9 to the preautophagosomal structure by Atg11 is essential for selective autophagy in budding yeast. *J Cell Biol* 175: 925-35

69. Heilbronn LK, Ravussin E. 2003. Calorie restriction and aging: review of the literature and implications for studies in humans. *Am J Clin Nutr* 78: 361-9

70. Hettema EH, Lewis MJ, Black MW, Pelham HRB. 2003. Retromer and the sorting nexins Snx4/41/42 mediate distinct retrieval pathways from yeast endosomes. *EMBO J* 22: 548-57

71. Honda Y, Honda S. 1999. The *daf-2* gene network for longevity regulates oxidative stress resistance and Mn-superoxide dismutase gene expression in *Caenorhabditis elegans*. *FASEB J* 13: 1385-93

72. Houthoofd K, Johnson TE, Vanfleteren JR. 2005. Dietary restriction in the nematode *Caenorhabditis elegans*. *J Gerontol A Biol Sci Med Sci* 60: 1125-31

73. Huang J, Klionsky DJ. 2007. Autophagy and human disease. *Cell Cycle* 6: 1837-49

74. Huang TT, Carlson EJ, Gillespie AM, Shi Y, Epstein CJ. 2000. Ubiquitous overexpression of CuZn superoxide dismutase does not extend life span in mice. *J Gerontol A Biol Sci Med Sci* 55: B5-9

75. Huang WP, Scott SV, Kim J, Klionsky DJ. 2000. The itinerary of a vesicle component, Aut7p/Cvt5p, terminates in the yeast vacuole via the autophagy/Cvt pathways. *J Biol Chem* 275: 5845-51

76. Hutchins MU, Klionsky DJ. 2001. Vacuolar localization of oligomeric α-mannosidase requires the cytoplasm to vacuole targeting and autophagy pathway components in *Saccharomyces cerevisiae*. *J Biol Chem* 276: 20491-8

77. Hwangbo DS, Gershman B, Tu MP, Palmer M, Tatar M. 2004. Drosophila dFOXO controls lifespan and regulates insulin signalling in brain and fat body. *Nature* 429: 562-6

78. Ishihara N, Hamasaki M, Yokota S, Suzuki K, Kamada Y, et al. 2001. Autophagosome requires specific early Sec proteins for its formation and NSF/SNARE for vacuolar fusion. *Mol Biol Cell* 12: 3690-702

79. Ishii N, Fujii M, Hartman PS, Tsuda M, Yasuda K, et al. 1998. A mutation in succinate dehydrogenase cytochrome b causes oxidative stress and ageing in nematodes. *Nature* 394: 694-7

80. James P, Halladay J, Craig EA. 1996. Genomic libraries and a host strain designed for highly efficient two-hybrid selection in yeast. *Genetics* 144: 1425-36

81. Jia K, Chen D, Riddle DL. 2004. The TOR pathway interacts with the insulin signaling pathway to regulate *C. elegans* larval development, metabolism and life span. *Development* 131: 3897-906

82. Jorgensen P, Rupes I, Sharom JR, Schneper L, Broach JR, Tyers M. 2004. A dynamic transcriptional network communicates growth potential to ribosome synthesis and critical cell size. *Genes Dev* 18: 2491-505

83. Juhasz G, Erdi B, Sass M, Neufeld TP. 2007. Atg7-dependent autophagy promotes neuronal health, stress tolerance, and longevity but is dispensable for metamorphosis in *Drosophila. Genes Dev* 21: 3061-6

84. Juhasz G, Neufeld TP. 2006. Autophagy: a forty-year search for a missing membrane source. *PLoS Biol* 4: e36

85. Juhasz G, Puskas LG, Komonyi O, Erdi B, Maroy P, et al. 2007. Gene expression profiling identifies FKBP39 as an inhibitor of autophagy in larval *Drosophila* fat body. *Cell Death Differ* 14: 1181-90

86. Kaeberlein M, Hu D, Kerr EO, Tsuchiya M, Westman EA, et al. 2005. Increased life span due to calorie restriction in respiratory-deficient yeast. *PLoS Genet* 1: e69

87. Kaeberlein M, McVey M, Guarente L. 1999. The SIR2/3/4 complex and SIR2 alone promote longevity in *Saccharomyces cerevisiae* by two different mechanisms. *Genes Dev* 13: 2570-80

88. Kaeberlein M, Powers RW, 3rd, Steffen KK, Westman EA, Hu D, et al. 2005. Regulation of yeast replicative life span by TOR and Sch9 in response to nutrients. *Science* 310: 1193-6

89. Kaiser CA, Schekman R. 1990. Distinct sets of SEC genes govern transport vesicle formation and fusion early in the secretory pathway. *Cell* 61: 723-33

90. Kamada Y, Funakoshi T, Shintani T, Nagano K, Ohsumi M, Ohsumi Y. 2000. Tor-mediated induction of autophagy via an Apg1 protein kinase complex. *J Cell Biol* 150: 1507-13

91. Kanki T, Klionsky DJ. 2008. Mitophagy in yeast occurs through a selective mechanism. *J Biol Chem* 283: 32386-93

92. Kapahi P, Zid BM, Harper T, Koslover D, Sapin V, Benzer S. 2004. Regulation of lifespan in Drosophila by modulation of genes in the TOR signaling pathway. *Curr Biol* 14: 885-90

93. Kawamata T, Kamada Y, Suzuki K, Kuboshima N, Akimatsu H, et al. 2005. Characterization of a novel autophagy-specific gene, ATG29. *Biochem Biophys Res Commun* 338: 1884-9

94. Kayser EB, Sedensky MM, Morgan PG. 2004. The effects of complex I function and oxidative damage on lifespan and anesthetic sensitivity in *Caenorhabditis elegans. Mech Ageing Dev* 125: 455-64

95. Kennedy BK, Austriaco NR, Jr., Zhang J, Guarente L. 1995. Mutation in the silencing gene SIR4 can delay aging in S. cerevisiae. *Cell* 80: 485-96

96. Kennedy BK, Steffen KK, Kaeberlein M. 2007. Ruminations on dietary restriction and aging. *Cell Mol Life Sci* 64: 1323-8

97. Kihara A, Noda T, Ishihara N, Ohsumi Y. 2001. Two distinct Vps34 phosphatidylinositol 3-kinase complexes function in autophagy and carboxypeptidase Y sorting in *Saccharomyces cerevisiae. J Cell Biol* 152: 519-30

98. Kim DW, Sacher M, Scarpa A, Quinn AM, Ferro-Novick S. 1999. High-copy suppressor analysis reveals a physical interaction between Sec34p and Sec35p, a protein implicated in vesicle docking. *Mol Biol Cell* 10: 3317-29

99.   Kim I, Rodriguez-Enriquez S, Lemasters JJ. 2007. Selective degradation of mitochondria by mitophagy. *Arch Biochem Biophys* 462: 245-53

100.   Kim J, Huang W-P, Klionsky DJ. 2001. Membrane recruitment of Aut7p in the autophagy and cytoplasm to vacuole targeting pathways requires Aut1p, Aut2p, and the autophagy conjugation complex. *J Cell Biol* 152: 51-64

101.   Kim J, Huang W-P, Stromhaug PE, Klionsky DJ. 2002. Convergence of multiple autophagy and cytoplasm to vacuole targeting components to a perivacuolar membrane compartment prior to de novo vesicle formation. *J Biol Chem* 277: 763-73

102.   Kim J, Kamada Y, Stromhaug PE, Guan J, Hefner-Gravink A, et al. 2001. Cvt9/Gsa9 functions in sequestering selective cytosolic cargo destined for the vacuole. *J Cell Biol* 153: 381-96

103.   Kim J, Scott SV, Oda MN, Klionsky DJ. 1997. Transport of a large oligomeric protein by the cytoplasm to vacuole protein targeting pathway. *J Cell Biol* 137: 609-18

104.   Kimura KD, Tissenbaum HA, Liu Y, Ruvkun G. 1997. daf-2, an insulin receptor-like gene that regulates longevity and diapause in *Caenorhabditis elegans*. *Science* 277: 942-6

105.   Kirisako T, Baba M, Ishihara N, Miyazawa K, Ohsumi M, et al. 1999. Formation process of autophagosome is traced with Apg8/Aut7p in yeast. *J Cell Biol* 147: 435-46

106.   Kirisako T, Ichimura Y, Okada H, Kabeya Y, Mizushima N, et al. 2000. The reversible modification regulates the membrane-binding state of Apg8/Aut7 essential for autophagy and the cytoplasm to vacuole targeting pathway. *J Cell Biol* 151: 263-76

107.   Kirkland RA, Adibhatla RM, Hatcher JF, Franklin JL. 2002. Loss of cardiolipin and mitochondria during programmed neuronal death: evidence of a role for lipid peroxidation and autophagy. *Neuroscience* 115: 587-602

108.   Kissova I, Deffieu M, Samokhvalov V, Velours G, Bessoule JJ, et al. 2006. Lipid oxidation and autophagy in yeast. *Free Radic Biol Med* 41: 1655-61

109.   Klionsky DJ. 2005. The molecular machinery of autophagy: unanswered questions. *J Cell Sci* 118: 7-18

110.   Klionsky DJ, Banta LM, Emr SD. 1988. Intracellular sorting and processing of a yeast vacuolar hydrolase: proteinase A propeptide contains vacuolar targeting information. *Mol Cell Biol* 8: 2105-16

111.   Klionsky DJ, Cregg JM, Dunn WA, Jr., Emr SD, Sakai Y, et al. 2003. A unified nomenclature for yeast autophagy-related genes. *Dev Cell* 5: 539-45

112.   Klionsky DJ, Cueva R, Yaver DS. 1992. Aminopeptidase I of *Saccharomyces cerevisiae* is localized to the vacuole independent of the secretory pathway. *J Cell Biol* 119: 287-99

113.   Klionsky DJ, Emr SD. 2000. Autophagy as a regulated pathway of cellular degradation. *Science* 290: 1717-21

114.   Komatsu M, Waguri S, Chiba T, Murata S, Iwata J, et al. 2006. Loss of autophagy in the central nervous system causes neurodegeneration in mice. *Nature* 441: 880-4

115. Koubova J, Guarente L. 2003. How does calorie restriction work? *Genes Dev* 17: 313-21

116. Kraft C, Deplazes A, Sohrmann M, Peter M. 2008. Mature ribosomes are selectively degraded upon starvation by an autophagy pathway requiring the Ubp3p/Bre5p ubiquitin protease. *Nat Cell Biol* 10: 602-10

117. Kuma A, Hatano M, Matsui M, Yamamoto A, Nakaya H, et al. 2004. The role of autophagy during the early neonatal starvation period. *Nature* 432: 1032-6

118. Kurosu H, Yamamoto M, Clark JD, Pastor JV, Nandi A, et al. 2005. Suppression of aging in mice by the hormone Klotho. *Science* 309: 1829-33

119. Larsen PL, Albert PS, Riddle DL. 1995. Genes that regulate both development and longevity in *Caenorhabditis elegans*. *Genetics* 139: 1567-83

120. Lee CK, Klopp RG, Weindruch R, Prolla TA. 1999. Gene expression profile of aging and its retardation by caloric restriction. *Science* 285: 1390-3

121. Lee CK, Weindruch R, Prolla TA. 2000. Gene-expression profile of the ageing brain in mice. *Nat Genet* 25: 294-7

122. Lee IH, Cao L, Mostoslavsky R, Lombard DB, Liu J, et al. 2008. A role for the NAD-dependent deacetylase Sirt1 in the regulation of autophagy. *Proc Natl Acad Sci U S A* 105: 3374-9

123. Lee RY, Hench J, Ruvkun G. 2001. Regulation of C. elegans DAF-16 and its human ortholog FKHRL1 by the daf-2 insulin-like signaling pathway. *Curr Biol* 11: 1950-7

124. Lee SS, Kennedy S, Tolonen AC, Ruvkun G. 2003. DAF-16 target genes that control C. elegans life-span and metabolism. *Science* 300: 644-7

125. Lee SS, Lee RY, Fraser AG, Kamath RS, Ahringer J, Ruvkun G. 2003. A systematic RNAi screen identifies a critical role for mitochondria in *C. elegans* longevity. *Nat Genet* 33: 40-8

126. Legakis JE, Yen WL, Klionsky DJ. 2007. A cycling protein complex required for selective autophagy. *Autophagy* 3: 422-32

127. Legesse-Miller A, Sagiv Y, Glozman R, Elazar Z. 2000. Aut7p, a soluble autophagic factor, participates in multiple membrane trafficking processes. *J Biol Chem* 275: 32966-73

128. Lemasters JJ. 2005. Selective mitochondrial autophagy, or mitophagy, as a targeted defense against oxidative stress, mitochondrial dysfunction, and aging. *Rejuvenation Res* 8: 3-5

129. Lemieux ME, Yang X, Jardine K, He X, Jacobsen KX, et al. 2005. The Sirt1 deacetylase modulates the insulin-like growth factor signaling pathway in mammals. *Mech Ageing Dev* 126: 1097-105

130. Levavasseur F, Miyadera H, Sirois J, Tremblay ML, Kita K, et al. 2001. Ubiquinone is necessary for mouse embryonic development but is not essential for mitochondrial respiration. *J Biol Chem* 276: 46160-4

131. Levine B, Klionsky DJ. 2004. Development by self-digestion: molecular mechanisms and biological functions of autophagy. *Dev Cell* 6: 463-77

132. Levine B, Yuan J. 2005. Autophagy in cell death: an innocent convict? *J Clin Invest* 115: 2679-88

133.   Liang J, Shao SH, Xu ZX, Hennessy B, Ding Z, et al. 2007. The energy sensing LKB1-AMPK pathway regulates p27(kip1) phosphorylation mediating the decision to enter autophagy or apoptosis. *Nat Cell Biol* 9: 218-24

134.   Lin SJ, Kaeberlein M, Andalis AA, Sturtz LA, Defossez PA, et al. 2002. Calorie restriction extends *Saccharomyces cerevisiae* lifespan by increasing respiration. *Nature* 418: 344-8

135.   Lin YJ, Seroude L, Benzer S. 1998. Extended life-span and stress resistance in the *Drosophila* mutant *methuselah*. *Science* 282: 943-6

136.   Loewith R, Jacinto E, Wullschleger S, Lorberg A, Crespo JL, et al. 2002. Two TOR complexes, only one of which is rapamycin sensitive, have distinct roles in cell growth control. *Mol Cell* 10: 457-68

137.   Longo VD. 2003. The Ras and Sch9 pathways regulate stress resistance and longevity. *Exp Gerontol* 38: 807-11

138.   Longtine MS, McKenzie III, Demarini DJ, Shah NG, Wach A, et al. 1998. Additional modules for versatile and economical PCR-based gene deletion and modification in *Saccharomyces cerevisiae*. *Yeast* 14: 953-61

139.   MacLean M, Harris N, Piper PW. 2001. Chronological lifespan of stationary phase yeast cells; a model for investigating the factors that might influence the ageing of postmitotic tissues in higher organisms. *Yeast* 18: 499-509

140.   Magwere T, West M, Riyahi K, Murphy MP, Smith RA, Partridge L. 2006. The effects of exogenous antioxidants on lifespan and oxidative stress resistance in *Drosophila melanogaster*. *Mech Ageing Dev* 127: 356-70

141.   Mammucari C, Milan G, Romanello V, Masiero E, Rudolf R, et al. 2007. FoxO3 controls autophagy in skeletal muscle in vivo. *Cell Metab* 6: 458-71

142.   Mammucari C, Schiaffino S, Sandri M. 2008. Downstream of Akt: FoxO3 and mTOR in the regulation of autophagy in skeletal muscle. *Autophagy* 4: 524-6

143.   Marino G, Ugalde AP, Salvador-Montoliu N, Varela I, Quiros PM, et al. 2008. Premature aging in mice activates a systemic metabolic response involving autophagy induction. *Hum Mol Genet* 17: 2196-211

144.   Masoro EJ. 2005. Overview of caloric restriction and ageing. *Mech Ageing Dev* 126: 913-22

145.   Matsui Y, Takagi H, Qu X, Abdellatif M, Sakoda H, et al. 2007. Distinct roles of autophagy in the heart during ischemia and reperfusion: roles of AMP-activated protein kinase and Beclin 1 in mediating autophagy. *Circ Res* 100: 914-22

146.   Melendez A, Tallóczy Z, Seaman M, Eskelinen E-L, Hall DH, Levine B. 2003. Autophagy genes are essential for dauer development and life-span extension in *C. elegans*. *Science* 301: 1387-91

147.   Migliaccio E, Giorgio M, Mele S, Pelicci G, Reboldi P, et al. 1999. The p66shc adaptor protein controls oxidative stress response and life span in mammals. *Nature* 402: 309-13

148.   Mihaylova VT, Borland CZ, Manjarrez L, Stern MJ, Sun H. 1999. The PTEN tumor suppressor homolog in *Caenorhabditis elegans* regulates longevity and dauer formation in an insulin receptor-like signaling pathway. *Proc Natl Acad Sci U S A* 96: 7427-32

149.   Miller RA, Buehner G, Chang Y, Harper JM, Sigler R, Smith-Wheelock M. 2005. Methionine-deficient diet extends mouse lifespan, slows immune and lens aging,

alters glucose, T4, IGF-I and insulin levels, and increases hepatocyte MIF levels and stress resistance. *Aging Cell* 4: 119-25

150.   Miwa S, Riyahi K, Partridge L, Brand MD. 2004. Lack of correlation between mitochondrial reactive oxygen species production and life span in Drosophila. *Ann N Y Acad Sci* 1019: 388-91

151.   Mizushima N, Levine B, Cuervo AM, Klionsky DJ. 2008. Autophagy fights disease through cellular self-digestion. *Nature* 451: 1069-75

152.   Mizushima N, Sugita H, Yoshimori T, Ohsumi Y. 1998. A new protein conjugation system in human. The counterpart of the yeast Apg12p conjugation system essential for autophagy. *J Biol Chem* 273: 33889-92

153.   Mizushima N, Yamamoto A, Matsui M, Yoshimori T, Ohsumi Y. 2004. In vivo analysis of autophagy in response to nutrient starvation using transgenic mice expressing a fluorescent autophagosome marker. *Mol Biol Cell* 15: 1101-11

154.   Monastyrska I, He C, Geng J, Hoppe AD, Li Z, Klionsky DJ. 2008. Arp2 links autophagic machinery with the actin cytoskeleton. *Mol Biol Cell* 19: 1962-75

155.   Morley JF, Morimoto RI. 2004. Regulation of longevity in *Caenorhabditis elegans* by heat shock factor and molecular chaperones. *Mol Biol Cell* 15: 657-64

156.   Mortimore GE, Poso AR, Lardeux BR. 1989. Mechanism and regulation of protein degradation in liver. *Diabetes Metab Rev* 5: 49-70

157.   Mostoslavsky R, Chua KF, Lombard DB, Pang WW, Fischer MR, et al. 2006. Genomic instability and aging-like phenotype in the absence of mammalian SIRT6. *Cell* 124: 315-29

158.   Nakai D, Shimizu T, Nojiri H, Uchiyama S, Koike H, et al. 2004. coq7/clk-1 regulates mitochondrial respiration and the generation of reactive oxygen species via coenzyme Q. *Aging Cell* 3: 273-81

159.   Nezis IP, Simonsen A, Sagona AP, Finley K, Gaumer S, et al. 2008. Ref(2)P, the *Drosophila melanogaster* homologue of mammalian p62, is required for the formation of protein aggregates in adult brain. *J Cell Biol* 180: 1065-71

160.   Nice DC, Sato TK, Stromhaug PE, Emr SD, Klionsky DJ. 2002. Cooperative binding of the cytoplasm to vacuole targeting pathway proteins, Cvt13 and Cvt20, to phosphatidylinositol 3-phosphate at the pre-autophagosomal structure is required for selective autophagy. *J Biol Chem* 277: 30198-207

161.   Noda T, Kim J, Huang W-P, Baba M, Tokunaga C, et al. 2000. Apg9p/Cvt7p is an integral membrane protein required for transport vesicle formation in the Cvt and autophagy pathways. *J Cell Biol* 148: 465-80

162.   Noda T, Matsuura A, Wada Y, Ohsumi Y. 1995. Novel system for monitoring autophagy in the yeast *Saccharomyces cerevisiae. Biochem Biophys Res Commun* 210: 126-32

163.   Nowikovsky K, Reipert S, Devenish RJ, Schweyen RJ. 2007. Mdm38 protein depletion causes loss of mitochondrial K^+/H^+ exchange activity, osmotic swelling and mitophagy. *Cell Death Differ* 14: 1647-56

164.   Obara K, Sekito T, Ohsumi Y. 2006. Assortment of phosphatidylinositol 3-kinase complexes--Atg14p directs association of complex I to the pre-autophagosomal structure in *Saccharomyces cerevisiae. Mol Biol Cell* 17: 1527-39

165.   Ogier-Denis E, Codogno P. 2003. Autophagy: a barrier or an adaptive response to cancer. *Biochim Biophys Acta* 1603: 113-28

166. Oka T, Ungar D, Hughson FM, Krieger M. 2004. The COG and COPI complexes interact to control the abundance of GEARs, a subset of Golgi integral membrane proteins. *Mol Biol Cell* 15: 2423-35

167. Oldham S, Hafen E. 2003. Insulin/IGF and target of rapamycin signaling: a TOR de force in growth control. *Trends Cell Biol* 13: 79-85

168. Orr WC, Sohal RS. 1994. Extension of life-span by overexpression of superoxide dismutase and catalase in *Drosophila melanogaster*. *Science* 263: 1128-30

169. Orr WC, Sohal RS. 2003. Does overexpression of Cu,Zn-SOD extend life span in *Drosophila melanogaster*? *Exp Gerontol* 38: 227-30

170. Paradis S, Ailion M, Toker A, Thomas JH, Ruvkun G. 1999. A PDK1 homolog is necessary and sufficient to transduce AGE-1 PI3 kinase signals that regulate diapause in *Caenorhabditis elegans*. *Genes Dev* 13: 1438-52

171. Parkes TL, Elia AJ, Dickinson D, Hilliker AJ, Phillips JP, Boulianne GL. 1998. Extension of Drosophila lifespan by overexpression of human SOD1 in motorneurons. *Nat Genet* 19: 171-4

172. Partridge L, Piper MD, Mair W. 2005. Dietary restriction in Drosophila. *Mech Ageing Dev* 126: 938-50

173. Pedruzzi I, Burckert N, Egger P, De Virgilio C. 2000. Saccharomyces cerevisiae Ras/cAMP pathway controls post-diauxic shift element-dependent transcription through the zinc finger protein Gis1. *EMBO J* 19: 2569-79

174. Pedruzzi I, Dubouloz F, Cameroni E, Wanke V, Roosen J, et al. 2003. TOR and PKA signaling pathways converge on the protein kinase Rim15 to control entry into G0. *Mol Cell* 12: 1607-13

175. Picard F, Kurtev M, Chung N, Topark-Ngarm A, Senawong T, et al. 2004. Sirt1 promotes fat mobilization in white adipocytes by repressing PPAR-gamma. *Nature* 429: 771-6

176. Piper MD, Mair W, Partridge L. 2005. Counting the calories: the role of specific nutrients in extension of life span by food restriction. *J Gerontol A Biol Sci Med Sci* 60: 549-55

177. Portela P, Moreno S. 2006. Glucose-dependent activation of protein kinase A activity in *Saccharomyces cerevisiae* and phosphorylation of its TPK1 catalytic subunit. *Cell Signal* 18: 1072-86

178. Powers RW, 3rd, Kaeberlein M, Caldwell SD, Kennedy BK, Fields S. 2006. Extension of chronological life span in yeast by decreased TOR pathway signaling. *Genes Dev* 20: 174-84

179. Ram RJ, Li B, Kaiser CA. 2002. Identification of Sec36p, Sec37p, and Sec38p: components of yeast complex that contains Sec34p and Sec35p. *Mol Biol Cell* 13: 1484-500

180. Rea SL. 2005. Metabolism in the *Caenorhabditis elegans Mit* mutants. *Exp Gerontol* 40: 841-9

181. Reggiori F, Klionsky DJ. 2002. Autophagy in the eukaryotic cell. *Eukaryot Cell* 1: 11-21

182. Reggiori F, Klionsky DJ. 2005. Autophagosomes: biogenesis from scratch? *Curr Opin Cell Biol* 17: 415-22

183.   Reggiori F, Monastyrska I, Shintani T, Klionsky DJ. 2005. The actin cytoskeleton is required for selective types of autophagy, but not nonspecific autophagy, in the yeast *Saccharomyces cerevisiae*. *Mol Biol Cell* 16: 5843-56

184.   Reggiori F, Pelham HRB. 2001. Sorting of proteins into multivesicular bodies: ubiquitin-dependent and -independent targeting. *EMBO J* 20: 5176-86

185.   Reggiori F, Shintani T, Nair U, Klionsky DJ. 2005. Atg9 cycles between mitochondria and the pre-autophagosomal structure in yeasts. *Autophagy* 1: 101-9

186.   Reggiori F, Tucker KA, Stromhaug PE, Klionsky DJ. 2004. The Atg1-Atg13 complex regulates Atg9 and Atg23 retrieval transport from the pre-autophagosomal structure. *Dev Cell* 6: 79-90

187.   Reggiori F, Wang C-W, Nair U, Shintani T, Abeliovich H, Klionsky DJ. 2004. Early stages of the secretory pathway, but not endosomes, are required for Cvt vesicle and autophagosome assembly in *Saccharomyces cerevisiae*. *Mol Biol Cell* 15: 2189-204

188.   Reggiori F, Wang C-W, Stromhaug PE, Shintani T, Klionsky DJ. 2003. Vps51 is part of the yeast Vps fifty-three tethering complex essential for retrograde traffic from the early endosome and Cvt vesicle completion. *J Biol Chem* 278: 5009-20

189.   Roberts P, Moshitch-Moshkovitz S, Kvam E, O'Toole E, Winey M, Goldfarb DS. 2003. Piecemeal microautophagy of nucleus in *Saccharomyces cerevisiae*. *Mol Biol Cell* 14: 129-41

190.   Robinson JS, Klionsky DJ, Banta LM, Emr SD. 1988. Protein sorting in *Saccharomyces cerevisiae*: isolation of mutants defective in the delivery and processing of multiple vacuolar hydrolases. *Mol Cell Biol* 8: 4936-48

191.   Rodriguez-Enriquez S, He L, Lemasters JJ. 2004. Role of mitochondrial permeability transition pores in mitochondrial autophagy. *Int J Biochem Cell Biol* 36: 2463-72

192.   Rogina B, Helfand SL. 2004. Sir2 mediates longevity in the fly through a pathway related to calorie restriction. *Proc Natl Acad Sci U S A* 101: 15998-6003

193.   Rohde J, Heitman J, Cardenas ME. 2001. The TOR kinases link nutrient sensing to cell growth. *J Biol Chem* 276: 9583-6

194.   Roosen J, Engelen K, Marchal K, Mathys J, Griffioen G, et al. 2005. PKA and Sch9 control a molecular switch important for the proper adaptation to nutrient availability. *Mol Microbiol* 55: 862-80

195.   Roth GS, Lane MA, Ingram DK, Mattison JA, Elahi D, et al. 2002. Biomarkers of caloric restriction may predict longevity in humans. *Science* 297: 811

196.   Roth GS, Mattison JA, Ottinger MA, Chachich ME, Lane MA, Ingram DK. 2004. Aging in rhesus monkeys: relevance to human health interventions. *Science* 305: 1423-6

197.   Santangelo GM. 2006. Glucose signaling in *Saccharomyces cerevisiae*. *Microbiol Mol Biol Rev* 70: 253-82

198.   Scherz-Shouval R, Elazar Z. 2007. ROS, mitochondria and the regulation of autophagy. *Trends Cell Biol* 17: 422-7

199.   Scherz-Shouval R, Shvets E, Fass E, Shorer H, Gil L, Elazar Z. 2007. Reactive oxygen species are essential for autophagy and specifically regulate the activity of Atg4. *EMBO J* 26: 1749-60

200. Scott SV, Baba M, Ohsumi Y, Klionsky DJ. 1997. Aminopeptidase I is targeted to the vacuole by a nonclassical vesicular mechanism. *J Cell Biol* 138: 37-44

201. Scott SV, Guan J, Hutchins MU, Kim J, Klionsky DJ. 2001. Cvt19 is a receptor for the cytoplasm-to-vacuole targeting pathway. *Mol Cell* 7: 1131-41

202. Scott SV, Hefner-Gravink A, Morano KA, Noda T, Ohsumi Y, Klionsky DJ. 1996. Cytoplasm-to-vacuole targeting and autophagy employ the same machinery to deliver proteins to the yeast vacuole. *Proc Natl Acad Sci U S A* 93: 12304-8

203. Seglen PO, Berg TO, Blankson H, Fengsrud M, Holen I, Stromhaug PE. 1996. Structural aspects of autophagy. *Adv Exp Med Biol* 389: 103-11

204. Senoo-Matsuda N, Hartman PS, Akatsuka A, Yoshimura S, Ishii N. 2003. A complex II defect affects mitochondrial structure, leading to ced-3- and ced-4-dependent apoptosis and aging. *J Biol Chem* 278: 22031-6

205. Seto NO, Hayashi S, Tener GM. 1990. Overexpression of Cu-Zn superoxide dismutase in Drosophila does not affect life-span. *Proc Natl Acad Sci U S A* 87: 4270-4

206. Shestakova A, Zolov S, Lupashin V. 2006. COG complex-mediated recycling of Golgi glycosyltransferases is essential for normal protein glycosylation. *Traffic* 7: 191-204

207. Shintani T, Huang WP, Stromhaug PE, Klionsky DJ. 2002. Mechanism of cargo selection in the cytoplasm to vacuole targeting pathway. *Dev Cell* 3: 825-37

208. Shintani T, Klionsky DJ. 2004. Autophagy in health and disease: a double-edged sword. *Science* 306: 990-5

209. Shintani T, Klionsky DJ. 2004. Cargo proteins facilitate the formation of transport vesicles in the cytoplasm to vacuole targeting pathway. *J Biol Chem* 279: 29889-94

210. Short KR, Bigelow ML, Kahl J, Singh R, Coenen-Schimke J, et al. 2005. Decline in skeletal muscle mitochondrial function with aging in humans. *Proc Natl Acad Sci U S A* 102: 5618-23

211. Simonsen A, Cumming RC, Lindmo K, Galaviz V, Cheng S, et al. 2007. Genetic modifiers of the *Drosophila blue cheese* gene link defects in lysosomal transport with decreased life span and altered ubiquitinated-protein profiles. *Genetics* 176: 1283-97

212. Sinclair DA, Guarente L. 1997. Extrachromosomal rDNA circles--a cause of aging in yeast. *Cell* 91: 1033-42

213. Slattery MG, Liko D, Heideman W. 2008. Protein kinase A, TOR, and glucose transport control the response to nutrient repletion in *Saccharomyces cerevisiae*. *Eukaryot Cell* 7: 358-67

214. Smith A, Ward MP, Garrett S. 1998. Yeast PKA represses Msn2p/Msn4p-dependent gene expression to regulate growth, stress response and glycogen accumulation. *EMBO J* 17: 3556-64

215. Spelbrink RG, Nothwehr SF. 1999. The yeast GRD20 gene is required for protein sorting in the trans-Golgi network/endosomal system and for polarization of the actin cytoskeleton. *Mol Biol Cell* 10: 4263-81

216. Stack JH, DeWald DB, Takegawa K, Emr SD. 1995. Vesicle-mediated protein transport: regulatory interactions between the Vps15 protein kinase and the Vps34

PtdIns 3-kinase essential for protein sorting to the vacuole in yeast. *J Cell Biol* 129: 321-34

217. Stasyk OV, Stasyk OG, Mathewson RD, Farre JC, Nazarko VY, et al. 2006. Atg28, a novel coiled-coil protein involved in autophagic degradation of peroxisomes in the methylotrophic yeast *Pichia pastoris*. *Autophagy* 2: 30-8

218. Stromhaug PE, Reggiori F, Guan J, Wang CW, Klionsky DJ. 2004. Atg21 is a phosphoinositide binding protein required for efficient lipidation and localization of Atg8 during uptake of aminopeptidase I by selective autophagy. *Mol Biol Cell* 15: 3553-66

219. Sun J, Folk D, Bradley TJ, Tower J. 2002. Induced overexpression of mitochondrial Mn-superoxide dismutase extends the life span of adult *Drosophila melanogaster*. *Genetics* 161: 661-72

220. Sun J, Tower J. 1999. FLP recombinase-mediated induction of Cu/Zn-superoxide dismutase transgene expression can extend the life span of adult *Drosophila melanogaster* flies. *Mol Cell Biol* 19: 216-28

221. Suvorova ES, Duden R, Lupashin VV. 2002. The Sec34/Sec35p complex, a Ypt1p effector required for retrograde intra-Golgi trafficking, interacts with Golgi SNAREs and COPI vesicle coat proteins. *J Cell Biol* 157: 631-43

222. Suzuki K, Kirisako T, Kamada Y, Mizushima N, Noda T, Ohsumi Y. 2001. The pre-autophagosomal structure organized by concerted functions of *APG* genes is essential for autophagosome formation. *EMBO J* 20: 5971-81

223. Suzuki K, Kubota Y, Sekito T, Ohsumi Y. 2007. Hierarchy of Atg proteins in pre-autophagosomal structure organization. *Genes Cells* 12: 209-18

224. Tatar M, Kopelman A, Epstein D, Tu MP, Yin CM, Garofalo RS. 2001. A mutant Drosophila insulin receptor homolog that extends life-span and impairs neuroendocrine function. *Science* 292: 107-10

225. Taub J, Lau JF, Ma C, Hahn JH, Hoque R, et al. 1999. A cytosolic catalase is needed to extend adult lifespan in *C. elegans daf-C* and *clk-1* mutants. *Nature* 399: 162-6d

226. Terman A, Brunk UT. 2004. Myocyte aging and mitochondrial turnover. *Exp Gerontol* 39: 701-5

227. Thevelein JM, Cauwenberg L, Colombo S, De Winde JH, Donation M, et al. 2000. Nutrient-induced signal transduction through the protein kinase A pathway and its role in the control of metabolism, stress resistance, and growth in yeast. *Enzyme Microb Technol* 26: 819-25

228. Tissenbaum HA, Guarente L. 2001. Increased dosage of a sir-2 gene extends lifespan in *Caenorhabditis elegans*. *Nature* 410: 227-30

229. Toth ML, Sigmond T, Borsos E, Barna J, Erdelyi P, et al. 2008. Longevity pathways converge on autophagy genes to regulate life span in *Caenorhabditis elegans*. *Autophagy* 4: 330-8

230. Tucker KA, Reggiori F, Dunn WA, Jr., Klionsky DJ. 2003. Atg23 is essential for the cytoplasm to vacuole targeting pathway and efficient autophagy but not pexophagy. *J Biol Chem* 278: 48445-52

231. Ungar D, Oka T, Brittle EE, Vasile E, Lupashin VV, et al. 2002. Characterization of a mammalian Golgi-localized protein complex, COG, that is required for normal Golgi morphology and function. *J Cell Biol* 157: 405-15

232.   Ungar D, Oka T, Krieger M, Hughson FM. 2006. Retrograde transport on the COG railway. *Trends Cell Biol* 16: 113-20

233.   Valenzano DR, Terzibasi E, Genade T, Cattaneo A, Domenici L, Cellerino A. 2006. Resveratrol prolongs lifespan and retards the onset of age-related markers in a short-lived vertebrate. *Curr Biol* 16: 296-300

234.   Van Remmen H, Ikeno Y, Hamilton M, Pahlavani M, Wolf N, et al. 2003. Life-long reduction in MnSOD activity results in increased DNA damage and higher incidence of cancer but does not accelerate aging. *Physiol Genomics* 16: 29-37

235.   VanRheenen SM, Cao X, Lupashin VV, Barlowe C, Waters MG. 1998. Sec35p, a novel peripheral membrane protein, is required for ER to Golgi vesicle docking. *J Cell Biol* 141: 1107-19

236.   VanRheenen SM, Cao X, Sapperstein SK, Chiang EC, Lupashin VV, et al. 1999. Sec34p, a protein required for vesicle tethering to the yeast Golgi apparatus, is in a complex with Sec35p. *J Cell Biol* 147: 729-42

237.   Vasile E, Oka T, Ericsson M, Nakamura N, Krieger M. 2006. IntraGolgi distribution of the Conserved Oligomeric Golgi (COG) complex. *Exp Cell Res* 312: 3132-41

238.   Vellai T, Takacs-Vellai K, Zhang Y, Kovacs AL, Orosz L, Muller F. 2003. Genetics: influence of TOR kinase on lifespan in *C. elegans*. *Nature* 426: 620

239.   Ventura N, Rea SL, Testi R. 2006. Long-lived *C. elegans* mitochondrial mutants as a model for human mitochondrial-associated diseases. *Exp Gerontol* 41: 974-91

240.   Vercammen D, Beyaert R, Denecker G, Goossens V, Van Loo G, et al. 1998. Inhibition of caspases increases the sensitivity of L929 cells to necrosis mediated by tumor necrosis factor. *J Exp Med* 187: 1477-85

241.   Volchuk A, Ravazzola M, Perrelet A, Eng WS, Di Liberto M, et al. 2004. Countercurrent distribution of two distinct SNARE complexes mediating transport within the Golgi stack. *Mol Biol Cell* 15: 1506-18

242.   von Heijne G. 1984. How signal sequences maintain cleavage specificity. *J Mol Biol* 173: 243-51

243.   Wallace DC. 2005. A mitochondrial paradigm of metabolic and degenerative diseases, aging, and cancer: a dawn for evolutionary medicine. *Annu Rev Genet* 39: 359-407

244.   Wei M, Fabrizio P, Hu J, Ge H, Cheng C, et al. 2008. Life span extension by calorie restriction depends on Rim15 and transcription factors downstream of Ras/PKA, Tor, and Sch9. *PLoS Genet* 4: e13

245.   Weindruch R, Naylor PH, Goldstein AL, Walford RL. 1988. Influences of aging and dietary restriction on serum thymosin alpha 1 levels in mice. *J Gerontol* 43: B40-2

246.   Westermann B, Neupert W. 2000. Mitochondria-targeted green fluorescent proteins: convenient tools for the study of organelle biogenesis in *Saccharomyces cerevisiae*. *Yeast* 16: 1421-7

247.   Whyte JR, Munro S. 2001. The Sec34/35 Golgi transport complex is related to the exocyst, defining a family of complexes involved in multiple steps of membrane traffic. *Dev Cell* 1: 527-37

248. Willcox DC, Willcox BJ, Todoriki H, Curb JD, Suzuki M. 2006. Caloric restriction and human longevity: what can we learn from the Okinawans? *Biogerontology* 7: 173-7

249. Wilson WA, Roach PJ. 2002. Nutrient-regulated protein kinases in budding yeast. *Cell* 111: 155-8

250. Wohlgemuth SE, Julian D, Akin DE, Fried J, Toscano K, et al. 2007. Autophagy in the heart and liver during normal aging and calorie restriction. *Rejuvenation Res* 10: 281-92

251. Wu X, Steet RA, Bohorov O, Bakker J, Newell J, et al. 2004. Mutation of the COG complex subunit gene COG7 causes a lethal congenital disorder. *Nat Med* 10: 518-23

252. Wu YT, Tan HL, Huang Q, Kim YS, Pan N, et al. 2008. Autophagy plays a protective role during zVAD-induced necrotic cell death. *Autophagy* 4: 457-66

253. Wuestehube LJ, Duden R, Eun A, Hamamoto S, Korn P, et al. 1996. New mutants of *Saccharomyces cerevisiae* affected in the transport of proteins from the endoplasmic reticulum to the Golgi complex. *Genetics* 142: 393-406

254. Wurmser AE, Emr SD. 2002. Novel PtdIns(3)P-binding protein Etf1 functions as an effector of the Vps34 PtdIns 3-kinase in autophagy. *J Cell Biol* 158: 761-72

255. Xie Z, Klionsky DJ. 2007. Autophagosome formation: core machinery and adaptations. *Nat Cell Biol* 9: 1102-9

256. Xie Z, Nair U, Klionsky DJ. 2008. Atg8 controls phagophore expansion during autophagosome formation. *Mol Biol Cell* 19: 3290-8

257. Xu Y, Kim SO, Li Y, Han J. 2006. Autophagy contributes to caspase-independent macrophage cell death. *J Biol Chem* 281: 19179-87

258. Yamamoto M, Clark JD, Pastor JV, Gurnani P, Nandi A, et al. 2005. Regulation of oxidative stress by the anti-aging hormone klotho. *J Biol Chem* 280: 38029-34

259. Yamasoba T, Someya S, Yamada C, Weindruch R, Prolla TA, Tanokura M. 2007. Role of mitochondrial dysfunction and mitochondrial DNA mutations in age-related hearing loss. *Hear Res* 226: 185-93

260. Yan L, Vatner DE, O'Connor JP, Ivessa A, Ge H, et al. 2007. Type 5 adenylyl cyclase disruption increases longevity and protects against stress. *Cell* 130: 247-58

261. Yang Z, Huang J, Geng J, Nair U, Klionsky DJ. 2006. Atg22 recycles amino acids to link the degradative and recycling functions of autophagy. *Mol Biol Cell* 17: 5094-104

262. Yen W-L, Klionsky DJ. 2008. How to live long and prosper: autophagy, mitochondria, and aging. *Physiology (Bethesda)* 23: 248-62

263. Yen W-L, Legakis JE, Nair U, Klionsky DJ. 2007. Atg27 is required for autophagy-dependent cycling of Atg9. *Mol Biol Cell* 18: 581-93

264. Yorimitsu T, Klionsky DJ. 2005. Autophagy: molecular machinery for self-eating. *Cell Death Differ* 12 Suppl 2: 1542-52

265. Yorimitsu T, Klionsky DJ. 2007. Eating the endoplasmic reticulum: quality control by autophagy. *Trends Cell Biol* 17: 279-85

266. Yorimitsu T, Zaman S, Broach JR, Klionsky DJ. 2007. Protein kinase A and Sch9 cooperatively regulate induction of autophagy in *Saccharomyces cerevisiae. Mol Biol Cell* 18: 4180-9

267. Young ARJ, Chan EYW, Hu XW, Köchl R, Crawshaw SG, et al. 2006. Starvation and ULK1-dependent cycling of mammalian Atg9 between the TGN and endosomes. *J Cell Sci* 119: 3888-900

268. Yu L, Alva A, Su H, Dutt P, Freundt E, et al. 2004. Regulation of an *ATG7-beclin 1* program of autophagic cell death by caspase-8. *Science* 304: 1500-2

269. Yu L, Wan F, Dutta S, Welsh S, Liu Z, et al. 2006. Autophagic programmed cell death by selective catalase degradation. *Proc Natl Acad Sci U S A* 103: 4952-7

270. Zatloukal K, Stumptner C, Fuchsbichler A, Heid H, Schnoelzer M, et al. 2002. p62 Is a common component of cytoplasmic inclusions in protein aggregation diseases. *Am J Pathol* 160: 255-63

271. Tomotake Kanki, Yang Cao, Misuzu Baba, and Daniel J. Klionsky. 2009. *Dev Cell*. Atg32 is a mitochondrial protein that confers selectivity during mitophagy. (manuscript accepted)